Collection Characteristics of Mist Aerosol Particles by Fibrous Filter

Punnida Suwanwong

A Thesis Submitted in Partial Fulfillment of the Requirements
for the Degree of Master of Science in Physical Chemistry
Prince of Songkla University
2008

Thesis Title	Collection Characteristics of Mist Aerosol Particles by Fibrous Filter
Author	Miss Punnida Suwanwong
Major Program	Physical Chemistry

Major Advisor

..……..……...

(Asst. Prof. Dr. Surajit Tekasakul)

Co-advisors

…….....……..…...……...

(Assoc. Prof. Dr. Perapong Tekasakul)

…….....……..…...……...

(Prof. Dr. Yoshio Otani)

Examining Committee:

……...……..Chairperson

(Asst. Prof. Dr. Orawan Sirichote)

..…...…….……Committee

(Asst. Prof. Dr. Surajit Tekasakul)

..…....……..……..Committee

(Assoc. Prof. Dr. Perapong Tekasakul)

….....……...……...……..Committee

(Assoc. Prof. Dr. Tawatchai Charinpanitkul)

The Graduate School, Prince of Songkla University, has approved this thesis as partial fulfillment of the requirements for the Master of Science Degree in Physical Chemistry

……..……

(Assoc. Prof. Dr. Krerkchai Thongnoo)

Dean of Graduate School

ชื่อวิทยานิพนธ์ คุณลักษณะการดักจับอนุภาคแอโรซอลประเภทละอองของเหลวด้วยตัวกรองเส้นใย
ผู้เขียน นางสาวพัณนิดา สุวรรณวงศ์
สาขาวิชา เคมีเชิงฟิสิกส์
ปีการศึกษา 2550

บทคัดย่อ

กระบวนการกรองด้วยตัวกรองเส้นใยเป็นวิธีที่ง่ายและให้ประสิทธิภาพสูงในการดักจับอนุภาคแอโรซอลที่แขวนลอยอยู่ในอากาศโดยเฉพาะอนุภาคขนาดเล็ก ในงานวิจัยนี้ได้ศึกษาคุณลักษณะการดักจับอนุภาคแอโรซอลประเภทละอองของเหลวด้วยตัวกรองเส้นใยโดยการเปลี่ยนตัวแปรต่าง ๆ หลายตัวแปร เช่นความเร็วของอนุภาค จำนวนแผ่นของตัวกรองเส้นใยและชนิดของของเหลวที่มีสมบัติเชิงฟิสิกส์ที่แตกต่างกัน รวมทั้งศึกษาการกระจายขนาดของอนุภาค ความเข้มข้นของอนุภาคของเหลวและประสิทธิภาพหรือสมรรถนะของตัวกรองเส้นใยบริสุทธิ์ จากผลการทดลองพบว่า ค่าความดันสูญเสียในระหว่างการดักจับอนุภาคของเหลวมีค่าเพิ่มขึ้นเมื่อความเร็วเพิ่มขึ้น และเมื่อความเร็วมีค่าสูง อนุภาคแอโรซอล ประเภทละอองของเหลวเกิดการดักจับบนผิวของตัวกรองเส้นใยได้อย่างรวดเร็วเป็นสาเหตุทำให้ค่าความดันสูญเสียของตัวกรองมีค่าเพิ่มขึ้น นอกจากนี้ค่าความดันสูญเสียมีค่าเพิ่มขึ้นเมื่อจำนวนแผ่นของตัวกรองเส้นใยเพิ่มขึ้นสำหรับทุกความเร็ว ขนาดของอนุภาค ความเข้มข้นของของเหลวและแรงตึงผิวของของเหลวมีบทบาทสำคัญต่อการดักจับอนุภาค ภาพถ่ายของตัวกรองที่สภาวะต่าง ๆ จากกล้องจุลทรรศน์พบว่าการดักจับอนุภาคน้ำมันปาล์มบนตัวกรองเส้นใยจะเกิดเพียงหยดของเหลวรอบ ๆ เส้นใย ในขณะที่การดักจับอนุภาคโพรพิลีนไกลคอลจะเกิดหยดของเหลวรอบ ๆ เส้นใย และเกิดการรวมตัวกันของหยดของเหลวเกิดเป็นฟิล์มของเหลวบนผิวของตัวกรอง นอกจากนี้ได้ทำการศึกษาพฤติกรรมการอิ่มตัวของตัวกรองเส้นใยที่อิ่มตัวด้วยน้ำ โพรพิลีนไกลคอลและน้ำมันปาล์ม จากผลการทดลองพบว่า ที่ความเร็วเริ่มต้นทุกความเร็ว ระยะเวลาที่ค่าความดันสูญเสียมีค่าคงที่ในกรณีของโพรพิลีนไกลคอลมีค่าสูงกว่าในกรณีของน้ำมันปาล์มและน้ำ และหลังจากค่าความดันสูญเสียมีค่าคงที่ที่ความเร็วเริ่มต้นทุกความเร็วพบว่า น้ำหนักของแผ่นกรองที่อิ่มตัวด้วยน้ำมีค่าต่ำกว่าในกรณีที่แผ่นกรองอิ่มตัวด้วยโพรพิลีนไกลคอลและน้ำมันปาล์ม

Thesis Title	Collection Characteristics of Mist Aerosol Particles by Fibrous Filter
Author	Miss Punnida Suwanwong
Major Program	Physical Chemistry
Academic Year	2007

ABSTRACT

Filtration by fibrous filters is one of the simplest and more effective means to remove contaminant aerosol particles from air streams, particularly in the smaller size ranges. In this work, the collection characteristics of mist aerosol particles by fibrous filter was studied by varying various parameters such as filtration velocity, numbers of fibrous filter and types of liquid with different physical properties. Moreover, size distribution, concentration of generated aerosol and performance of virgin filter were also investigated. The results show that the pressure drop evolutions during clogging increases when the filtration velocity increases. At high filtration velocity, the mist aerosol particles deposit on the collecting surface rapidly. This result causes the pressure drop of filter to increase. Furthermore, the change in pressure drop increases with increasing the number of filter sheets for all filtration velocities. Particle size, concentration and surface tension of the liquids have an influence on clogging. From the optical microscope photographs of a single filter at different stages, the deposition of palm oil aerosol particles is only made up of droplets deposited around the fibers as the deposition of propylene glycol aerosol particles is made up of droplets deposited around the fibers and join to form bridges and liquid films on the surface of the filter. In addition, the saturation characteristics of the medium performance fibrous filter saturated with water, propylene glycol and palm oil were studied. The results show that the period that the saturation pressure drop from all the initial velocity for propylene glycol is longer than that for palm oil and water while the remained mass on the filter sheet saturated with water after the pressure drop is constant at all the initial velocity is lower than when filter sheet saturated with propylene glycol and palm oil.

ACKNOWLEDGEMENT

I wish to express my deep and sincere gratitude to my advisor, Assistant Professor Dr. Surajit Tekasakul, for her valuable instructions, expert guidance, excellent suggestions and kindness throughout my graduate study. I am also grateful to her for providing help during the research.

My sincere thank is expressed to Associate Professor Dr. Perapong Tekasakul my co-advisor for his kindness, valuable suggestion and correction in the thesis. I would like to express thank to Professor Dr. Yoshio Otani of Kanasawa University, Japan for his helpful comments.

I would like to express thank to Assistant Professor Dr. Orawan Sirichote and Associate Professor Dr. Tawatchai Charinpanitkul for helpful suggestion and effort to thesis examination.

I would like to thank Mr. Prapas Chaitape for his suggestions and providing help during construction of experimental devices.

I would like to thank all member of CH 403 laboratory for their kindness, help, friendship and understanding.

I am very much thankful to Higher Education Development Project, Ministry of Education: Center for Innovation in Chemistry: Postgraduate Education and Research Program in Chemistry (PERCH-CIC) and Graduate School for partial financial supports.

I would also like to thank Department of Chemistry for making available the facilities used in this research.

Finally, none of this would have been possible without love, understand and encouragement of my family.

Punnida Suwanwong

THE RELEVANT OF THE RESEARCH WORK TO THAILAND

Collection Characteristics of Mist Aerosol Particles by Fibrous Filter is a Master of Science Thesis in Physical Chemistry. Organizations that could use the outcome of this thesis work include for examples

- Ministry of Industry
- Ministry of Education

CONTENTS

CONTENTS (Continued)

LIST OF TABLES

LIST OF FIGURES

LIST OF FIGURES (Continued)

LIST OF FIGURES (Continued)

LIST OF FIGURES (Continued)

LIST OF FIGURES (Continued)

LIST OF FIGURES (Continued)

LIST OF ABBREVIATIONS

d_{ave}	=	average aerodynamic diameter
d_c	=	characteristic length of collecting media
d_f	=	fiber diameter
$d_{f\ Davies}$	=	fiber Davies diameter
$d_{f\ Davies\ wet}$	=	mean wet fiber Davies diameter
d_p	=	droplet (particle) diameter
dZ	=	filter layer thickness
f	=	mass fraction
g	=	acceleration of gravity
k	=	Boltzmann constant
m_{liq}	=	collected liquid mass
t	=	sample time
u	=	gas velocity at filter face
u'	=	interstitial gas velocity
w_0	=	weight of clean filter
w_t	=	weight of clogged filter at any filtration time
A	=	filter cross-sectional area
C	=	aerosol concentration
C_c	=	Cunningham correction factor
C_{in}	=	inlet concentration
C_{out}	=	downstream concentration
D	=	particle diffusion coefficient
E	=	Efficiency (or total efficiency)
Gr	=	dimensionless parameter governing the gravitational sedimentation mechanism
K	=	slope of straight line linking ΔP to u

LIST OF ABBREVIATIONS (Continued)

M	=	total collected mass
N_{inlet}	=	number concentrations of particles at the upstream of the filter
N_{outlet}	=	number concentrations of particles at the downstream of the filter
N_R	=	interception parameter
P	=	penetration
Pe	=	Peclet number
Q	=	flow rate
QF	=	quality factor
R_f	=	fiber of radius
Stk	=	Stokes number
T	=	absolute temperature
U	=	average air velocity inside the filter medium (flow velocity)
V	=	sampling volume
V_g	=	settling velocity of the particle
Y	=	layer of thickness
Z	=	filter thickness
Ω	=	filtration surface
α_f	=	solidity or packing density of the filter
α_{film}	=	maximum liquid packing density
α_l	=	liquid packing density
α_{tube}	=	liquid packing density at the end of the first stage
η	=	single-fiber efficiency
$\eta_{\text{int}\,er}$	=	single-fiber efficiency by interception

LIST OF ABBREVIATIONS (Continued)

η_{imp}	=	single-fiber efficiency by inertial impaction
η_{diff}	=	single-fiber efficiency by diffusion or Brownian motion
η_{grav}	=	single-fiber efficiency due to gravity
λ	=	mean free path of the gas molecules
μ	=	liquid viscosity
μ_g	=	air viscosity
μ_g	=	gas viscosity
ρ	=	liquid density
ρ_g	=	density of gas
ρ_{liq}	=	liquid density
Δd	=	particle size interval for each stage of the Andersen Sampler
ΔP	=	pressure drop across the filter media
ΔP_0	=	pressure drop across a dry fibrous filter

CHAPTER 1
INTRODUCTION

1.1 General Background

Mist aerosol particles can be generated in several production processes including chemical production, mechanical atomization, evaporation-condensation, entrainment by the gas flow in liquid-gas contactors, and other processes (Frising *et al*., 2005). Mist aerosol particles such as metalworking fluids (MWFs), bis (2-ethylhexyl) sebacate (BEHS), di (2-ethylhexyl) sebacate (DEHS), di-ethyl sebacate (DES), di-octyl phthalate (DOP), decamethylcyclopentasiloxane (DMP) are used to cool and lubricate the chip-tool-workpiece interface during machining. MWFs can evaporate and then condense into small droplets and can also be ejected into the air during application (Letts *et al.,* 2003). People can be exposed to fine aerosol particles through deep inhalation into human lungs and contact with the skin. These exposures are associated with a variety of adverse health effects, most commonly skin disorders such as rashed, dermatitis, folliculitis and keratosis. Eye, nose, and throat irritation and respiratory disorders such as breathing problems, coughing, asthma, lipid pneumonia, chromic bronchitis are also health effects associated with exposure to aerosol particles. Therefore it is necessary to remove these mist aerosol particles (Letts *et al.,* 2003).

Filtration is the most common method of aerosol collection and is widely used for air cleaning. It is also simple, versatile and economical (Hinds, 1999). At present, fibrous filtration is the most common means used to separate liquid aerosol particles from an industrial and household gas streams. Liquid aerosol particles are collected by many collection mechanisms, including interception, impaction and diffusion. When the deposit is made up of droplets collected around the fibers, droplets join together to cover the fiber and distribute themselves over the surfaces of the fibers to form a liquid film on the surface of the filter. This causes a decrease of penetration (or increase of collection efficiency), an increase of pressure

drop. In addition, it would appear preferable to work at high filtration velocities as the penetration of the filter is minimized and collection efficiency increases (Contal *et al.,* 2004).

This research focuses on studying collection characteristics and performance of fibrous filter as it collects mist aerosol particles. Among all the devices designed to eliminate small aerosol particles from air streams, fibrous filters are economically the most interesting technology since they are both effective and simple to use.

1.2 Review of Literature

1.2.1 Size distribution of mist aerosol particles

In order to select an appropriate method or device for collection of liquid aerosol particles, it is essential to study the size distribution of liquid aerosol particles first. The size distribution of liquid aerosol particles has been investigated by many research attempts.

Penicot *et al.* (1999) studied size distribution of the liquid particles from a di-octyl phthalate (DOP) aerosol generated by an aerosol generator. Compressed air at a pressure of 1.1 bar was used to generate the liquid aerosol. Particle size distribution was measured using two techniques: Differential Mobility Particle Sizer (DMPS TSI 3071) associated with Condensation Nucleus Counter (CNC TSI 3020) and an Impactor Marple Personal Sampler 290, and the liquid particles had mean diameter of 0.6 micrometer and the geometric standard deviation (GSD) was 1.46.

Raynor *et al.* (2000) investigated size distribution of mist particles generated by the collison nebulizer. Their results indicated that the mists had mass median diameters (MMDs) ranging from 1.2 to 2.8 micrometer by the time the mist reached the test filter. Log-normal distribution fitted to the data showed geometric standard deviations (GSD) between 1.7 and 2.5.

Hajra *et al.* (2003) investigated size distribution of propylene glycol generated by a Laskin nozzle. Results showed that the oil droplets had mean diameter of 0.21 micrometer and the standard deviation was 0.0266 micrometer.

Vasudevan *et al.* (2004) studied size distribution of propylene glycol aerosol droplets produced by a Laskin nozzle. Results indicated that the droplets had mean diameter of 0.2 micrometer and standard deviation of 0.074 micrometer.

1.2.2 Particulate Control

There are currently a range of technologies used to remove particulate matters from air stream in order to prevent or to reduce emission of aerosol particles escaping to the atmospheric air such as electrostatic precipitators or ESPs, gravitational settlers, centrifuged cyclones, venturi scrubbers, etc. However, these methods are not effective for collecting liquid aerosol particles and small particles, especially for fine particles between submicron and micron size ranges (0.01 to 10 micrometer particle sizes). Electrostatic precipitators and venturi scrubbers, although theirs collection efficiency approach that of filters for particles in some size ranges, are overall less efficient. Gravitational settlers can capture only large aerosol particles (greater than 10 micrometer) and require large space for installation. Cyclones give low collection efficiency for aerosol particles smaller than 5-10 micrometer in diameter. The most efficient method to remove liquid aerosol particles is by the use of filters which are widely used since they can remove sufficient quantities of contaminated particles. Filters are used to remove the particles in the range of submicron particle size. Nowadays, filtration method is one of the most frequently used in diverse applications such as respiratory protection, air cleaning of smelter effluent, processing of nuclear and hazardous materials, and clean rooms. Fibrous filter is a common cleaning device often used to remove contaminated particles from industrial gas stream. At low dust concentration, fibrous filters are the most economical means for achieving high collection efficiency for submicrometer particles (Hinds, 1999). Filtration is a simple, versatile, economical means for aerosol collection and there is no limit to solid or liquid particles. However, there are some

disadvantages and the most significant disadvantages of filters are the requirement for frequent filter cleaning, the change in efficiency and the pressure drop in the filter during operation.

Walsh *et al.* (1996) investigated the effect of solid and liquid particles on the microstructure of the filter samples and the variation in pressure drop of filter as it collected solid and liquid particles. For solid aerosol loading, samples of prefilter material of 12% packing density had been loaded with solid particles of 0.6, 1.4 and 2.2 micrometer stearic acid aerosol particles, at an air velocity of 0.10 m s^{-1}. Results showed that smaller particles cause filter clogging more quickly because they have larger specific surface. As the coverage of fiber surface is related to the projected areas of the particles, then clearly one would expect smaller particles to have a more clogging effect (higher pressure drop). For liquid aerosol loading, experiments were conducted where a Bekaert stainless steel filter material was loaded with 3 micrometer di-ethyl sebacate at 0.2 m s^{-1}. From their results, the behavior of fibrous filters under liquid particle loading was largely different from that under solid particle loading. It was found that when loaded with solid aerosol, dendrites were formed, and when loaded with liquid aerosol, bridges were formed.

Hajra *et al.* (2003) studied the effects of temperature, humidity, and the addition of polymer nanofiber to coalescence performance of glass fiber filter media. Experiment was carried out at conditions commonly found in industry. Results indicated that temperature, humidity and fiber sizes affected the coalescence performance of the glass fiber filter media. The addition of polymer polyamide nanofiber to the glass fiber media significantly improved its collection performance. At higher temperatures, the glass fiber media had better coalescence filtration performance. For the effect of humidity, the glass fiber media performed better at a dewpoint of -15 °C compared with dewpoints of -10 and -20 °C which suggested that optimum performance may occur at an intermediate humidity value.

Letts *et al.* (2003) studied the filters such as glass fiber, polyester fiber and polyaramid fiber as they collected droplets and retained liquid. Results showed

that efficiency of the filter declined while the pressure drop increased. This indicated that filters drained more effectively and retained less liquid which may minimize efficiency losses and increase the pressure drop. Microscope was employed to examine the surface of the filter as it collected BEHS droplets. It was found that polyaramid fiber allowed collected fluid to spread more easily than glass or polyester fibers. It was suggested that the polyaramid fiber had higher surface energy than other fibers. Experiments were performed on polyaramid and glass fibers to investigate the effect of fiber material on wet filter performance. Using fiber with higher surface energy might decrease the pressure drop through wet filter and allowed liquid to spread and drain out of filter more effectively.

Contal *et al.* (2004) studied phenomena occurring during the clogging of fibrous filters by submicron liquid particles. They measured simultaneously the changes in the pressure drop and efficiency of filter media in relation to the generated aerosol mass per unit area. Results showed that at the beginning of filtration, the pressure drop and penetration increased because the droplets were deposited around the fibers and the beads then became bigger and joined together to form bridges at the intersections of the fibers. This then caused the less collection surface of the filters. Subsequently all interstices were bridged and these bridges combined to form a liquid film on the surface of the filter. This effect generated the increase of pressure drop and the decrease of the penetration. At the end of the clogging, the pressure drop and penetration no longer changed because liquid films were formed throughout the thickness of the filter. Furthermore, they studied effects of filtration velocity, filter properties (fiber diameter, packing density, wettability) and physicochemical characteristics of the liquid on the change in pressure drop. Effect of each parameter was studied by eliminating the effect of other factors. Results showed that the higher the filtration velocity, the higher the pressure drop evolution. Aerosol concentration had no influence on pressure drop evolutions of the filter. For the influence of the nature of the filter during clogging by DOP aerosol, the Whatman-type glass fiber medium had highest change in the pressure drop because this filter was composed of the fine fibers.

Frising *et al.* (2004) investigated clogging of fibrous filters by liquid aerosol particles. Experimental and modelling results described the pressure drop and penetration evolutions of a glass microfiber HEPA filter (D309 HEPA filter) using three filtration velocities: 5.8, 15.4 and 25 cm s^{-1}. Experimental results showed that the pressure drop increased as the velocity increased. Initially, the penetration increased identically for each filtration velocity until it reached maximum values. Then the penetration decreased and the pressure drop increased due to rearrangement of the liquid in the filter such as the forming of liquid bridges between fibers and at the fiber intersections. In mathematical modelling, the collection mechanisms were taken into account. Experimental values were then compared to their modelling counterparts for different filtration velocities. It was found the pressure drop evolution from modelling was close to that obtained from the experiment. However, the penetration values obtained from modeling are much higher than those obtained from the experiment. The penetration was lowest at the highest filtration velocity (v = 25 cm s^{-1}).

Vasudevan *et al.* (2004) designed an experimental setup to operate at conditions encountered in industrial applications. They studied the performance of filter media in coalescence filtration. Three types of filter media were prepared: (1) B-glass fibers and acrylic binder, CARBOSET 560, (2) E-glass fibers and acrylic binder, CARBOSET 560, and (3) a mixture of E and B glass fibers. Results indicated that the B-E-glass media performed significantly better than the media with the organic binders both in terms of collection efficiency and quality factor (QF) which is defined as $QF = -\ln(C_{out}/C_{in})/\Delta P$, where C_{out} is the downstream concentration of oil, C_{in} is the inlet concentration of oil and ΔP is the pressure drop across the filter media (Brown, 1993). The advantage of the B-E-glass media was its flexibility and its ability to maintain its hardness over longer periods of time after exposure to oil.

1.3 Research Objectives

Although there are some investigation of collection characteristics of liquids aerosol by fibrous filters, the knowledge is limited. In this research work, collection characteristics of mist aerosol by fibrous filter will be further explored. Initially, an appropriate experimental set-up will be designed and built. Its collection performance will then be investigated by varying various parameters. The objectives for this work are:

1. To investigate the collection characteristics of mist aerosol particles by fibrous filter at various basic operating parameters such as filtration velocity, number of fibrous filters and physicochemical properties of the liquids.
2. To investigate saturation characteristics of a medium-performance fibrous filter (glass fiber filter).

CHAPTER 2
THEORY

2.1 Filtration

Filtration is the most efficient method for the removal of solid and liquid aerosol particles. The rapid development of industrial processes such as surface lubrication, composite manufacture and machining operation has given rise to a need for highly efficient air quality control equipment. A variety of techniques is currently available for the removal of alien particles from air streams. They include electrostatic precipitators, venturi scrubbers, cyclones, settling chambers, etc. However, fibrous filtration is by far the most efficient means of removing contaminant aerosol particles from gas streams, particularly in the smaller size ranges. Devices such as electrostatic precipitators and venturi scrubbers, although approaching the removal efficiency of filters for particles in some size ranges, are far less efficient overall.

Filtration by fibrous filter is the most commonly used process to remove liquid aerosols. Fibrous filter captures aerosol particles on fibers within the filter depth through several mechanisms including diffusion, interception and inertia. Performance of fibrous filter is characterized by the proportion of liquid aerosol particles which get through the material and the pressure drop across the filter.

2.2 Types of Filters

There is a wide range of filters that could be used for the removal of particulate matters from air streams. These can be separated into two broad types, surface filters and depth filters. Surface filters collect particulate contaminants on the upstream face of the filter, and depth filters collect particles throughout the entire filter. The principal types of filters used for aerosol collection may be classified as fibrous filters, porous-membrane filters, straight-through pore membrane filters, and

granular-bed filters. The most important types are fibrous and porous membrane filters. The salient characteristics of each type of filters are also summarized in Table 2.1 (Baron and Willeke, 2005).

Table 2.1 Salient Characteristics of the Various Types of Filters Commonly Utilized for Aerosol Measurement (Baron and Willeke, 2005)

Filter Type	Characteristics
Fibrous filters	Mat/weave of fibers with diameters of 0.1-100 μm Cellulose or wood (paper), glass, quartz, and polymer fiber filters are available Porosities of 60 - 99%, thickness of 0.15 – 0.5 mm Particle collection is throughout the depth of the filter from interception, impaction, and diffusion onto fibers High particle collection efficiencies require low air velocities Pressure drops are the lowest among all filters under comparable conditions
Porous-membrane filters	Microporous membranes with tortuous pores throughout the structure Polymer, sintered metal, and ceramic microporous filters available Pore sizes (determined from liquid filtration) in the range 0.02 – 10 μm Porosities of < 85% and thickness of 0.05 – 0.2 mm Particle collection through attachment to microstructure elements High collection efficiencies, but highest pressure drop among all filters

Filter Type	Characteristics
Straight-through pore filters	Thin polycarbonate films (10 μm) with cylindrical pores perpendicular to film surface, with diameters in the range 0.1 – 8 μm Porosities are low, in the range of 5 – 10% Particle collection through impaction and interception near the pores and diffusion to tube walls of pores Collection efficiencies are intermediate between fibrous and microporous membrane Pressure drops are significantly higher than fibrous filters and comparable with or higher than microporous membrane filters for equivalent collection efficiency
Granular-bed filters	For special sampling, granules of specially chemicals, sugar, naphthalene, sand, metal, and glass beads are used Samples are recovered by washing or volatilization Granular bead size range from 200 μm to a few millimeters Filtration is achieved by impaction, interception, diffusion, and gravitation Filter porosities of 40 – 60% for stationary beds Low collection efficiency due to large granule size To enhance diffusion, low flow is used; bed depth is increased, or smaller granules are used
Porous-foam filters	Porosities of < 97% Pore diameters from 10 to 50 μm are common Collection efficiencies are low

2.2.1 Fibrous Filters

Fibrous filters, the type to be discussed in most detail here, consist of a mat of individual fibers (fiber diameter < 100 μm) arranged so that most are perpendicular to the direction of air flow as shown in Fig. 2.1 (Hinds, 1999). In general, filter porosity is relatively high, ranging from about 0.6 to 0.999. Porosities of less than 0.6 are not typically found in fibrous filters because of the difficulties in effectively compressing the component fibers into a smaller thin layer. The most common types of fiber are cellulose, glass, quartz, and plastic fibers. Sometimes, mixed fibers of cellulose, asbestos, and glass are also used as filters for certain low-cost qualitative sampling applications. Particles are removed by a fibrous filter when they collide and attach to the surface of the fibers.

Fibrous filters are generally depth filters for the initial portion of their operation. However as the filtration continues and the mass of collected particles increases, the filtration regime changes to surface filtration and besides influent particles are captured by the "cake" of collected particles on the surface of the filter, rather than the fibers themselves. This switch from depth to surface filtration is accompanied by an increase in collection efficiency of the filter, however at the cost of increase of the pressure drop across the filter. Finally, while the filter begins to clog, the pressure drop will increase exponentially as does the energy requirement to force air through the filter.

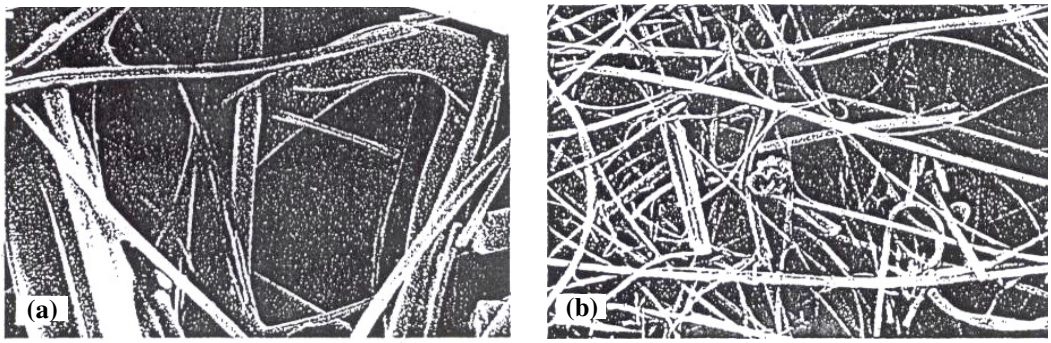

Figure 2.1 Scanning electron microscope photograph of a high efficiency glass fiber filter. Magnification (a) 4150×, (b) 800×. (Hinds, 1999)

Cellulose fiber (wood or paper fibers) filters were once used very widely for general-purpose air sampling. Whatman (*WHA*) filters are one of the most representative filters in this type. These filters are inexpensive, come in various sizes, and have good mechanical strength and low pressure drop characteristics. Some of the limitations of cellulose fiber filters are their moisture sensitivity and relatively low filtration efficiency of submicrometer particles.

Glass fiber filters typically have a higher pressure drop than cellulose fiber filters and often provide filtration efficiencies of greater than 99% for particles > 0.3 μm. These filters are more expensive than cellulose fiber filters. Glass fiber filters are less affected by moisture than are cellulose fiber filters. Then they are extensively used as the standard filter media for high-volume air sampling.

Quartz fiber filters are commonly used in high-volume air sampling applications including subsequent chemical analyzes such as atomic absorption, ion chromatography and carbon analysis due to their low trace contamination levels as well as to their relative inertness and ability to be baked at high temperature to eliminate trace organic contaminants.

Polystyrene fiber filters have been used for air sampling purposes to a limited extent. These filters have less mechanical strength than cellulose fiber filters. However, their filtration efficiency is comparable with that of glass fiber filters. Other plastic materials used in filters including polyvinyl chloride and Dacron®. For special applications involving high temperatures and corrosive environments, the filters made of stainless steel fibers have also been recently introduced.

2.2.2 Porous-Membrane Filters

Fig. 2.2 shows porous membrane filters which have a structure different from that of fibrous filters, with less porosity (50 to 90%) (Hinds, 1999). The air flowing through the filter follows an irregular path through the complex pore structure. Particles are lost from the air stream as they deposit on the structural elements that form the pores. A variety of porous membrane filters made of cellulose esters, polyvinyl chloride, sintered metals and Teflon™ are commercially available. Other types of porous membrane filters are gels formed from a colloidal solution and

have a very complicated and uniform microstructure providing a tortuous or irregular gas flow path. Frequently, the complex filter structure consists of a series of layers formed by different processes, depending on the manufacturing technique. Generally, the resistance to airflow (or pressure drop) and the particle collection efficiency are very high, even for particles significantly smaller than the characteristic pore size. Aerosol particles are captured by the surfaces provided by the filter structure, principally by Brownian motion (diffusion) and inertial impaction mechanisms.

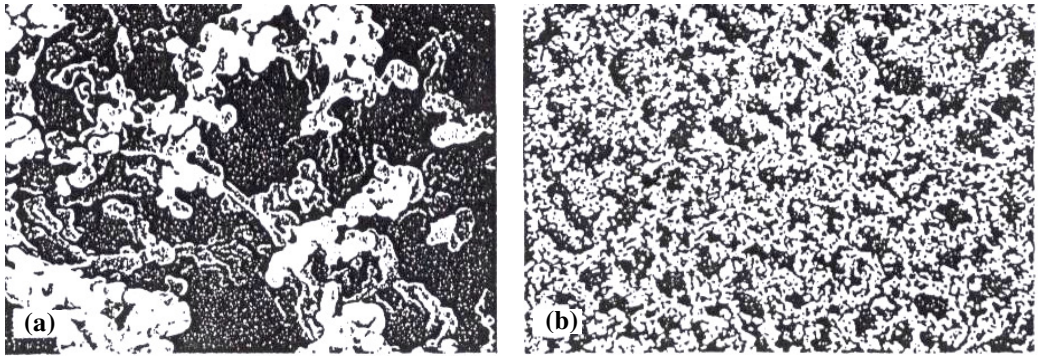

Figure 2.2 Scanning electron microscope photograph of a 0.8 μm pore size cellulose ester porous membrane filter. Magnification (a) 4150×, (b) 800×. (Hinds, 1999)

2.3 Filtration Theory

A great portion of the fundamentals of filtration and filtration theory has been described and developed by Walsh et al. (1996), Hinds (1999), Raynor and Leith (2000), Contal et al. (2004), Frising et al. (2004) and Baron and Willeke (2005).

In this section, filtration theory for fibrous filters is discussed. Filtration mechanisms and some useful predictive equations for collection efficiency of filter and the pressure drop across a filter are introduced for practical application.

2.3.1 Single-Fiber Efficiency

The most commonly used model for collection efficiency calculation is the single-fiber efficiency model. This model views the void space inside the filter as so great compared to the volume of fiber. Then only the interaction between particles

and a single fiber needs to be considered. From the single-fiber efficiency, the total efficiency can be calculated.

The beginning point in characterizing fiber filtration is to consider the capture of particles by a single fiber. The single-fiber efficiency, η, is then defined as the ratio of the number of particles striking the fiber to the number that would strike if the streamlines were not diverted around the fiber (Baron and Willeke, 2005). If a fiber of radius R_f removes all the particles contained in a layer of thickness Y as shown in Fig. 2.3, the single fiber efficiency, η, is defined as Y / R_f.

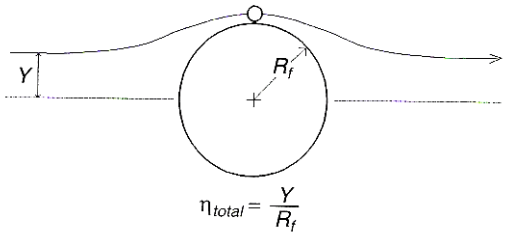

Figure 2.3 Definition of the single-fiber efficiency (Baron and Willeke, 2005).

The total efficiency, E, of a filter composed of many fibers in a mat can be related to the single-fiber efficiency as follows (Baron and Willeke, 2005):

$$E = 1 - \exp\left[\frac{-4\eta\alpha_f Z}{\pi d_f (1-\alpha_f)}\right] \tag{2.1}$$

where η is the single-fiber efficiency, α_f is the solidity or packing density of the filter (1 - porosity), Z is the filter thickness, and d_f is the fiber diameter. Often, Eq. (2.1) is used to calculate the single-fiber efficiency from the total filter efficiency, E, which can be measured experimentally.

2.3.2 Filtration Mechanisms

While air penetrates a filter, the trajectories of particles deviate from the streamlines due to several mechanisms. As a result, particles may collide with the surface of fiber and deposit on it. The important mechanisms causing aerosol particle deposition are inertial impaction, interception, diffusion and gravitational settling. The single-fiber efficiency, η, can then be assumed in the first approximation to be composed of the arithmetic sum of the individual efficiencies from inertial impaction (η_{imp}), interception ($\eta_{\text{int}er}$), diffusion (η_{diff}) and gravitational settling (η_{grav}) mechanisms.

Inertial Impaction. The gas streamlines around the fiber are curved. Particles with a finite mass and moving with the flow may not follow the gas streamlines exactly due to their inertia. If the curvature of a gas streamline is sufficiently large and the mass of a particle is sufficiently high, the particle may deviate far enough from the gas streamline to collide with the media surface as shown in Fig. 2.4 (Hinds, 1999). The importance of this inertial impaction mechanism increases with increasing particle size and increasing flow velocity, as shown in Fig. 2.7. Therefore, the effect of increasing flow velocity on the initial impaction of particles is contrary to that for the diffusive deposition. The inertial impaction mechanism can be studied by the use of the dimensionless Stokes number, Stk, defined by

$$Stk = \frac{\rho d_p^2 C_c u'}{18 \mu_g d_f} \tag{2.2}$$

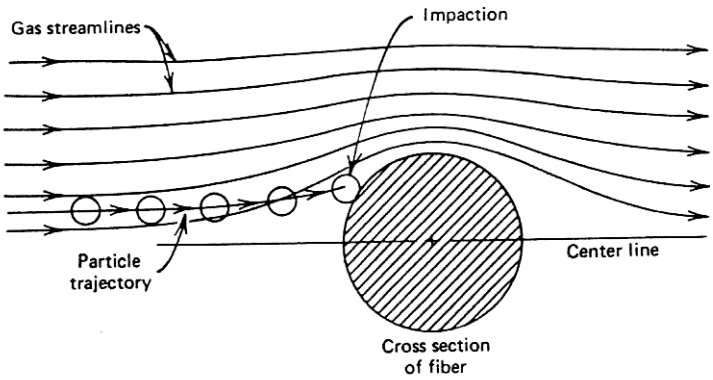

Figure 2.4 Single-fiber collection of a particle by inertial impaction.

where ρ is the liquid density, μ_g is the gas viscosity, u' is the interstitial gas velocity, d_f is the fiber diameter and C_c is the Cunningham correction factor defined as

$$C_c = 1 + \frac{2.52\lambda}{d_p} \qquad \text{for } d_p > 0.1\ \mu m \tag{2.3}$$

Here d_p is the droplet diameter and λ is the gas molecular mean free path.

The Stokes number is the basic parameter describing the inertial impaction mechanism for particle collection in a filter. A large Stokes number implies a higher probability of collection by impaction.

The single-fiber efficiency by inertial impaction, η_{imp}, was proposed by Stechkina et al. (1969):

$$\eta_{imp} = \frac{1}{(2Ku)^2}\left[\left(29.6 - 28\alpha_f^{0.62}\right)N_R^2 - 27.5N_R^{2.8}\right]Stk \tag{2.4}$$

for N_R smaller than 0.4. If N_R is greater than 0.4, a value of N_R = 0.4 can be used for the calculation. Eq. (2.4) has been used extensively for calculating the contribution by the inertial impaction mechanism.

Interception. Even the trajectory of a particle does not depart from the gas streamline, a particle may still be captured if the streamline brings the particle center to within one particle radius of the surface of a fiber, as shown in Fig. 2.5 (Hinds, 1999). One would expect the interception to be relatively independent of flow velocity for a given fiber, and this characteristic can be contrasted to the flow-dependent characteristics of Brownian motion and inertial impaction. The dimensionless parameter describing the interception effect is the interception parameter, N_R, defined as the ratio of the droplet diameter to the fiber diameter:

$$N_R = \frac{d_p}{d_f} \tag{2.5}$$

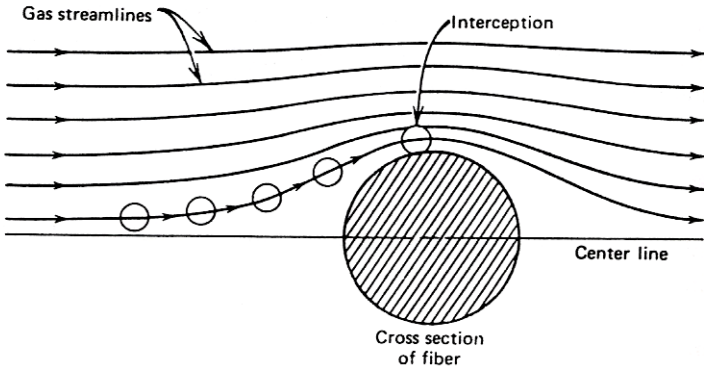

Figure 2.5 Single-fiber collection of a particle by interception.

The single-fiber efficiency by interception, $\eta_{\text{int}\,er}$, is given by Raynor and Leith (2000) as

$$\eta_{\text{int}\,er} = \frac{1+N_R}{Ku}\left[2\ln(1+N_R)-1+\alpha_f+\left(\frac{1}{1+N_R}\right)^2\left(1-\frac{\alpha_f}{2}\right)-\frac{\alpha_f}{2}(1+N_R)^2\right] \tag{2.6}$$

Although Eq. (2.6) is a complete expression for the interception efficiency, the form of the equation is somewhat long, and it can be shown to be approximated into the following simpler form:

$$\eta_{\text{int}\,er} = \frac{1-\alpha_f}{Ku}\frac{N_R^2}{(1+N_R)} \tag{2.7}$$

Enhanced collection of particles by a fiber can also occur from the interception of diffusing particles as was proposed by Stechkina et al. (1969). The magnitude of this additional efficiency term is of the same order as that of the errors involved in the approximation method used in the analysis. Spielman and Goren (1968) also indicated that the term is not theoretically consistent and is, consequently, not introduced here.

Diffusion. Under normal conditions, the diffusion or Brownian motion of small particles generally does not follow the streamlines but continuously diffuse away from them. Once a particle is captured on a surface, it would adhere to it due to the van der waals force. The trajectory of one such particle is shown in Fig. 2.6 (Hinds, 1999).

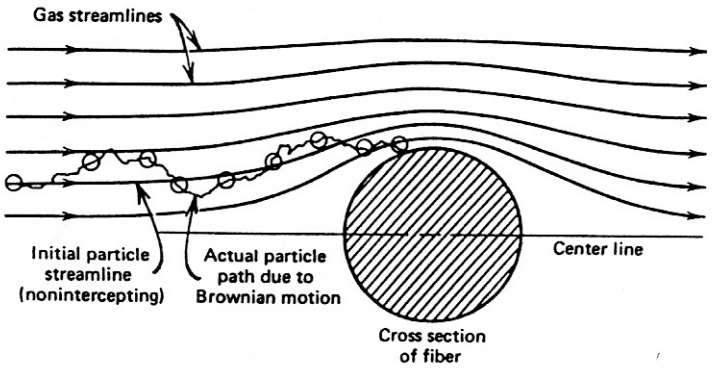

Figure 2.6 Single-fiber collection of a particle by diffusion.

In general, Brownian motion increases with decreasing particle size; the diffusive deposition of particles is increased when the particle size is reduced. This phenomenon is illustrated in Fig. 2.7 (Baron and Willeke, 2005). Similarly at low air velocities, particles can spend more time in the vicinity of the fiber surfaces, thus enhancing diffusional collection. From the convective diffusion equation describing this process, a dimensionless parameter called the Peclet number, Pe , is defined as

$$Pe = \frac{d_c U}{D} \tag{2.8}$$

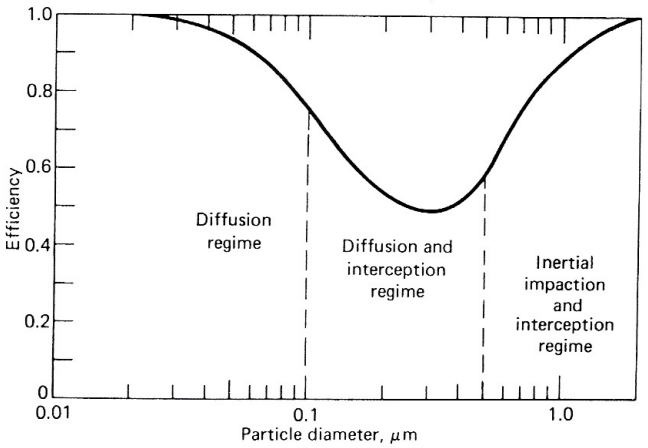

Figure 2.7 Filter collection efficiency versus particle size illustrating the different filtration regimes.

where d_c is the characteristic length of collecting media, U is the average air velocity inside the filter medium, and D is the particle diffusion coefficient. For pure molecular diffusion, D is expressed as

$$D = \frac{kTC_c}{3\pi\mu_g d_p} \tag{2.9}$$

where k is the Boltzmann constant, T is the absolute temperature, μ_g is the air viscosity, d_p is the particle diameter, and C_c is the Cunningham correction factor. From the above discussion, particle collection by diffusion is expected to decrease with increasing Peclet number. The Cunningham correction factor can be written as

$$C_c = 1 + 2.492\frac{\lambda}{d_p} + 0.84\frac{\lambda}{d_p}\exp\left(-0.435\frac{d_p}{\lambda}\right) \tag{2.10}$$

where λ is the mean free path of the gas molecules (Hinds, 1999).

The single-fiber efficiency by diffusion, η_{diff}, was developed by Lee and Liu (1982):

$$\eta_{diff} = 2.6\left(\frac{1-\alpha_f}{Ku}\right)^{1/3} Pe^{-2/3} \quad (2.11)$$

Where α_f is the packing density of the filter. Ku is the Kuwabara hydrodynamic factor, a dimensionless factor that compensates for the effect of distortion of the flow field around the fiber because of its proximity to other fibers defined as

$$Ku = -\frac{1}{2}\ln\alpha_f - \frac{3}{4} + \alpha_f - \frac{\alpha_f^2}{4} \quad (2.12)$$

Gravitational Settling. Particles will settle with a finite air velocity in a gravitational force field. When the settling velocity is sufficiently large, the particles may deviate from the gas streamline. Under downward filtration conditions, this would cause an increased collection due to gravity. When flow is upward, this mechanism causes particles to move away from the collector, resulting in a negative contribution to filtration. This mechanism is important only for particles larger than at least a few micrometers in diameter and at low air velocity. The dimensionless parameter governing the gravitational sedimentation mechanism is

$$Gr = \frac{V_g}{U} = \frac{\rho_g d_p^2 C_c g}{18\mu_g U} \quad (2.13)$$

where U is the flow velocity, V_g is the settling velocity of the particle, ρ_g is the density of gas, d_p is the particle diameter, C_c is the Cunningham correction factor, g is the acceleration of gravity and μ_g is the gas viscosity.

The single-fiber filtration efficiency due to gravity, η_{grav}, can be approximated as (Davies, 1973):

$$\eta_{grav} = \frac{Gr}{1+Gr} \quad (2.14)$$

In filtration theories, it is common to consider that the individual filtration mechanisms discussed above are independent of each other and additive. Hence, η, the overall single-fiber collection efficiency in Eq. (2.1), can be written as

the sum of individual single-filter efficiencies contributed by the different mechanisms. This approximation has been found to serve adequately in predicting the total collection efficiencies of fibrous filters [Eq. (2.1)], owing to the different ranges in particle sizes and face velocities in which the different filtration mechanisms predominate, as illustrated in Fig. 2.7.

2.3.3 Pressure Drop

In a fibrous filter, pressure drop is the resistance to airflow across a filter and is caused by the combined effect of each filter resisting the flow of air past through it. A consideration of the pressure drop across filter media is essential in choosing a specific filter type in a particular application. The pressure drop is easily measurable and can be used as a check on the flow fields on which collection mechanisms are based. More importantly, the measurement of the pressure drop across filter media plays a central role in the practical estimation of collection efficiency. Ideality, filters that exhibit a high collection efficiency at a low pressure drop are the most desirable ones.

Davies (1952) gives the pressure drop across a dry fibrous filter, ΔP_0, as

$$\Delta P_0 = \frac{u\mu_g Z}{d_f^2}\left[64\alpha_f^{1.5}(1+56\alpha_f^3)\right] \tag{2.15}$$

where u is the gas velocity at filter face, μ_g is the gas viscosity, Z is the filter thickness, α_f is the filter solidity, and d_f is the fiber diameter. This shows that the pressure drop is directly proportional to Z and inversely proportional to d_f^2. It is also directly proportional to the gas velocity at the filter face, as expected for laminar flow inside the filter.

The fiber diameter, $d_{f\,Davies}$, can be calculate from (Penicot et al. 1999)

$$d_{f\ Davies} = 2\sqrt{\frac{16\mu_g Z\alpha_f^{3/2}(1+56\alpha_f^3)}{K}} \quad (2.16)$$

where K is the slope of straight line between ΔP and u.

The change in the pressure drop of a fibrous filter when loaded with liquid aerosol is quite different from that obtained with solid aerosol as shown in Figs. 2.8 and 2.9. The pressure drop starts off at its lowest value to increase slowly in the first stage. In this stage the droplets are deposited mainly on the fiber surface where they only interfere marginally with the flow, so the pressure drop increases slowly (Walsh et al. 1996) as shown in Fig. 2.9. Liew and Conder (1985) explained the increase of pressure drop is quickly in the second and the third stages due to the formation of liquid bridges, coalesces and films between fibers and at fiber intersections. This result was confirmed by Contal et al. (2004) as shown in Fig. 2.10.

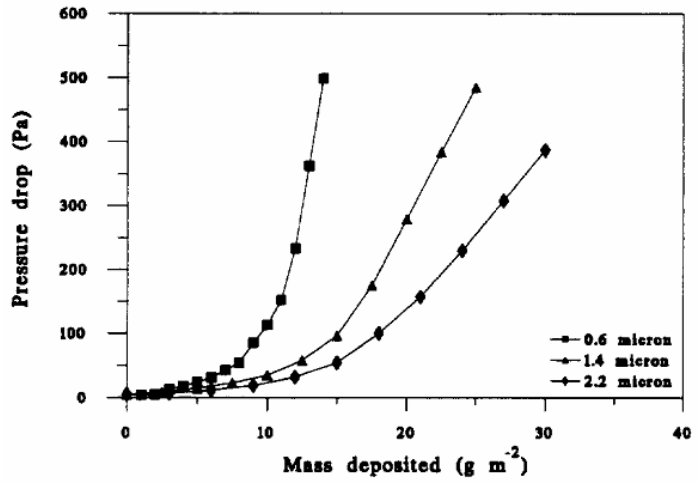

Figure 2.8 Pressure drop across fibrous filter samples (α = 12 %) loaded at 0.10 m s^{-1} with 0.6, 1.4 and 2.2 μm particles (Walsh et al. 1996).

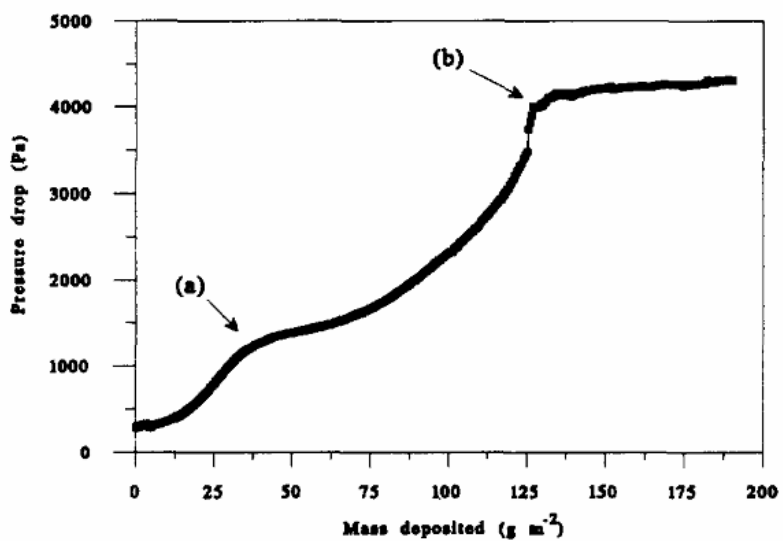

Figure 2.9 Pressure drop across a fibrous filter samples loaded with 3 µm Di-Ethyl Sebacate at 0.2 m s^{-1} (Walsh et al. 1996).

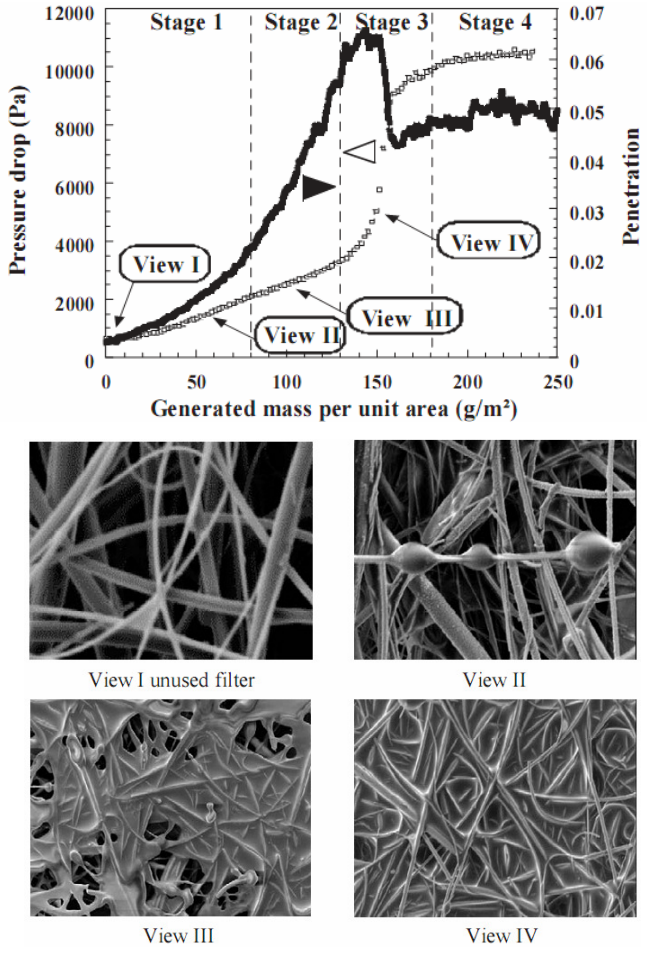

Figure 2.10 Change in the deposit during clogging by liquid aerosol (Contal et al. 2004).

Even though the pressure drop has been quite extensively studied experimentally, very few modelling studied investigating the evolution of the pressure drop across a fibrous filter during a filtration have been published to date.

Davies (1973) presents a modification of his own pressure drop model

$$\Delta P = \mu Z U_0 \frac{64\alpha_f^{1.5}(1+56\alpha_f^3)}{d_{f\,Davies\,wet}^2} \tag{2.17}$$

where the wet fiber diameter $d_{f\,Davies\,wet}$ is defined as

$$d_{f\,Davies\,wet} = d_{f\,Davies}\sqrt{1+\frac{m_{liq}}{\Omega\rho_{liq}Z\alpha_f}} \tag{2.18}$$

where m_{liq} is the collected liquid mass, Ω is filtration surface, ρ_{liq} is liquid density and α_f is clean filter packing density.

Fig. 2.11 represents pressure drop evolution for a D309 HEPA filter throughout the filtration experiment for three different velocities with a challenge aerosol of DEHS.

In the first stage, the liquid is only deposited on the surface of a fiber. No drainage or the migration of liquid from one layer to the next is observed. The pressure drop is calculated by an adapted version of Davies' equation (1973):

$$\Delta P = 64\mu u\, dZ \frac{(\alpha_f+\alpha_l)(\alpha_f+\alpha_l)^{0.5}}{d_{f\,Davies\,wet}^2} \times \left[1+16(\alpha_f+\alpha_l)^{2.5}\right] \tag{2.19}$$

where μ is liquid viscosity, u is filtration velocity, $d_{f\,Davies\,wet}$ is the mean wet fiber Davies diameter, dZ is filter layer thickness, α_f is clean filter packing density, and α_l is liquid packing density defined as

$$\alpha_l = \frac{Volume\ of\ \ collected\ \ particles}{Volume\ \ \ layer} = \frac{m/\rho}{\pi r^2 Z} \tag{2.20}$$

where m is the collected liquid mass and ρ is liquid density.

In the second stage, the liquid bridges between fibers and liquid films at intersections of fibers are formed. Some of the collected liquid particles migrate to the next layer downstream. In this stage, the collection surface decreases due to the formation of liquid bridges and films. The flow will be largely disturbed by the liquid bridges and films. So the pressure drop expression has to take the modified filtration velocity into account:

$$\Delta P = 64\mu dZ \frac{\left(\alpha_f + \alpha_{tube}\right)\left(\alpha_f + \alpha_l\right)^{0.5}}{d_{f\,Davies\,wet}^2} \times \left[1 + 16\left(\alpha_f + \alpha_l\right)^{2.5}\right] \frac{u}{1 - \alpha_l + \alpha_{tube}} \qquad (2.21)$$

where α_{tube} is liquid packing density at the end of the first stage.

In the third stage, all the collected liquid particles are supposed to migrate to the downstream layer due to capillary (wetting) or flow (migration) forces. The pressure drop is constant in this stage:

$$\Delta P = 64\mu dZ \frac{\left(\alpha_f + \alpha_{tube}\right)\left(\alpha_f + \alpha_{film}\right)^{0.5}}{d_{f\,Davies\,wet}^2} \times \left[1 + 16\left(\alpha_f + \alpha_{film}\right)^{2.5}\right] \frac{u}{1 - \alpha_{film} + \alpha_{tube}} \qquad (2.22)$$

where α_{film} is maximum liquid packing density.

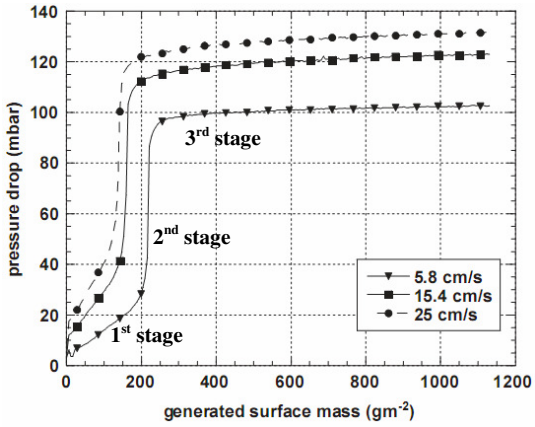

Figure 2.11 Pressure drop evolution for a D309 HEPA filter throughout the filtration experiment for three different velocities with a challenge aerosol of DEHS (Frising et al. 2005).

CHAPTER 3
EXPERIMENT

In the present work, a Laskin nozzle and a mist aerosol generator were built, and an experimental set-up was designed to investigate evolutions of collection efficiency and pressure drop of a medium-performance fibrous filter for various conditions. Basic operating parameters include filtration velocity, number of filter sheets and types of mist aerosols. Characteristics of filter clogging by mist aerosols were studied by visualization of deposits on the surface of the filter.

3.1 Size Distribution and Stability of Generated Aerosol

Mist aerosol used in this study was generated from the Laskin nozzle (see detail in Appendix A). Size distribution and concentration of generated aerosols were determined to study their characteristics and stability. The liquids used for aerosol generation were propylene glycol and palm oil. Their physical properties are summarized in Table 3.1. The surface tension was determined at 25°C using a tensiometer (CSC, DuNouy) and the viscosity was measured at 29.5°C using a rotational viscometer (Brookfield, DV-□+). The experimental setup used for determination of aerosol size distribution and concentration is shown in Fig. 3.1 and 3.2. Compressed air at a pressure of 1.4 bar was used to generate the mist aerosol. Moisture in the compressed air was removed by a diffusion dryer, an annular cylinder in which the space is filled with silica gel. It was constructed from a 65-mm-diameter and 290-mm-long PVC. After passing through the HEPA filter, the clean air entered the Laskin nozzle at the flow rate of 3 L min^{-1}, measured and controlled by an orifice meter and a needle valve, respectively. The mist aerosol generated from the Laskin nozzle was diluted by mixing with clean air passing through an absolute filter (Cambridge Filter, 1GC-50-2-MCL). Photograph of the Laskin nozzle and an absolute filter are shown in Fig. 3.3 (a) and (b), respectively. To provide sufficient mixing between clean air and aerosol particles, a 40-mm-diameter and 80-mm-long

nozzle and a 54-mm-diameter and 485-mm-long clear acrylic tube were used. The mixture of air and aerosol particles flowed into the system by means of a vacuum pump.

Table 3.1 Physical properties of the liquids used for aerosol generation

Aerosol	Propylene glycol	Palm oil
[a] Viscosity (cP)	64.6	94.6
[b] Surface tension (dynes/cm)	47.6	42.2
[c] Density (g/cm^3)	1.034	0.914

[a]T = 29.5°C; 100 RPM

[b]T = 25°C

[c]T = 30°C

An 8-stage Andersen sampler (Dylec, AN 200) with the cut sizes of 11.0, 7.0, 4.7, 3.3, 2.1, 1.1, 0.65 and 0.43 micron was used to determine the aerosol concentration and the size distribution of the generated aerosol. Aerosol particles were collected on HEPA filters (Cambridge Filter) cut into 80-mm-diameter circular sheets and placed on the impaction plates. Sampling flow rate measured by a rotameter (Cole Parmer, N044-40) was 28.3 L min^{-1}. The HEPA filters were treated in a desiccator at room temperature (25°C) and 50-60 % relative humidity for at least 24 hours and then weighed using a five-digit-readability analytical balance (Sartorius, CP225D) before being placed in the Andersen Sampler.

Liquid aerosol particles were sampled for 10 minutes and HEPA filters were weighed again. After each sampling, the filters were replaced and the experiment was carried out in a repeated manner for 5 hours. There were 6 sets of sample in total:

Set 1: After aerosol was generated for 60 minutes.

Set 2: After aerosol was generated for 90 minutes.

Set 3: After aerosol was generated for 120 minutes.

Set 4: After aerosol was generated for 180 minutes.

Set 5: After aerosol was generated for 240 minutes.

Set 6: After aerosol was generated for 300 minutes.

To determine the size distribution of generated liquid aerosol the normalized mass fraction, $f/\Delta d$, was plotted as a function of the average aerodynamic diameter, d_{ave} [μm]. Here f is the mass fraction and Δd is the particle size interval for each stage of the Andersen sampler. Aerosol concentration (C) can be calculated from

$$C = \frac{M}{V} \tag{3.1}$$

where M is the total collected mass and V is the sampling volume determined from

$$V = Q\,t \tag{3.2}$$

Here Q is the flow rate and t is the sampling time.

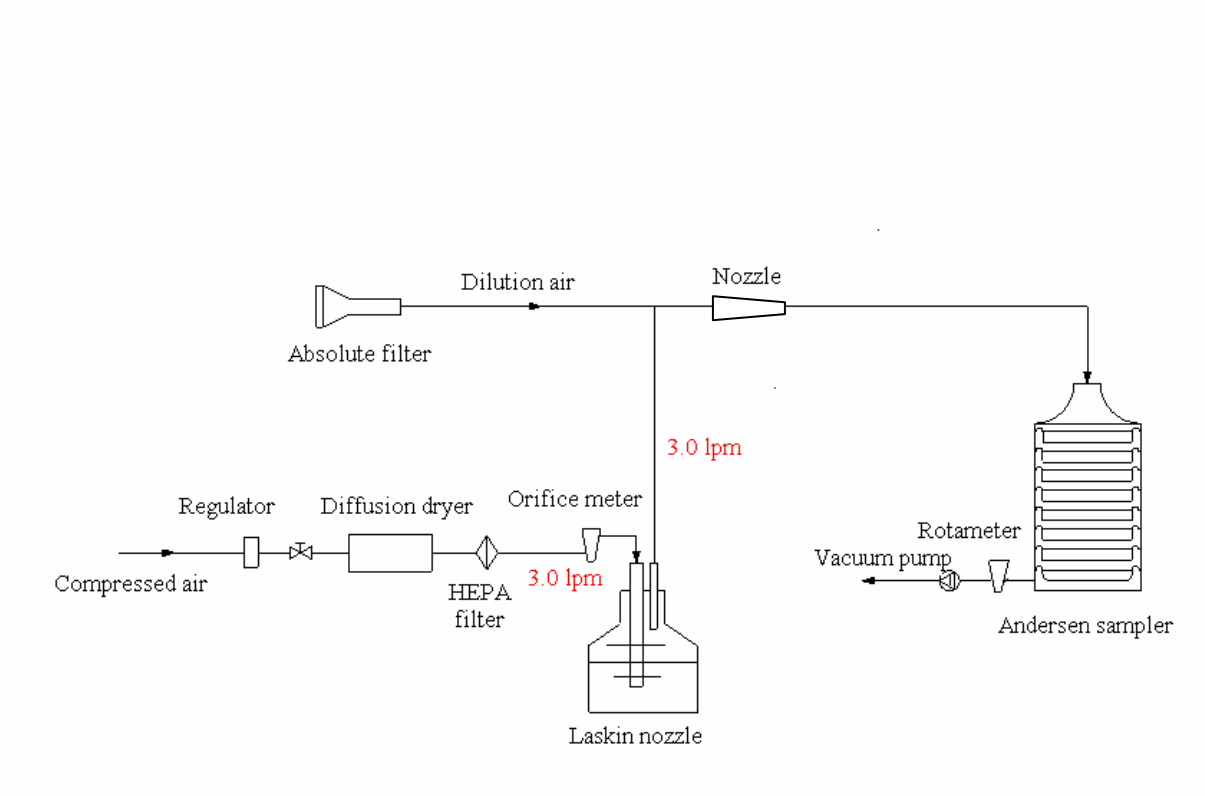

Figure 3.1 The schematic representation of the experimental set-up for examining size distribution and stability of generated aerosol.

Figure 3.2 Photograph of the experimental set-up for examining size distribution and stability of generated aerosol.

(a)

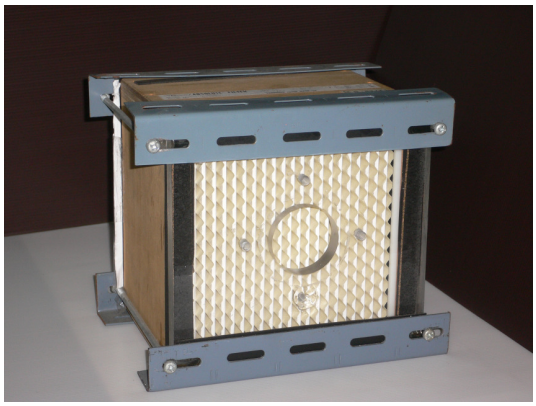

(b)

Figure 3.3 Photograph of (a) the Laskin nozzle and (b) an absolute filter.

3.2 Performance of Virgin Filter

Performance of a single virgin filter was evaluated by determining filtration efficiency (or penetration) and pressure drop.

Liquid used for aerosol generation is propylene glycol. Compressed air at a pressure of 1.4 bar was used to generate the mist aerosol after moisture was removed by the diffusion dryer. Partial liquid aerosol from the Laskin nozzle was removed by the use of a cotton box before dilution with clean air passing through the absolute filter (Cambridge Filter, 1GC-50-2-MCL). The mist aerosol particles were then introduced to the test filter using a vacuum pump (Gast, 0523-V4-G21DX).

Flow rate was measured and controlled by a rotameter (Cole Parmer, N044-40). The HEPA filter was used to prevent the re-entrained mist aerosol particles from passing through the rotameter during the experiment. The test filter is a medium-performance glass fiber filter in which the properties are given in Table 3.2.

Table 3.2 Properties of the test filter

Test filter	Thickness, L [mm]	Fiber diameter, d_f [μm]	Packing density, α [-]
Medium performance glass fiber filter	0.56	3.65	0.061

The schematic representation of the experimental set-up for measuring the efficiency of a virgin filter is shown in Figure 3.4, and its photograph is shown in Figure 3.5. Flow rates introduced through the Laskin nozzle and the test filter were 3.0 and 0.2 L min^{-1}, respectively. Excessive liquid particles were trapped in a buffer chamber at a flow rate of 2.8 L min^{-1} by the use of a vacuum pump. The flow rate was controlled by adjusting the needle valve and measured by an orifice meter and the corresponding U-tube manometer. A HEPA filter was used to prevent the mist aerosol particles from passing through the orifice meter.

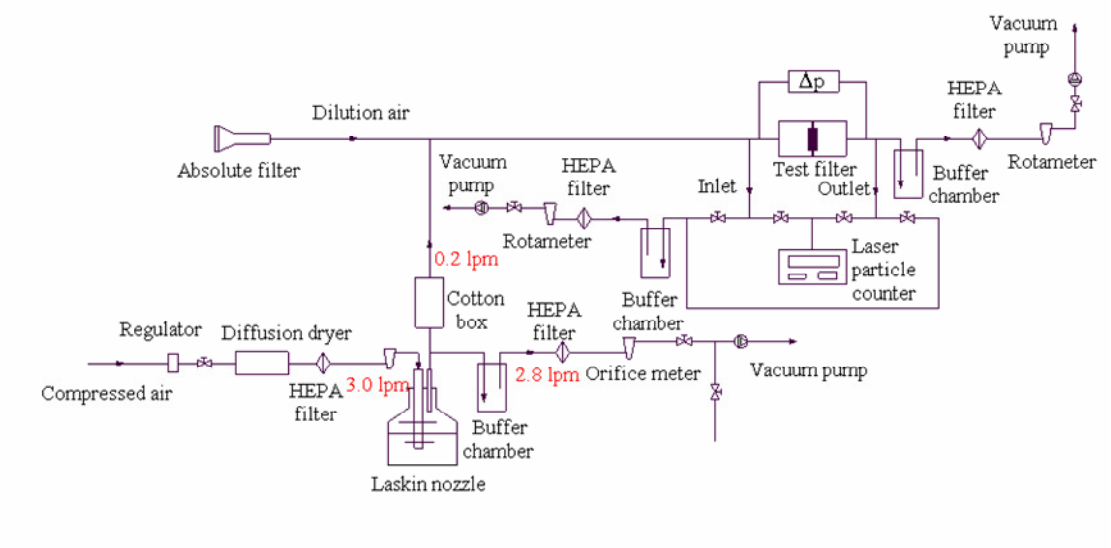

Figure 3.4 The schematic representation of the experimental set-up for measuring the efficiency of a virgin filter.

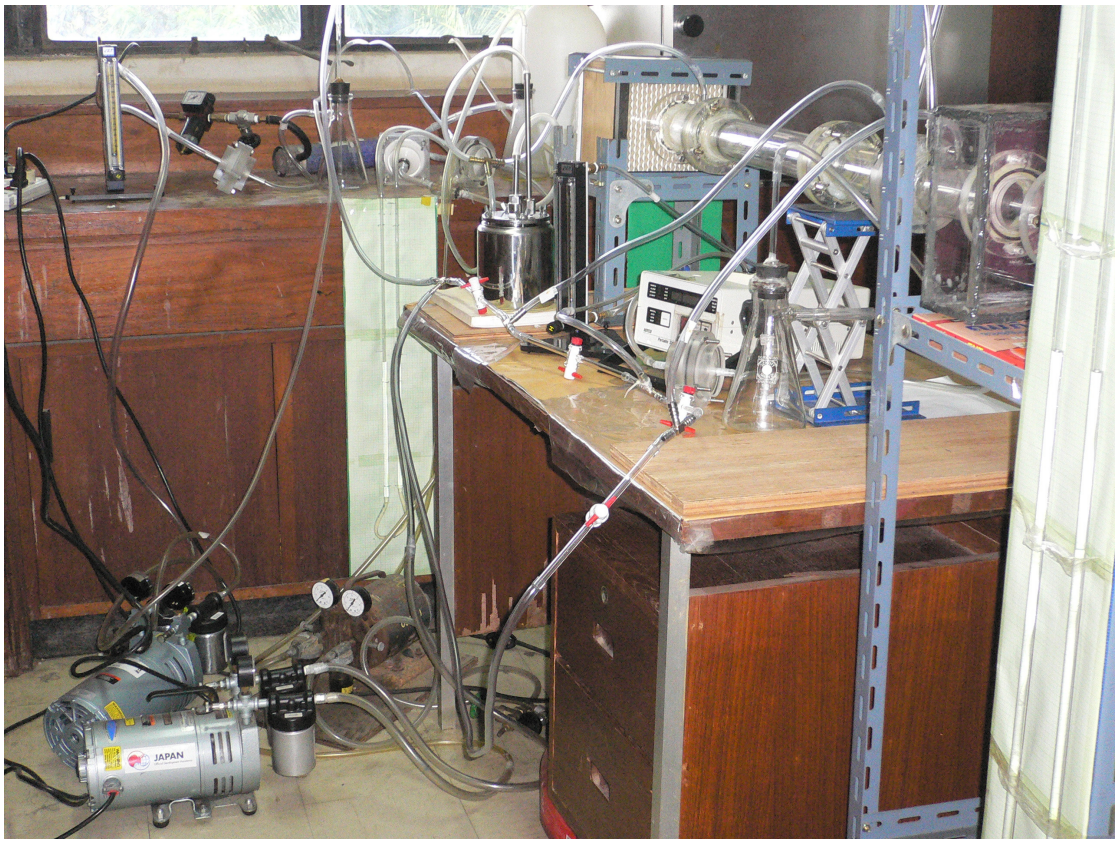

Figure 3.5 Photograph of the experimental set-up for measuring the efficiency of a virgin filter.

The test filters (glass fiber filters) were treated in the desiccator using silica gel at room temperature (25°C) and 50-60 % relative humidity for at least 24 hours. They were then weighed using the five-digit readability analytical balance (Sartorius, CP225D). The test filter was first weighed and then placed in the filter holder and the pressure drop was measured at different filtration velocities. The photograph of the filter holder was shown in Fig. 3.6. Filter loading was monitored by measuring pressure drop. After 30 minutes, particle concentrations of the liquid aerosol were sampled upstream and downstream of the filter simultaneously using a laser particle counter (Royco, Portable 330B). The weight of the collected liquid particles on the filter was measured using the identical analytical balance.

The filtration velocities were 5, 7, 10, 14, 21 and 28 cm s^{-1}. A rotameter with a control valve (Cole Parmer, N044-40) was used to adjust and monitor the flow rate.

To evaluate the performance of a single virgin filter, filtration efficiency (or penetration) and pressure drop were measured. The efficiency (E) can be calculated from

$$E = 1 - \frac{N_{outlet}}{N_{inlet}} \tag{3.3}$$

where N_{inlet} and N_{outlet} are number concentrations of particles at the upstream and downstream of the filter. The penetration (P) can then be calculated from

$$P = 1 - E \tag{3.4}$$

The pressure drop across the filter was measured by a U-tube manometer.

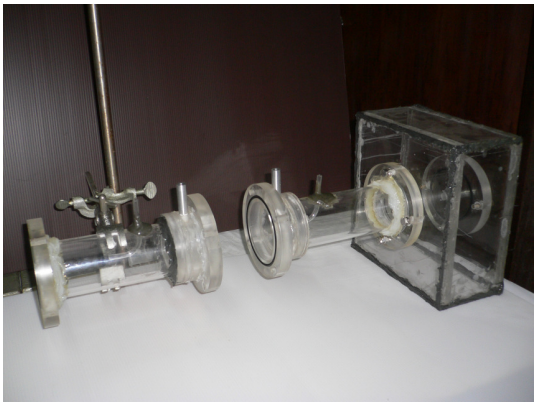

Figure 3.6 Photograph of the filter holder (the test filter).

3.3 Mist Aerosol Particles Collection Characteristics of a Fibrous Filter

To evaluate the collection characteristics of mist aerosol particles by the fibrous filter, the relationship between pressure drop and collected mass at various conditions including number of filter sheets, filtration velocity, and physical properties of liquids were investigated.

The schematical diagram of the experimental set-up for studying mist aerosol collection characteristics of a fibrous filter is shown in Fig. 3.7, and its photograph is shown in Fig. 3.8. Similar to Sec. 3.2, compressed air at a pressure of 1.4 bar was used to generate the mist aerosol. The flow rate of the compressed air introduced through the Laskin nozzle was 3.0 L min^{-1}. Only 1.0 L min^{-1} of generated aerosol was introduced to the system and diluted with the clean air. Excessive liquid aerosol was removed by passing through a buffer chamber using a vacuum pump at a flow rate of 2.0 L min^{-1}.

The glass fiber filters were treated in the same manner as done in the preceding section. The change in the pressure drop across a single filter and five filters were investigated at four different filtration velocities: 7, 14, 21 and 28 cm s^{-1}, by adjusting the flow rate using the rotameter.

3.3.1 Effect of the Filtration Velocity

A single-filter was first weighed and then placed in the filter holder. Then the pressure drop was measured at different filtration velocities. Filter loading was monitored by measuring the pressure drop. The weight of the collected liquid particles on the filter was measured every 10 minutes until the pressure drop reached three times of the initial value.

3.3.2 Effect of the Number of Filter Sheets

To highlight experimentally any possible redistribution of the liquid particles within the medium, five-filter experiment was conducted. Each filter was first weighed and then place in the filter holder in a series side by side. The weight of the collected liquid particles on each filter was measured at every 10 minutes until the pressure drop reached three times of the initial value.

3.3.3 Effect of the Physical Properties of the Aerosol Particles

The influence of the physical properties of the aerosol particles was investigated by using liquids with different physical properties. Propylene glycol and palm oil were chosen. Single-filter and five-filter experiments were conducted in the same manner as done in the Sec. 3.3.1 and 3.3.2**.** The pressure drop across the single filter and five filters were measured at a filtration velocity of 14 cm s^{-1}.

To better understand the phenomena occurring and to be able to explain the profile of the clogging, an optical microscope (OLYMPUS, BX60F5) was employed to examine the surface of the filter at different stages. The glass fiber filter was photographed after aerosol collection of 20, 40, 60 and 80 minutes for a single filter and of 20 and 50 minutes for five filters to compare the appearance of deposits within the filter when the filter was collected by propylene glycol and palm oil aerosol particles.

Pressure drop across a single filter and five filters were plotted as a function of the filtration time (t) and the collected aerosol mass (M).

The collected aerosol mass (M) during clogging of five filters were plotted as a function of particle loading Cvt [g/m^2] which describes the amount of liquid particle that flows to the filter per cross section. Here C is the initial particle concentration, v is the filtration velocity and t is the filtration time.

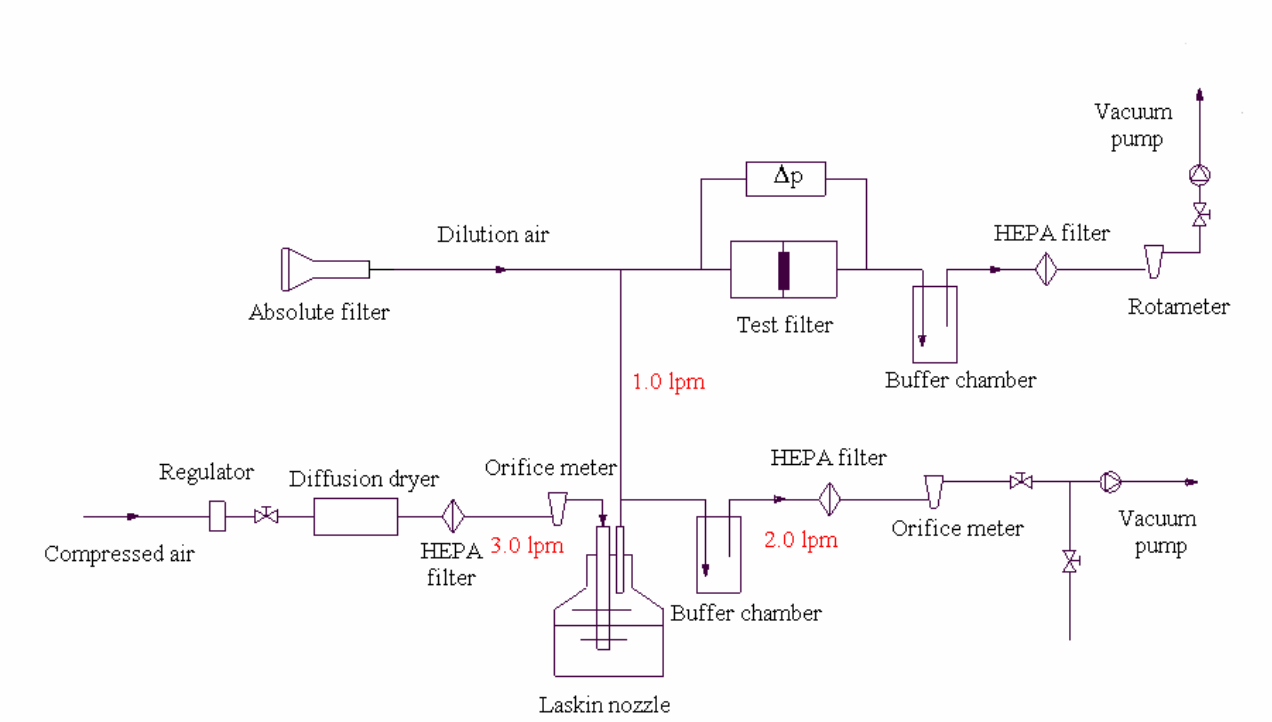

Figure 3.7 The schematic representation of the experimental set-up for studying the collection characteristics of mist aerosol particles.

Figure 3.8 Photograph of the experimental set-up for studying the collection characteristics of mist aerosol particles.

3.4 The Saturation Characteristic of a medium-performance fibrous filter (glass fiber filter)

The characteristics of a medium-performance fibrous filter (glass fiber filter) saturated with liquids (water, propylene glycol and palm oil) were studied by measuring the pressure drop and examining the surface of the glass fiber filter using the optical microscope.

The experimental set-up, as shown in Fig. 3.9 and Fig. 3.10, composed of a filter holder and an absolute filter. To test the influence of the surface tension and viscosity of the liquids; water, propylene glycol and palm oil were used.

A filter was treated in a desiccator using silica gel at room temperature (25°C) and 50-60 % relative humidity for at least 24 hours. The filter was first weighed using a five-digit readability analytical balance. It was then immersed in a

liquid (water, propylene glycol or palm oil) until it was saturated and then placed in the filter holder. The clean air passing through an absolute filter was introduced to the filter until the pressure drop was constant. The pressure drop was measured by a U-tube manometer. The collected liquid particles on glass fiber filter were weighed using the same balance. Then the filtration velocity was reduced from the initial velocity to the minimum velocity of 1 cm s^{-1}. The constant pressure drop was recorded at each step of reducing velocity. The initial velocities and the steps of reducing velocities are shown in Table 3.3.

Table 3.3 Values of velocity set in the experiment to determine the saturation characteristics of a medium-performance fibrous filter (glass fiber filter).

Initial velocity (cm s^{-1})	Reducing velocities (cm s^{-1})
28	24, 20, 16, 12, 8, 4 and 1
21	18, 15, 12, 9, 6, 3 and 1
14	12, 10, 8, 6, 4, 2 and 1
7	6, 5, 4, 3, 2 and 1

To better understand the aerosol deposition, optical microscope (OLYMPUS, BX60F5) was employed to examine the surface of the fibrous filter when saturated with liquids (water, propylene glycol and palm oil) at different initial velocities.

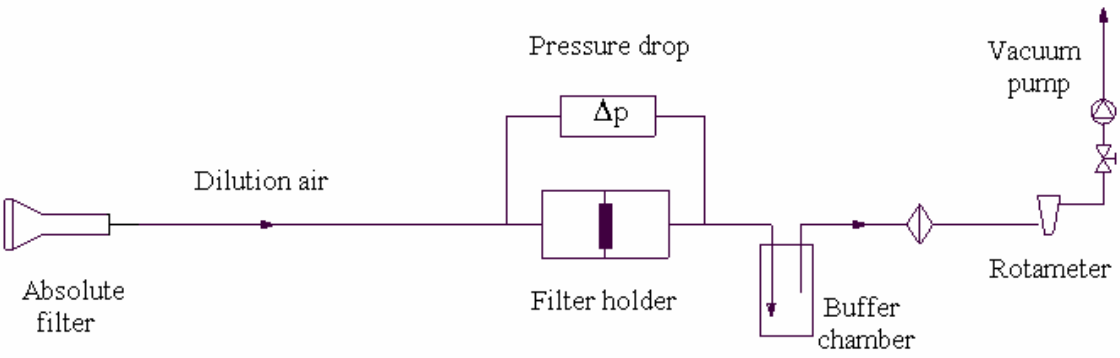

Figure 3.9 The schematic representation of the experimental set-up for studying the saturation characteristic of a medium-performance fibrous filter (glass fiber filter).

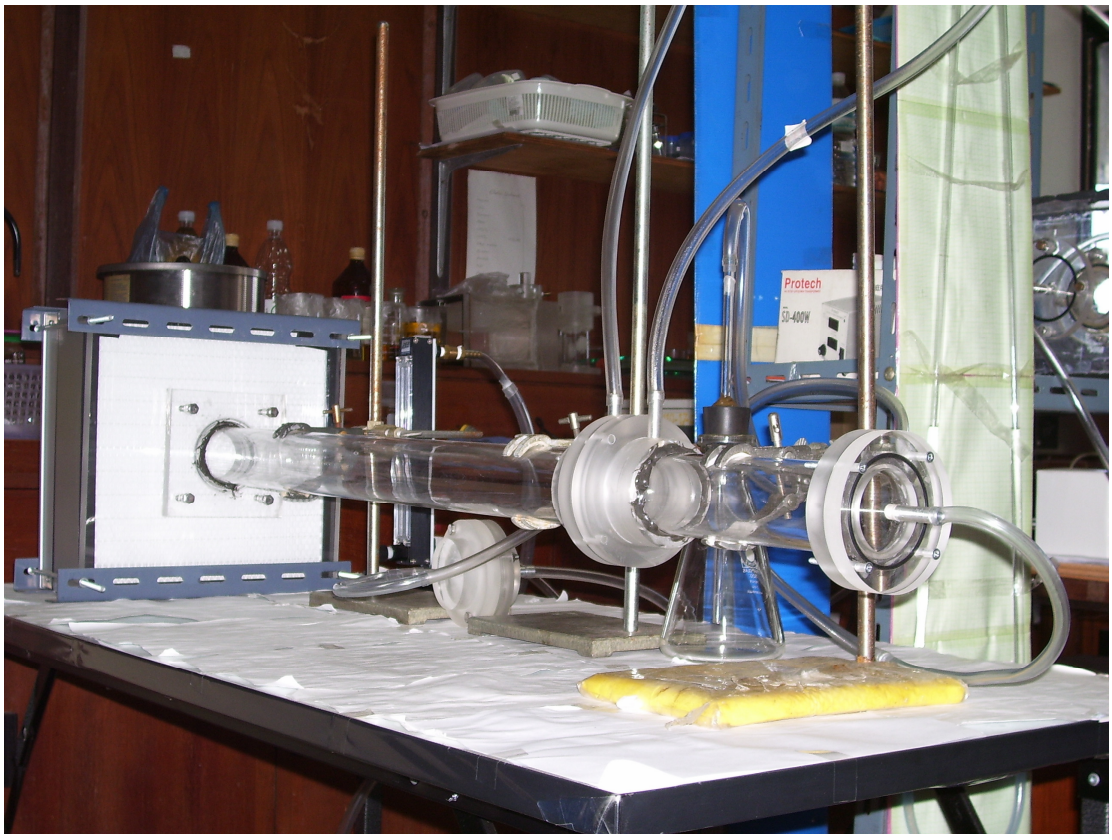

Figure 3.10 Photograph of the experimental set-up for studying the saturation characteristic of a medium-performance fibrous filter (glass fiber filter).

CHAPTER 4
RESULTS AND DISCUSSION

4.1 Size Distribution of Generated Liquid Aerosol

In this work, an experimental set-up was designed to investigate collection performance of a medium performance glass fiber filter subjected to liquid aerosol. The concentration and the size distribution of mist aerosol generated from different liquids (propylene glycol and palm oil) were measured using an 8-stage Andersen sampler (Dylec, AN 200). The stability of aerosol generation was examined and the results are shown in Fig. 4.1 to Fig. 4.2 for propylene glycol and Fig. 4.3 to Fig. 4.4 for palm oil aerosol. The size distribution appears very stable. The average mass median aerodynamic diameter (MMAD) of propylene glycol aerosol is about 2.24 and 2.35 μm for the first and the second tests while the average geometric standard deviation (GSD) of propylene glycol aerosol is about 2.32 and 2.42 μm for the first and the second tests. The average MMAD of palm oil aerosol is about 1.43 and 1.40 μm for the first and the second tests while the average GSD of palm oil aerosol is about 2.10 μm for both tests. From the result of Hajra *et al.* (2003), the mean diameter of propylene glycol droplets generated by a Laskin nozzle was 0.21 μm when the Laskin nozzle was operated under the supply pressure of 172 kPa (25 psi or 1.7 bar). Vasudevan *et al.* (2004) showed that propylene glycol aerosol produced by a Laskin nozzle had mean diameter of 0.2 μm when the compressed air at a pressure of 1.1 bar was used to generate the droplets of propylene glycol and Frising *et al.* (2005) showed that the average aerodynamic particle diameter of di-(2-ethyl hexyl) sebacate (DEHS) generated by a Laskin nozzle was 0.18 μm.

The mass median aerodynamic diameter and the geometric standard deviation can be determined directly from a log-probability plot. The geometric standard deviation, being the ratio between the size associated with a cumulative count of 84.1% and the median size (a cumulative count of 50%) or between the 50%

cumulative size and the 15.9% cumulative size must usually be greater than or equal to 1.0. It can be expressed as

$$GSD = \sigma_g = \frac{d_{84\%}}{d_{50\%}} = \frac{d_{50\%}}{d_{16\%}} = \left(\frac{d_{84\%}}{d_{16\%}}\right)^{1/2} \quad (4.1)$$

The data in a log-probability graph of aerosol particles is linear which shows a lognormal distribution behavior of the generated aerosol. The MMAD and GSD can be determined from the 50th percentile size and Eq. 4.1 (Hinds, 1999).

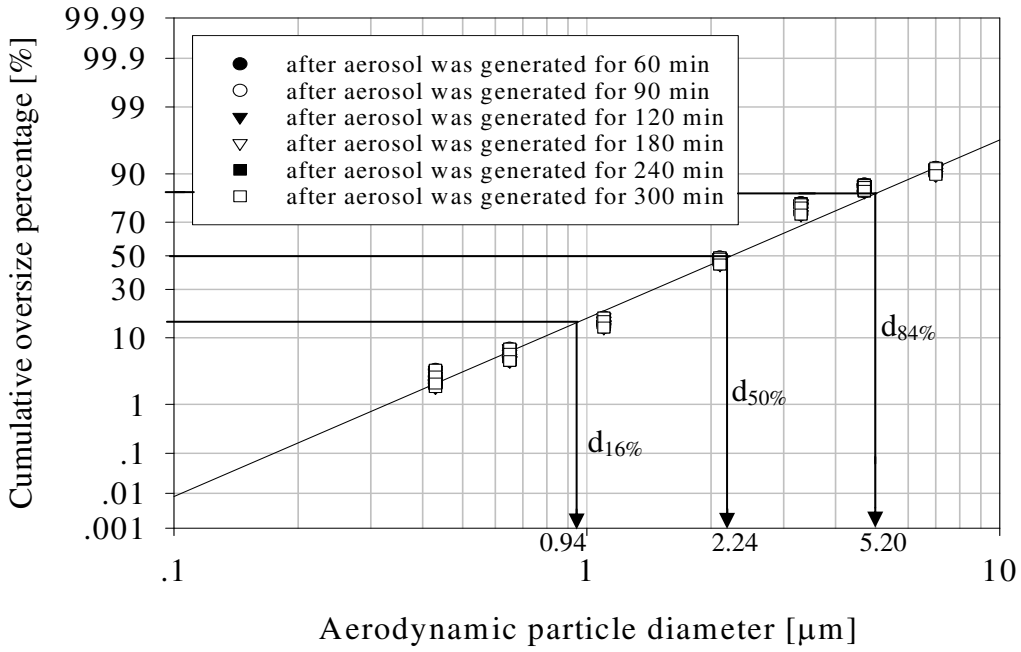

Figure 4.1 Characteristics of propylene glycol aerosol particles from the Laskin nozzle (Test#1).

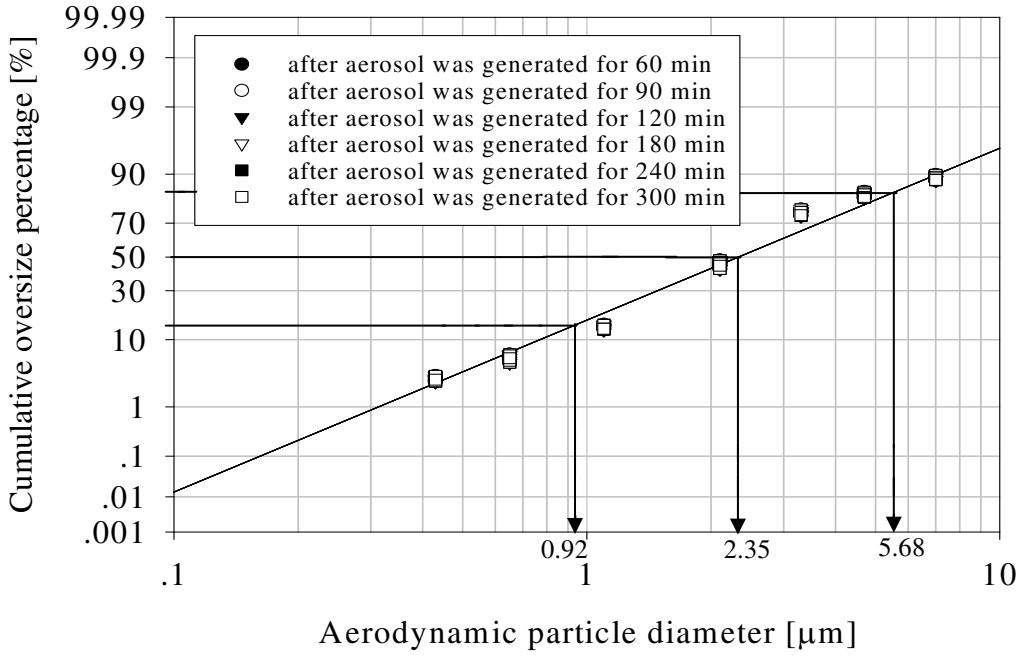

Figure 4.2 Characteristics of propylene glycol aerosol particles from the Laskin nozzle (Test#2).

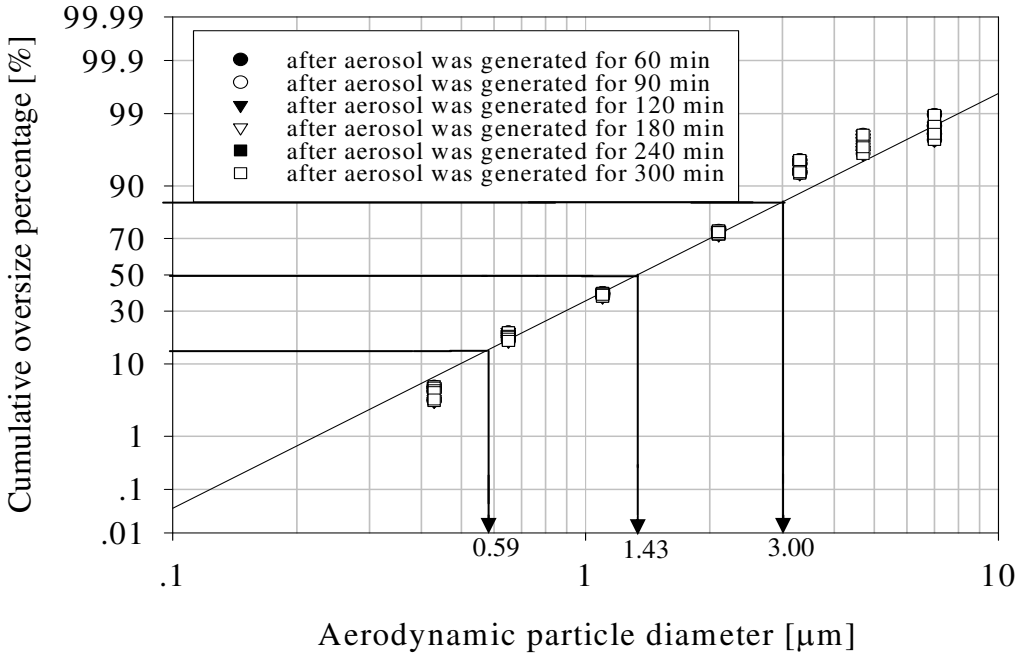

Figure 4.3 Characteristics of palm oil aerosol particles from the Laskin nozzle (Test#1).

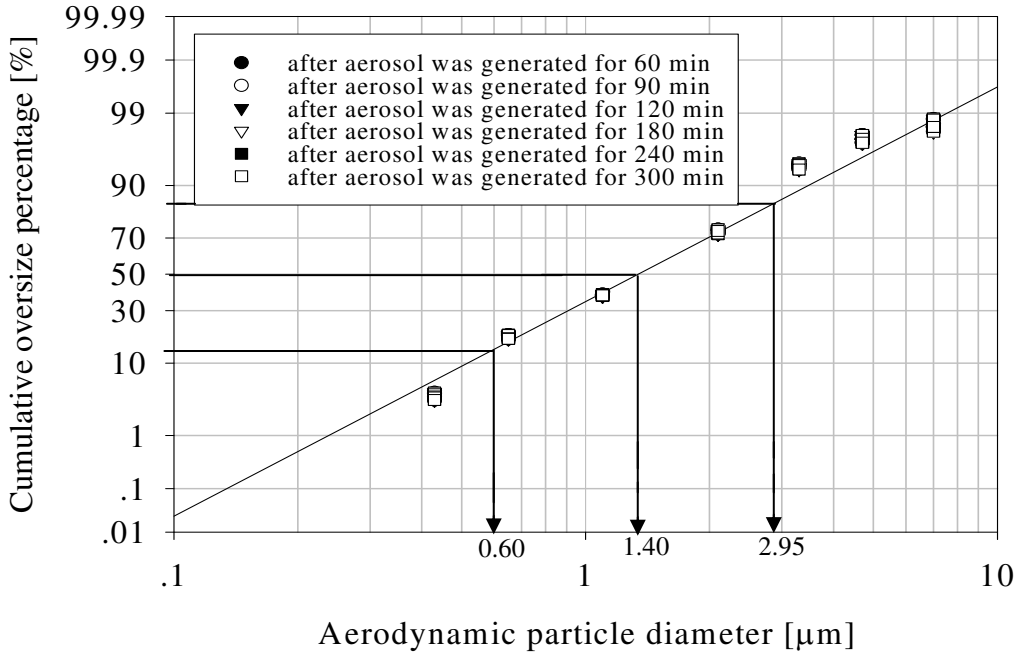

Figure 4.4 Characteristics of palm oil aerosol particles from the Laskin nozzle (Test#2).

Fig. 4.5 shows that the concentration of palm oil droplets generated from the Laskin nozzle was slightly more stable than propylene glycol droplets. The relationship between concentration of oil mist and collected mass is shown in Fig. 4.6. Average aerosol concentrations of propylene glycol are 0.487 and 0.559 g m^{-3} for the first and the second tests, respectively while the average aerosol concentrations of palm oil are 0.295 and 0.311 g m^{-3} for the first and the second tests. For identical operating condition, the average concentration of propylene glycol is higher than that of palm oil because propylene glycol is less viscous than palm oil and then easier to be atomized by the Laskin nozzle.

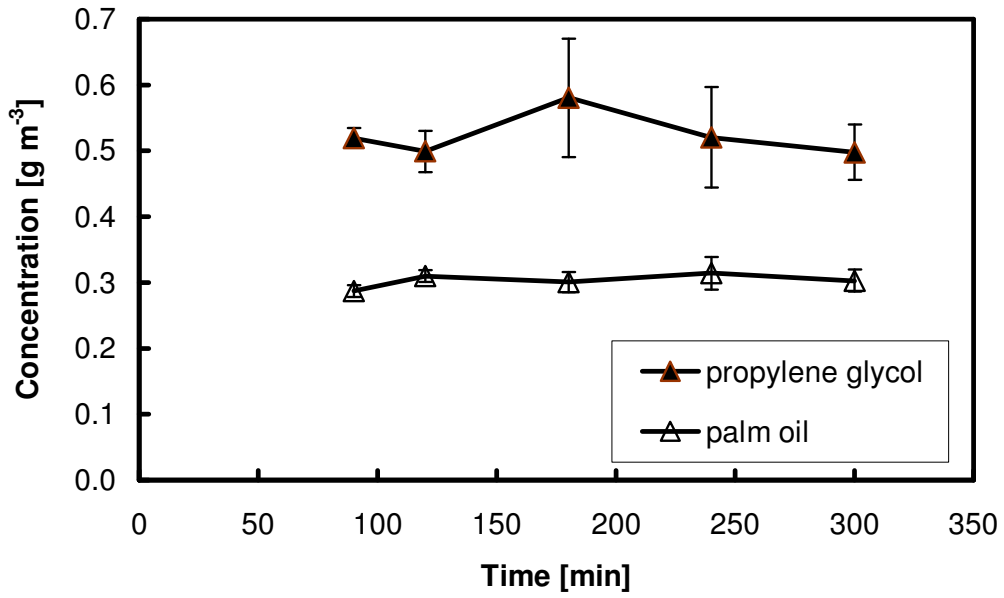

Figure 4.5 Concentration of oil mist from the Laskin nozzle as a function of the filtration time.

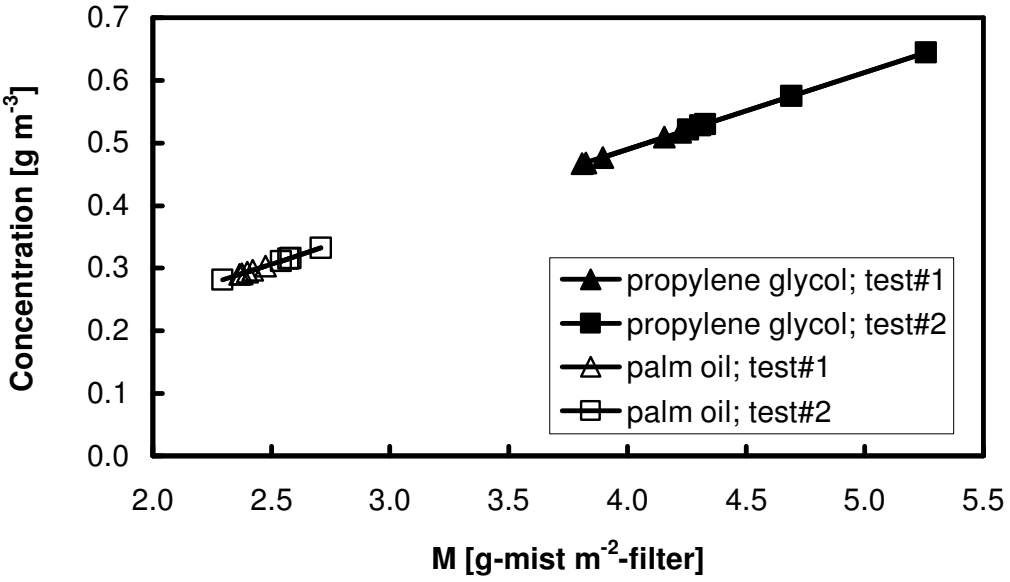

Figure 4.6 Concentration of oil mist from the Laskin nozzle as a function of the collected mass.

4.2 Performance of a Virgin Filter

4.2.1 Effect of Particle Size and Velocity on Efficiency

Effects of velocity and particle size on filtration efficiency of the virgin filter using propylene glycol aerosol particles are shown in Figs. 4.7 and 4.8, respectively. Filtration time was 30 min. The results indicate that the efficiency of a virgin filter slightly decreases when the filtration velocity increases for all particle sizes and increases when the particle size increases for all filtration velocities. Moreover, the efficiency is nearly independent of particle sizes for filtration velocity of 5 to 21 cm s^{-1}. At the highest velocity of 28 cm s^{-1}, the difference in efficiency is significant for all particle sizes. However, at the same filtration velocity (v = 28 cm s^{-1}) it was found that the filter shows a better collection efficiency for larger particles than smaller particles. This is due to the influence of impaction mechanism (Hinds, 1999). The importance of this inertial impaction mechanism increases with increasing particle size and increasing flow velocity. The collection efficiencies are about 97%, 89%, 76% and 26% for the particle size of 1.0, 0.7, 0.5 and 0.3 μm particles, respectively, at a filtration velocity of 28 cm s^{-1}. In addition, at the same particle size, it was found that at the lower filtration velocity shows better efficiency than at the higher filtration velocity. This is due to the influence of Brownian motion of small particles (Hinds, 1999). Brownian motion increases when particle size and flow velocity are decreased.

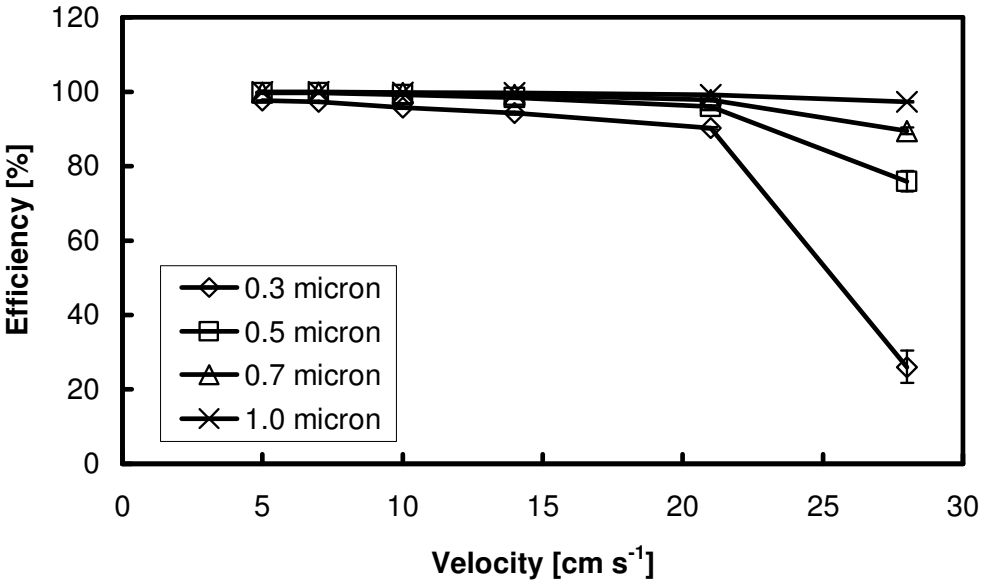

Figure 4.7 Effect of velocity on efficiency of a filter using propylene glycol particles of 0.3, 0.5, 0.7 and 1.0 μm after filtration for 30 min.

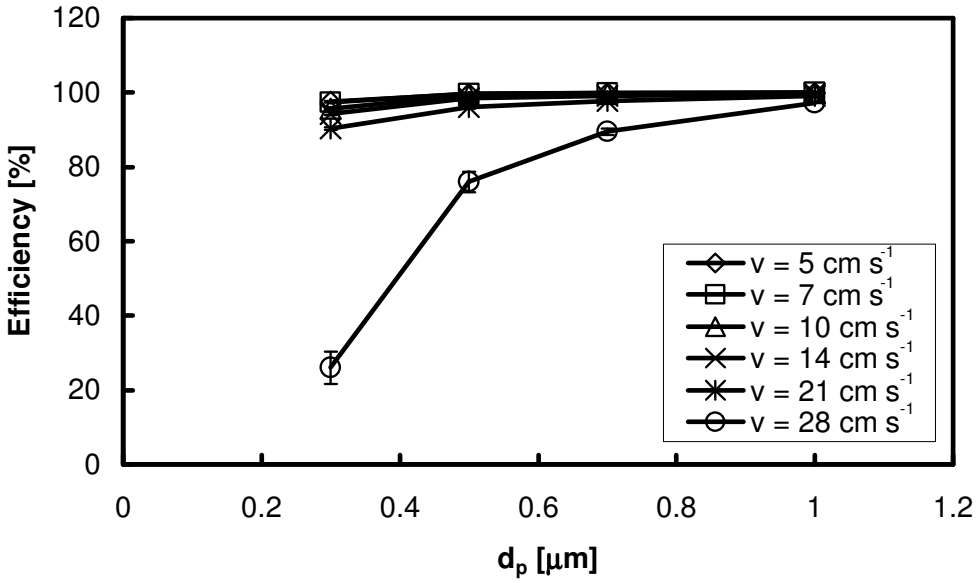

Figure 4.8 Effect of particle size on efficiency of a filter using propylene glycol particles at different velocities and after filtration for 30 min.

4.2.2 Effect of Velocity on Pressure drop Evolutions

Pressure drop across a filter is a parameter used to determine the collection performance. The pressure drop is the resistance to the air which flows through the fibrous filter. The liquid used for mist generation in this experiment was propylene glycol. The pressure drop across the virgin filter after filtration for 30 min at different velocities is shown in Fig. 4.9.

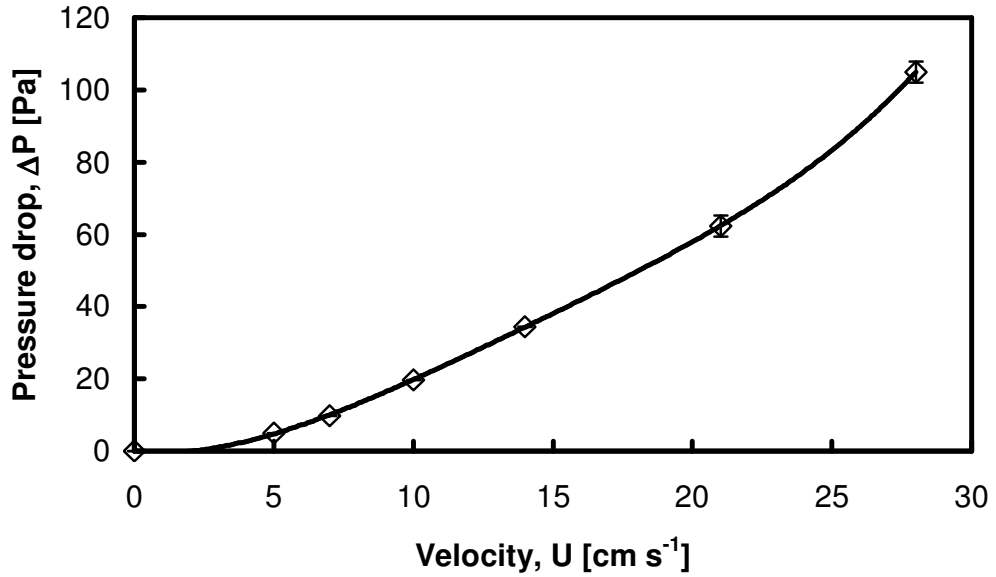

Figure 4.9 Pressure drop across a filter where the oil mist is propylene glycol and after filtration for 30 min at different velocities.

The results show that the pressure drop of the fibrous filter increases with increasing the filtration velocity as commonly known. The increase is, however, is not linear.

4.3 Collection Characteristics of Mist Aerosol Particles

Different clogging tests were conducted by varying the operating conditions, including filtration velocity, number of filter sheets and aerosol particles with different physical properties. The influence of each parameter is studied by eliminating the effect of other factors.

4.3.1 Effect of Filtration Velocity

Figs. 4.10 and 4.11 represent the pressure drop evolutions of a single filter as functions of filtration time and collected mass, respectively, during clogging by propylene glycol aerosol with different filtration velocities: 7, 14, 21 and 28 cm s^{-1}.

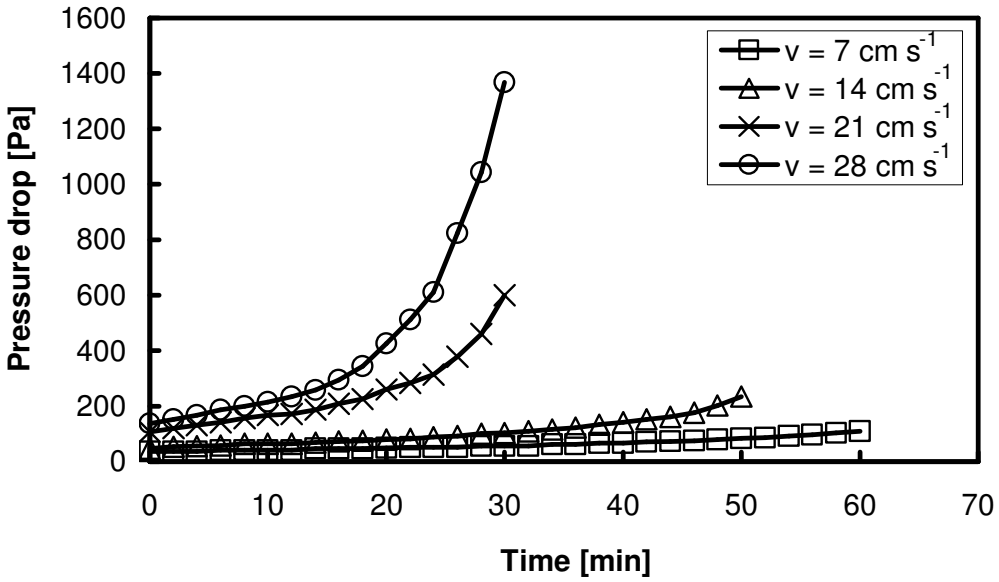

Figure 4.10 Pressure drop evolutions of a single filter as a function of filtration time during clogging by propylene glycol aerosol with different filtration velocities.

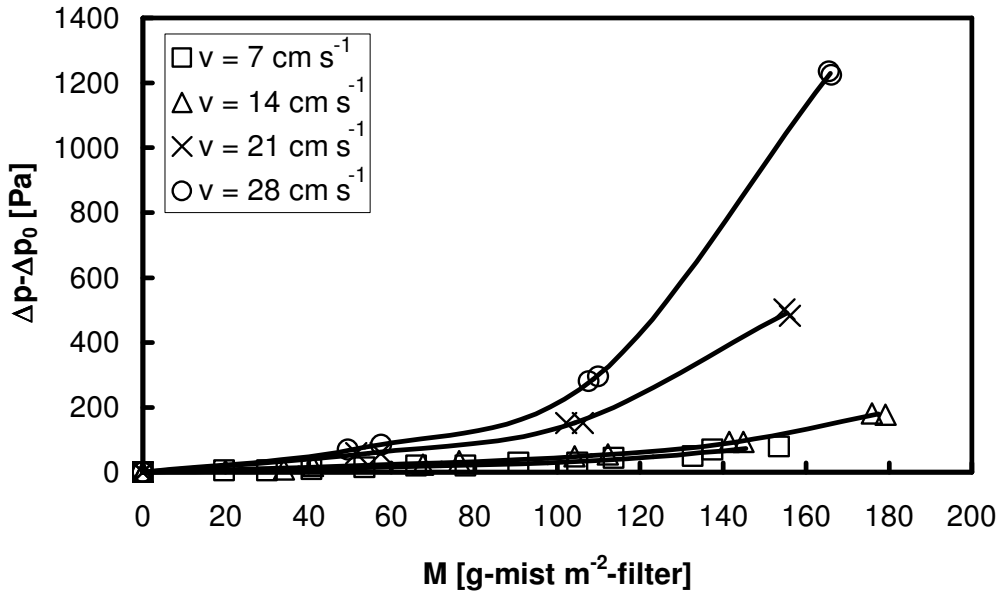

Figure 4.11 Pressure drop evolutions of a single filter as a function of collected mass during clogging by propylene glycol aerosol with different filtration velocities.

From the results, it was found that the change in the pressure drop during clogging as functions of filtration time and collected mass are in the same direction for all filtration velocities. At high filtration velocity, the initial single fiber collection efficiency is higher so that more droplets were collected in a thin layer of filter surface. At the same filtration time, mass collected (M) on the filter at high filtration velocity is greater than that at low filtration velocity since the liquid aerosol particles deposit on the collecting surface rapidly. This result causes the pressure drop of a single filter increases as the filtration time and the collected mass increase which is similar to the result of Contal et al. (2004). They studied the change in pressure drop of a D309 filter during clogging by a di-octyl phthalate (DOP) aerosol for different filtration velocities ranging from 2.5 to 19 cm s^{-1}. Their result showed that at high filtration velocity, the collected mass on the filter is higher than that at low filtration velocity.

At the beginning of the filtration process (the initial stage), the whole pressure drop is caused by the porous medium itself which maintains nearly constant. As filtration time progresses, the particles retained in the filter increase the resistance to the flow. A liquid film starts to build up on the surface of the filter so that,

gradually, a greater proportion of pressure drop is due to the liquid particle resistance to the flow.

For a filtration velocity of 28 cm s^{-1}, the final pressure drop is barely 91.9% of that at a filtration velocity of 7 cm s^{-1}. At filtration velocity of 28 and 21 cm s^{-1}, the pressure drop reached three times of the initial value after 30 minutes and at filtration velocity of 14 and 7 cm s^{-1}, the pressure drop reached three times of the initial value after 50 and 60 min, respectively. The change in the pressure drop increases when the filtration velocity increases. At the highest filtration velocity the change in the pressure drop is maximum since the pressure drop is proportional to the filtration velocity. At high filtration velocity the liquid aerosol particles deposit on the collecting surface rapidly which causes the pressure drop increases more when compared with lower filtration velocity. The filtration velocity, hence, plays a significant role during clogging.

4.3.2 Effect of the Number of Filter Sheets

The pressure drop evolutions for 1 and 5 filters at different filtration velocity as functions of filtration time and collected mass are shown in Figs. 4.12 to 4.19. The generated aerosol is propylene glycol. Results show that the change in pressure drop increases with increasing the number of filter sheet for all velocities. The changes in pressure drop during clogging as functions of filtration time and collected mass are in the same direction for all filtration velocities. It was noted that the changes in pressure drop of five identical filters in series were similar to that of a single filter. When the number of filter sheets increases, the change in the pressure drop increases since the pressure drop is directly proportional to the thickness of the filter. The number of filter sheets plays an important role during clogging.

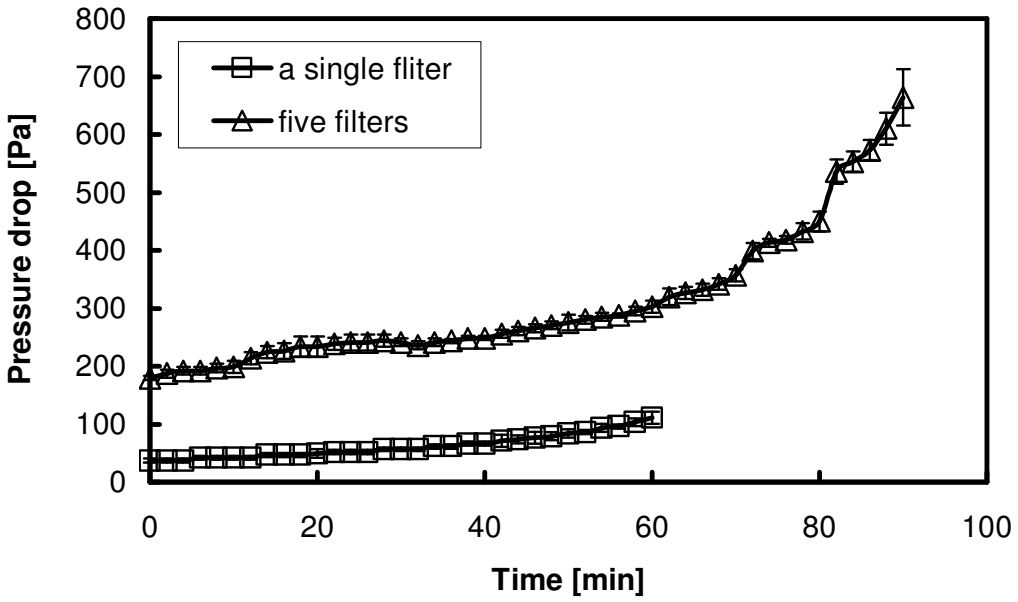

Figure 4.12 Effect of the number of filter sheets on the pressure drop evolutions as a function of filtration time for propylene glycol aerosol particles at filtration velocity of 7 cm s^{-1}.

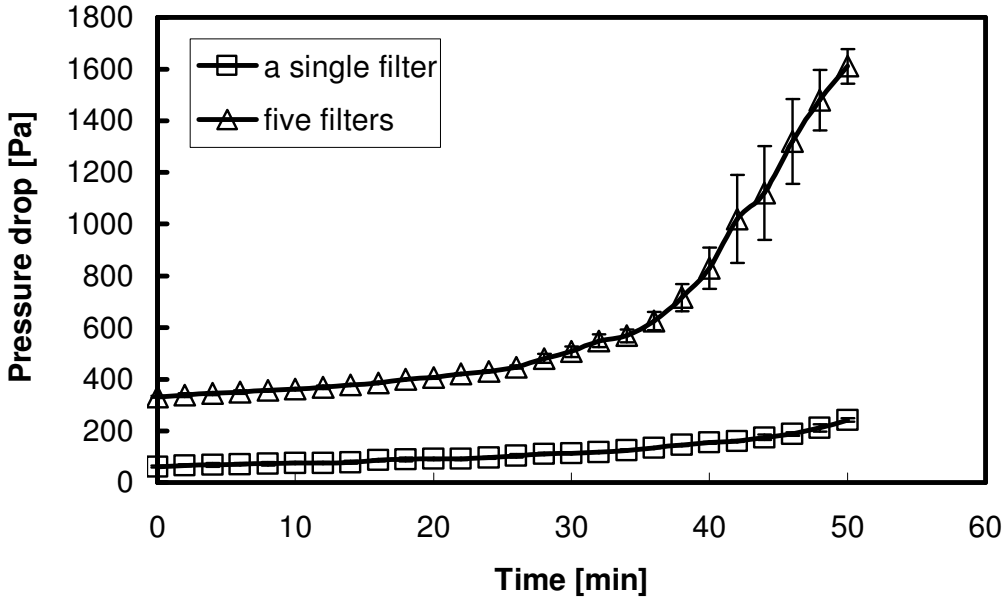

Figure 4.13 Effect of the number of filter sheets on the pressure drop evolutions as a function of filtration time for propylene glycol aerosol particles at filtration velocity of 14 cm s^{-1}.

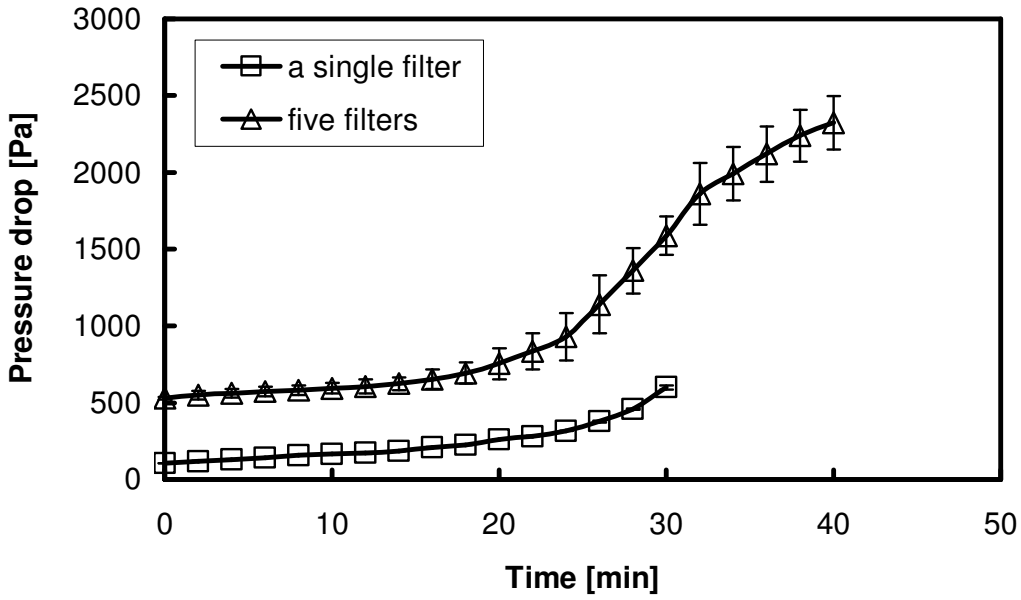

Figure 4.14 Effect of the number of filter sheets on the pressure drop evolutions as a function of filtration time for propylene glycol aerosol particles at filtration velocity of 21 cm s^{-1}.

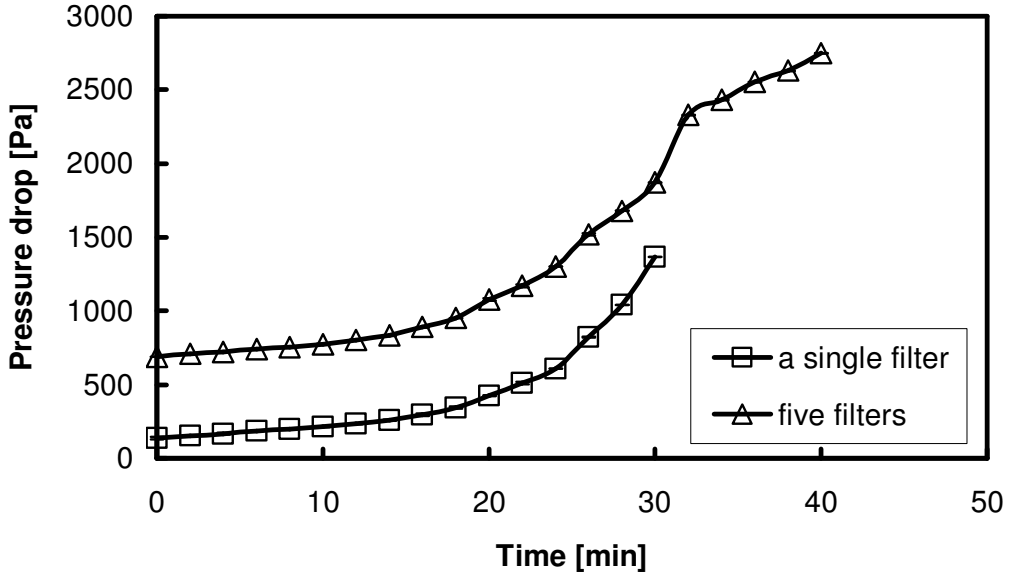

Figure 4.15 Effect of the number of filter sheets on the pressure drop evolutions as a function of filtration time for propylene glycol aerosol particles at filtration velocity of 28 cm s^{-1}.

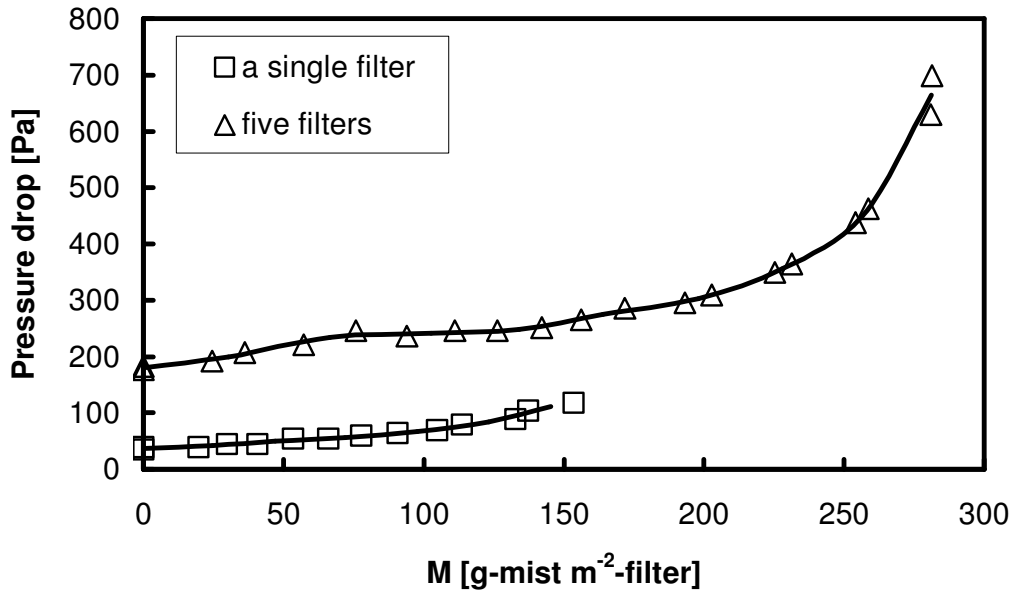

Figure 4.16 Effect of the number of filter sheets on the pressure drop evolutions as a function of collected mass for propylene glycol aerosol particles at filtration velocity of 7 cm s^{-1}.

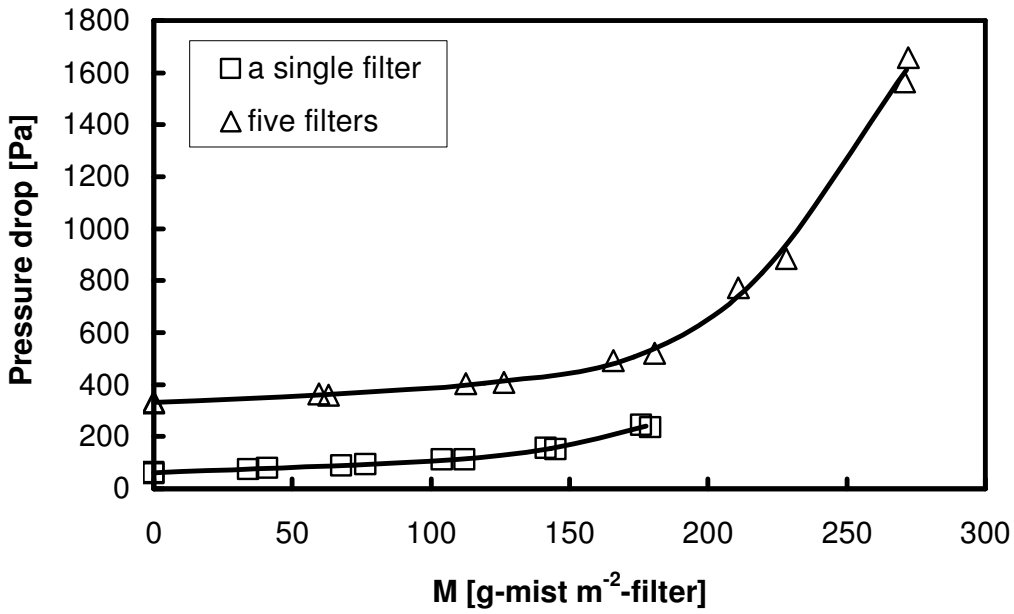

Figure 4.17 Effect of the number of filter sheets on the pressure drop evolutions as a function of collected mass for propylene glycol aerosol particles at filtration velocity of 14 cm s^{-1}.

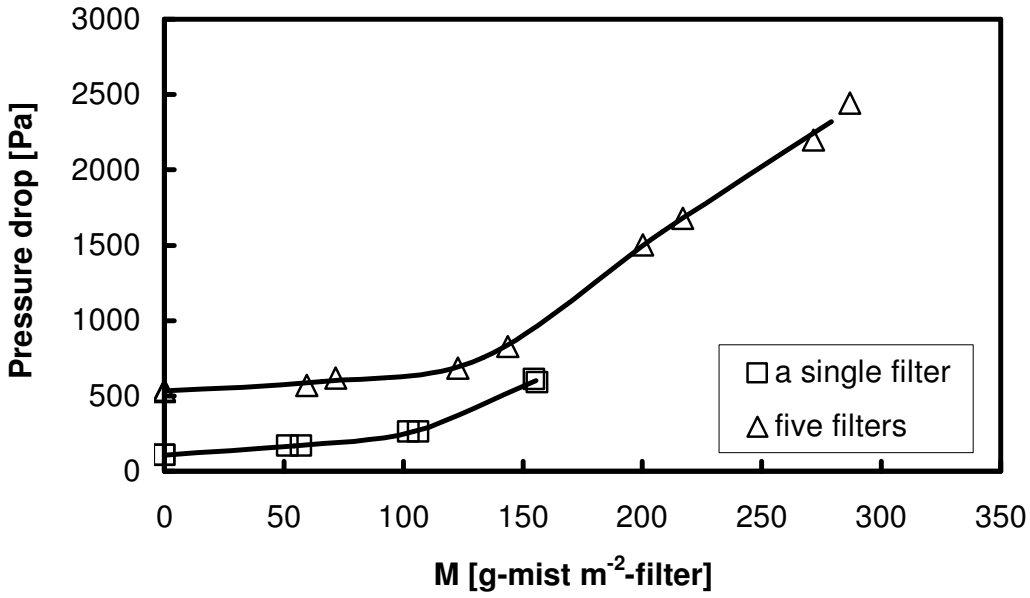

Figure 4.18 Effect of the number of filter sheets on the pressure drop evolutions as a function of collected mass for propylene glycol aerosol particles at filtration velocity of 21 cm s^{-1}.

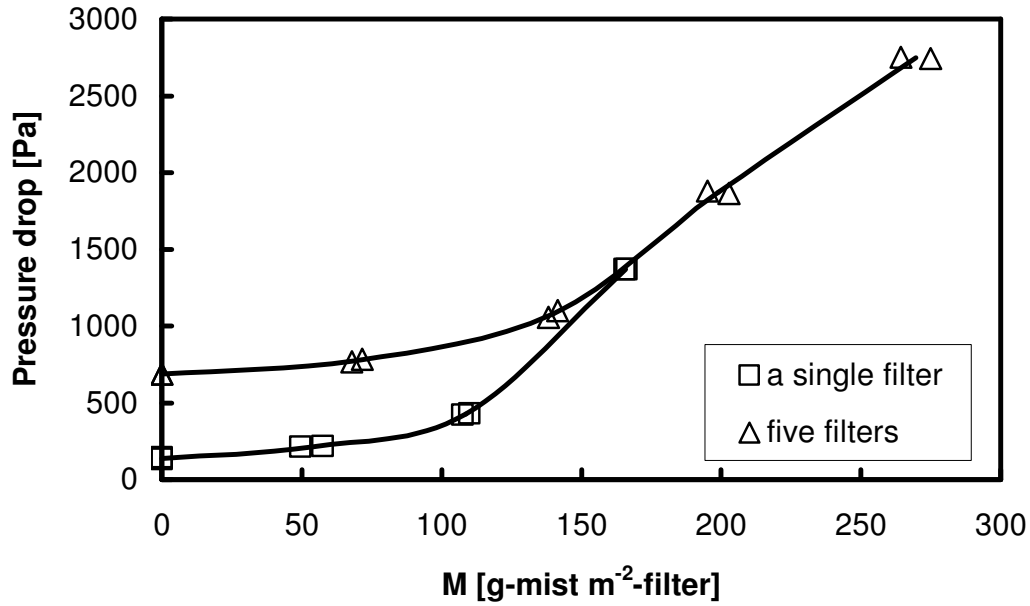

Figure 4.19 Effect of the number of filter sheets on the pressure drop evolutions as a function of collected mass for propylene glycol aerosol particles at filtration velocity of 28 cm s^{-1}.

Figs. 4.20 to 4.23 show the change in the collected mass as a function of filtration time during clogging of five filters for filtration velocity of 7, 14, 21 and 28 cm s^{-1}, respectively. The aerosol generated is propylene glycol. It can be observed that as filtration time increases, the collected mass of filter increases. Weighing each filter at different degree of clogging yielded the change in the collected mass as a function of filtration time (t). The collected mass (M) can be calculated from

$$M = \frac{w_t - w_0}{A} \tag{4.2}$$

where w_t is the weight of clogged filter at any filtration time, w_0 is the weight of clean filter and A is the filter cross-sectional area. When the filtration was carried out with the filters placed in series, it was noted that the evolution of pressure drop was similar to that of a single filter as shown in Figs. 4.12 to 4.19. Changes in the pressure drop during clogging of five identical glass fiber filters and a single filter are in the same direction. Observation of these results revealed that five filters are clogged up one after another. For five filters, while liquid aerosol particles were collected on the surface of the filter, these aerosol particles can partially penetrate to the thickness of the medium.

It can be seen that in the first stage of clogging, the collected mass of the filters is dependent on the filtration velocity as shown in Figs. 4.20 to 4.23. After 10 min, the collected mass on the first filter sheet increases when the filtration velocity increases. The collected mass on the first filter sheet after 10 min is about 24, 52, 55 and 59 g m^{-2} at the filtration velocity of 7, 14, 21 and 28 cm s^{-1}, respectively, as shown in Figure 4.24. Moreover, when the pressure drop reached three times of the initial value, the collected mass on the first filter sheet is identical for each filtration velocity. Most of liquid aerosol particles are collected on the first filter sheet. The collected mass on the first filter sheet is about 255 (90.6%), 246 (78.9%), 259 (78.8%) and 251 (76.5%) g m^{-2} at the filtration velocity of 7, 14, 21 and 28 cm s^{-1}, respectively. Deposited mass of droplets on the second filter sheet through the fifth filter sheet remained fairly constant during the course of filtration. At the same filtration time, it was found that the collected mass on the first filter sheet at

higher filtration velocity is higher than that at lower filtration velocity because the mist aerosol particles deposited on the collecting surface rapidly. The collected mass on each filter was measured every 10 min. The results indicate that the collected mass on the first filter sheet at the highest filtration velocity increases rapidly while that at the lowest filtration velocity increases slightly. At filtration velocity of 7 cm s^{-1}, liquid aerosol particles can partially penetrate to other filter sheet because the test period is longer compared to other filtration velocities.

At filtration velocity of 7 and 14 cm s^{-1}, the pressure drop across five filters reached three times of the initial value after 90 and 50 min, respectively as shown in Figs. 4.12 and 4.13 and at filtration velocity of 21 and 28 cm s^{-1}, the pressure drop across five filters reached three times of the initial value after 40 min as shown in Figs. 4.14 and 4.15.

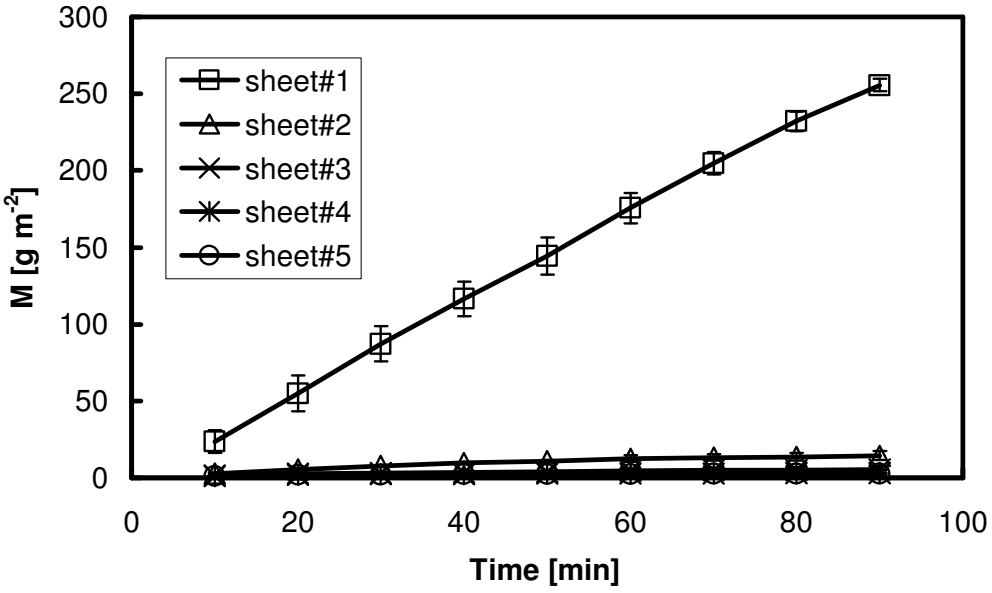

Figure 4.20 The change in the distribution profile during clogging of five identical filters in series for propylene glycol aerosol particles. (v = 7 cm s^{-1}; t = 10, 20, 30, 40, 50, 60, 70, 80 and 90 minutes)

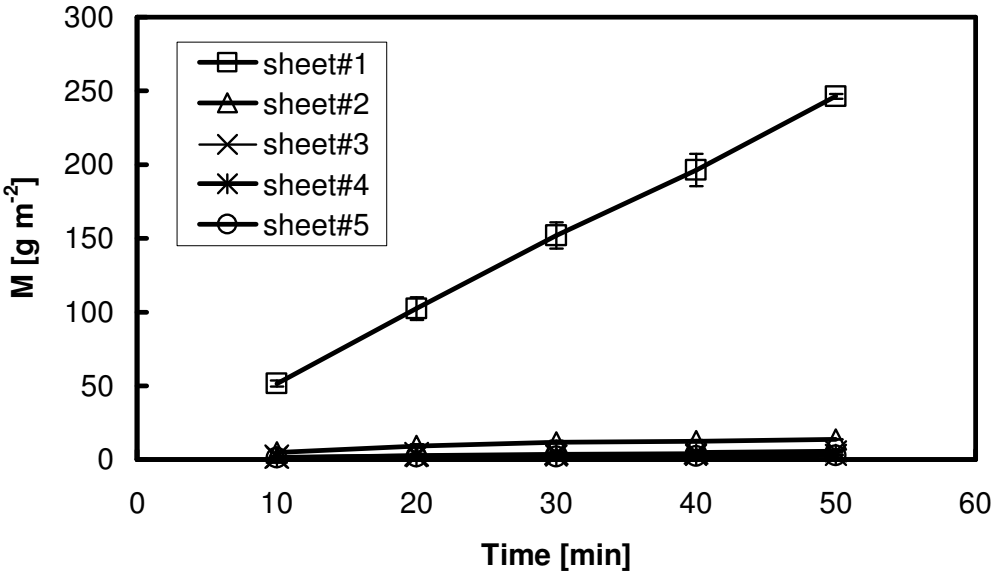

Figure 4.21 The change in the distribution profile during clogging of five identical filters in series for propylene glycol aerosol particles. (v = 14 cm s^{-1}; t = 10, 20, 30, 40 and 50 minutes)

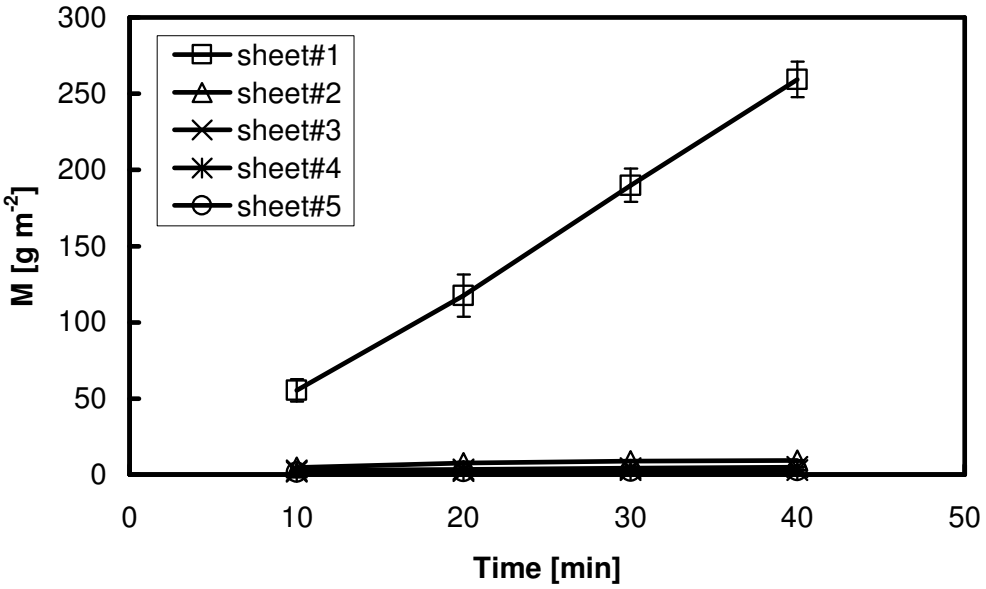

Figure 4.22 The change in the distribution profile during clogging of five identical filters in series for propylene glycol aerosol particles. (v = 21 cm s^{-1}; t = 10, 20, 30 and 40 minutes)

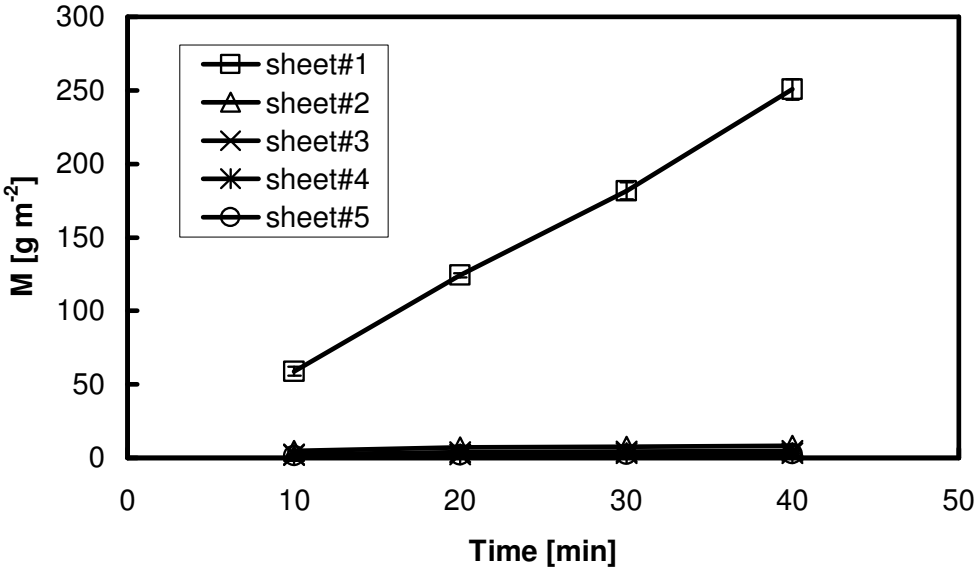

Figure 4.23 The change in the distribution profile during clogging of five identical filters in series for propylene glycol aerosol particles. (v = 28 cm s^{-1}; t = 10, 20, 30 and 40 minutes)

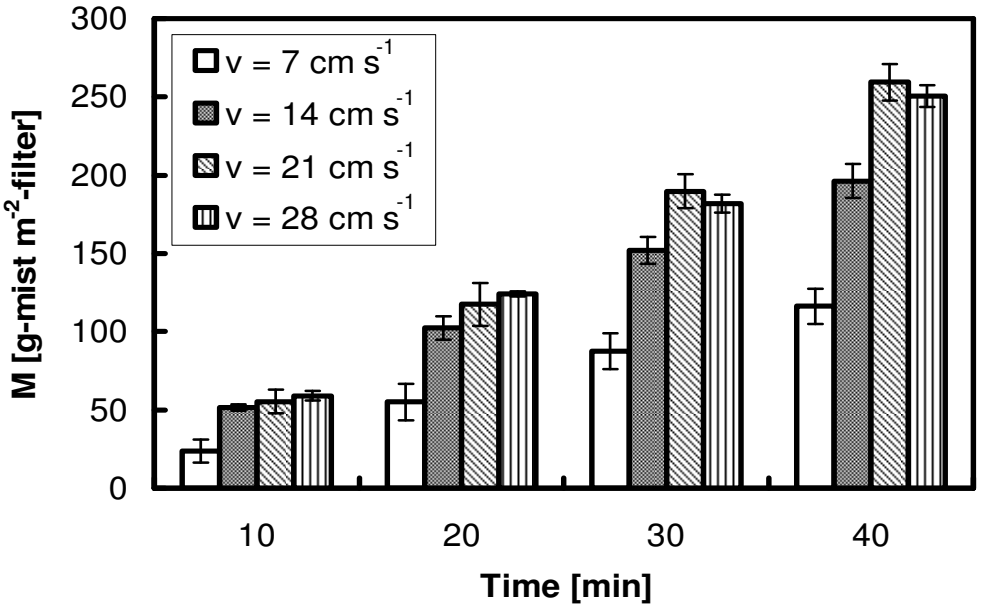

Figure 4.24 Collected mass evolutions on the first filter sheet as a function of the filtration time for propylene glycol aerosol particles at different filtration velocities.

Figs. 4.25 and 4.26 show the optical microscope photographs of five filters clogged by propylene glycol aerosol after filtration for 20 and 50 min, respectively. The photographs show that after 20 minutes of filtration, the deposit is made up of droplets around the fibers of the first filter sheet [Fig. 4.25 (a)]. Propylene glycol aerosol particles can partially penetrate to the second and the third filter sheets. They seem not to penetrate to the fourth and the fifth filter sheets. After 50 min of filtration, the quantity of liquid droplets increase and form a liquid film on the surface of the first filter sheet and liquid particles can penetrate to the second and third filter sheets and can partially penetrate to the fourth and the fifth filter sheets. This results in an increase of pressure drop because the quantity of the collected liquid particles on filter sheets increase.

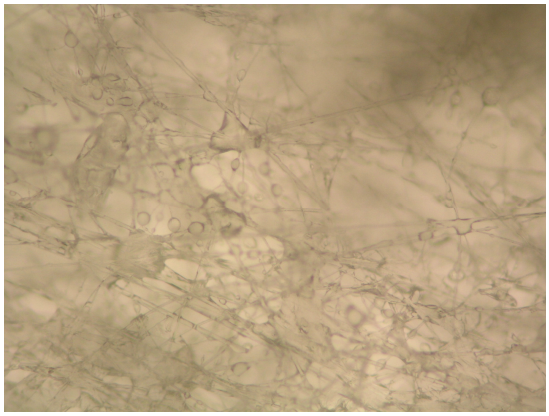

(a) sheet 1

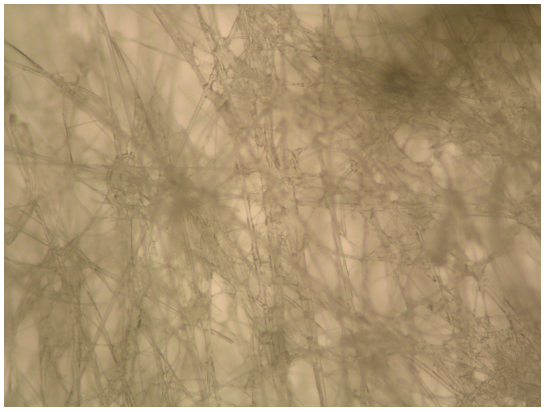

(b) sheet 2

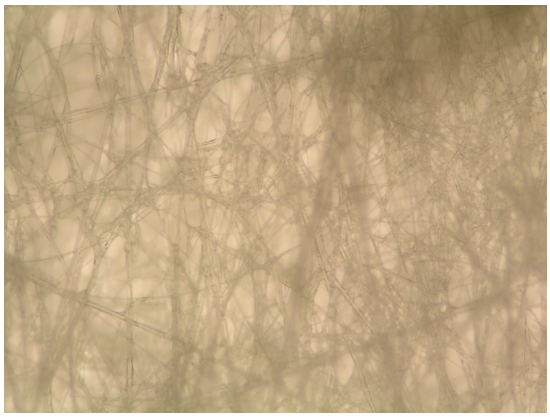

(c) sheet 3

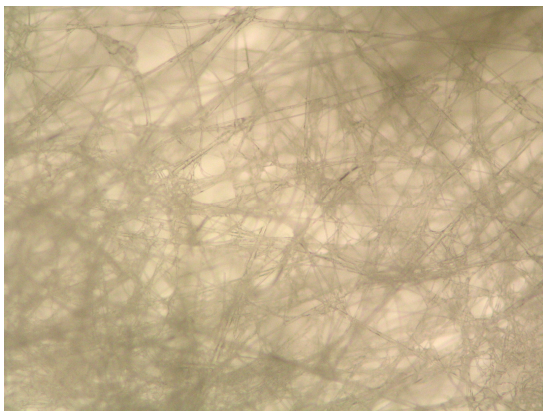

(d) sheet 4

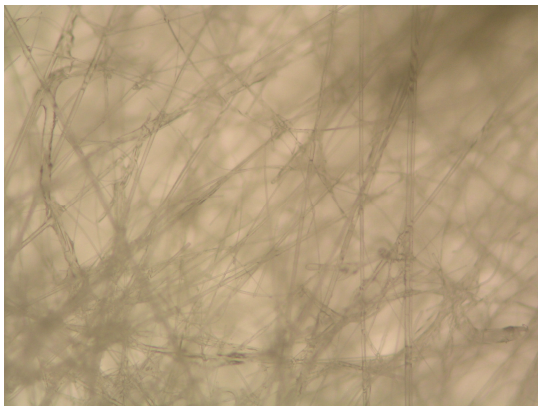

(e) sheet 5

Figure 4.25 Optical microscope photographs of five filters exposed to propylene glycol aerosol for 20 min (100×).

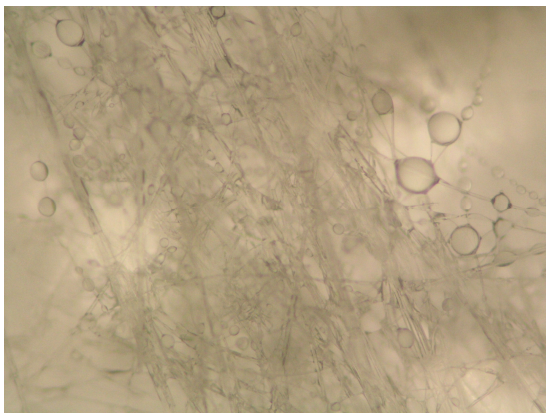

(a) sheet 1

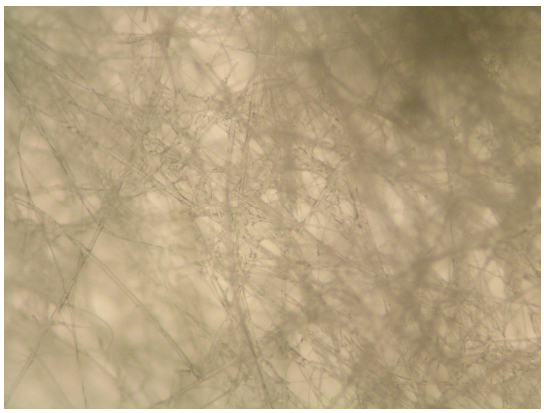

(b) sheet 2

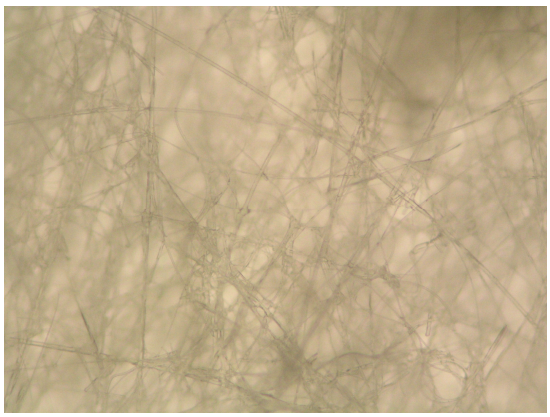

(c) sheet 3

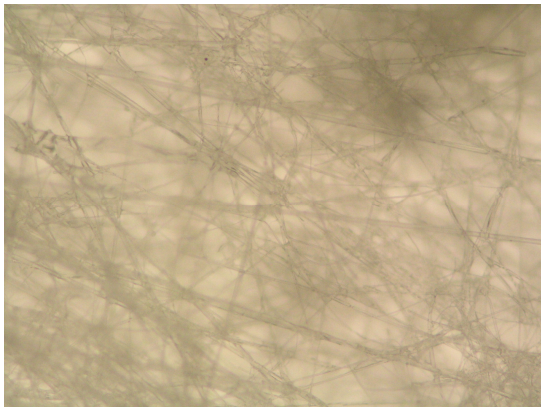

(d) sheet 4

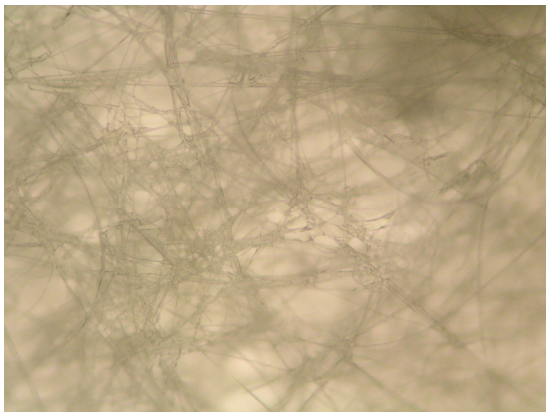

(e) sheet 5

Figure 4.26 Optical microscope photographs of five filters exposed to propylene glycol aerosol after 50 min (100×).

Figs. 4.27 and 4.28 show the optical microscope photographs of five filters collected by palm oil aerosol for 20 and 50 min, respectively. The photographs show that after 20 min of filtration the deposit is made up of droplets around the fibers of the first filter sheet [Fig. 4.27 (a)]. Palm oil aerosol particles can penetrate to the second and the third filter sheets, but not to the fourth and the fifth filter sheets. After filtration for 50 min, the quantity of liquid droplets on the first filter sheet increases. Liquid particles can penetrate to the second, the third, the fourth and the fifth filter sheets. The quantity of liquid droplets on the surface of the second and third filter sheets is greater when compared with propylene glycol aerosol particles, as shown in Figs. 4.26 (b) and (c). This is because palm oil aerosol particles have smaller particle size and larger surface area than propylene glycol aerosol particles so more palm oil aerosol particles can penetrate to the subsequent filter sheets. This result generates the low collection efficiency.

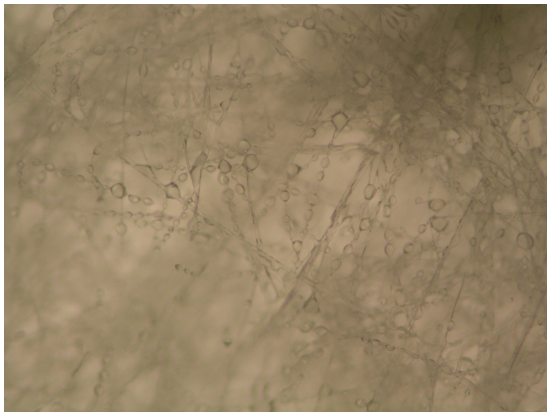

(a) sheet 1

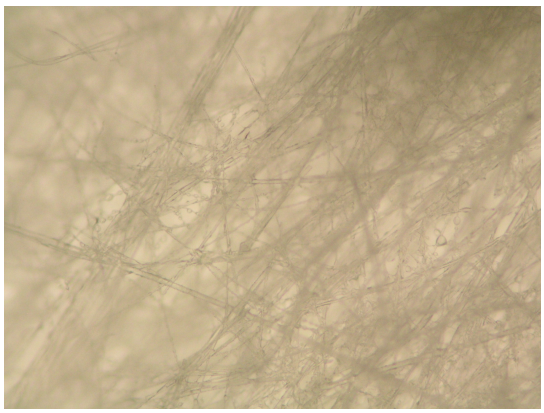

(b) sheet 2

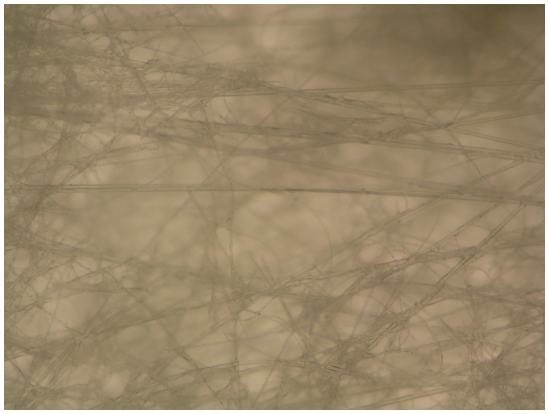

(c) sheet 3

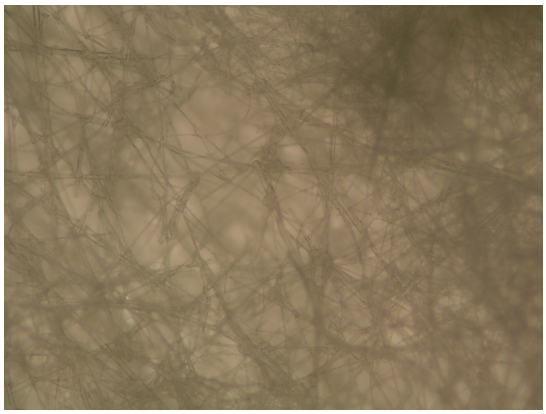

(d) sheet 4

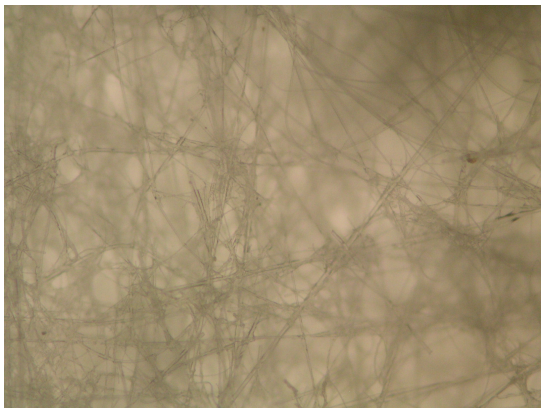

(e) sheet 5

Figure 4.27 Optical microscope photographs of five filters exposed to palm oil aerosol for 20 min (100×).

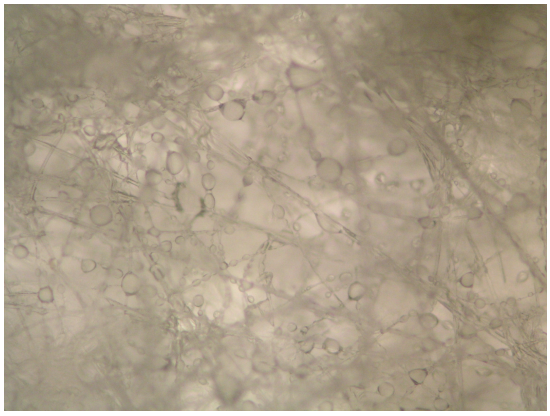

(a) sheet 1

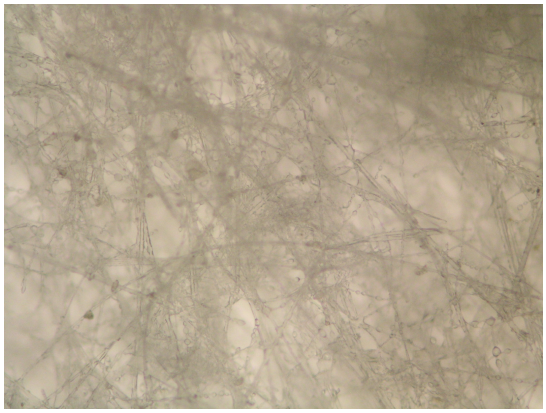

(b) sheet 2

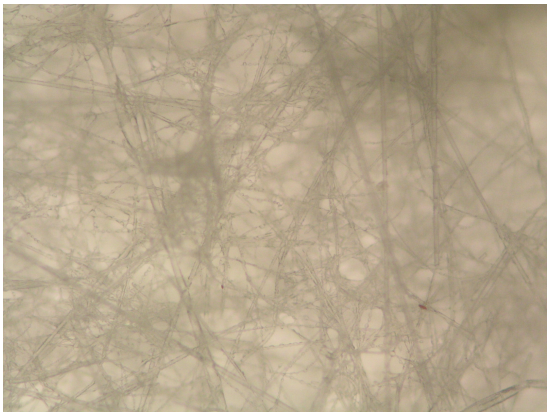

(c) sheet 3

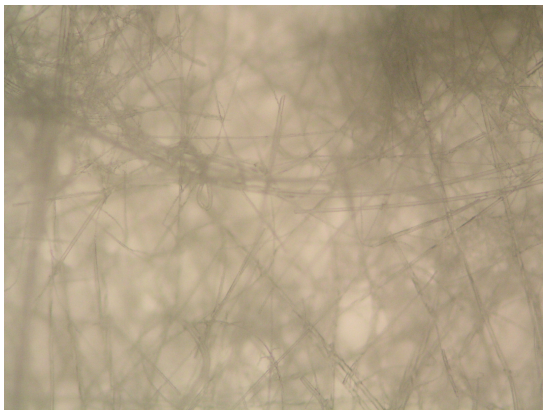

(d) sheet 4

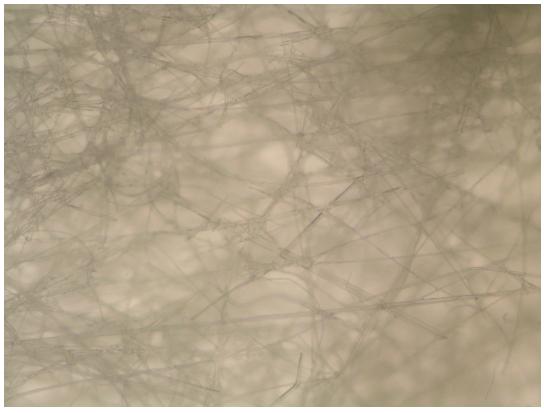

(e) sheet 5

Figure 4.28 Optical microscope photographs of five filters exposed to palm oil aerosol for 50 min (100×).

4.3.3 Effect of Physical Properties of the Aerosol Particles

The change in the pressure drop across a single filter and five filters as functions of the filtration time and the collected aerosol mass are shown in Figs. 4.29 to 4.32 when the glass fiber filters are exposed to liquid aerosol particles of propylene glycol and palm oil at filtration velocity of 14 cm s^{-1}. It was found that in an initial period, the clogging of the filter by palm oil aerosol is faster than that by propylene glycol aerosol. This is because of the particle size effect. Palm oil mist has smaller particle size and larger surface area than that of propylene glycol. Then the amount of collected palm oil aerosol on the surface of the filter medium is greater than propylene glycol aerosol. After some periods the fibrous filter that is exposed to propylene glycol aerosol has a higher pressure drop. This is because propylene glycol is less viscous (64.6 cP) than palm oil (94.6 cP) and then easier to be atomized by the Laskin nozzle so the concentration of propylene glycol is higher than that of palm oil and the large propylene glycol droplets deposited on the fibrous filter join to form bridges at the intersection of fibers. Subsequently all interstices are bridged and these bridges combine to form a liquid film on the surface of the filter medium. However, the palm oil aerosol deposit is only made up of droplets collected around the fibers. This is because propylene glycol has a higher surface tension (47.6 dynes/cm) than palm oil (42.2 dynes/cm) which is in agreement with the result of Contal et al. (2004). They studied the influence of the surface tension of three generated liquids: decamethylcyclopentasiloxane (DMP), di-octyl phthalate (DOP) and glycerol, and found that the filter that was exposed to glycerol aerosol had the highest pressure drop. This is because glycerol has a higher surface tension (92 dynes/cm) than DOP (35 dynes/cm) and DMP (19 dynes/cm) and the deposit of mainly spherical glycerol aerosol particles offers a specific surface area larger than that of DOP.

From the Figs. 4.29 to 4.32, the pressure drop curves are divided into two periods. Initially the pressure drop is linearly related to the collected mass. After some periods the pressure drop also increases almost linearly but at a higher rate.

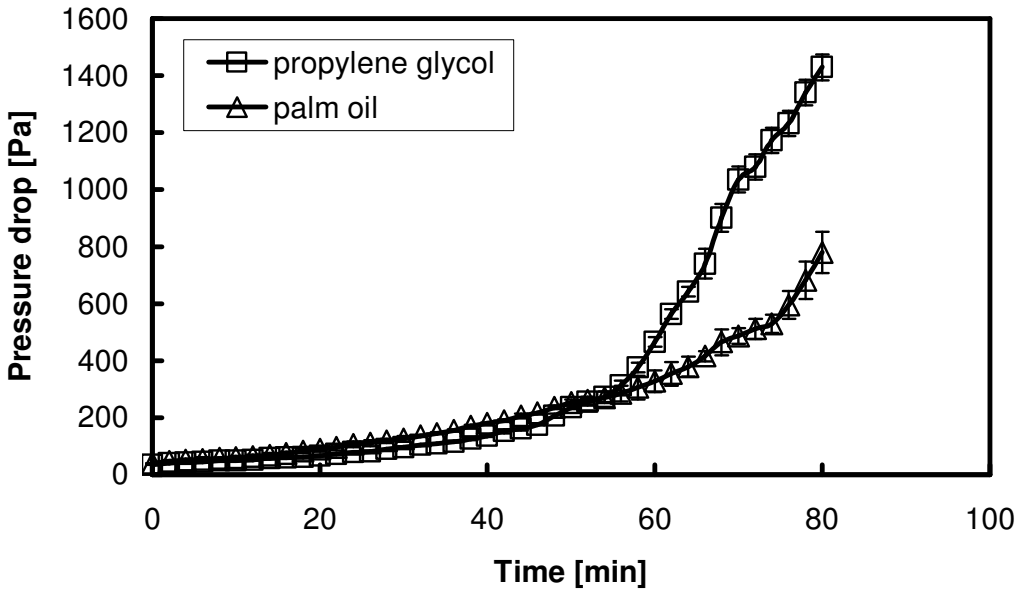

Figure 4.29 The change in the pressure drop across a single filter as a function of filtration time at 14 cm s^{-1}.

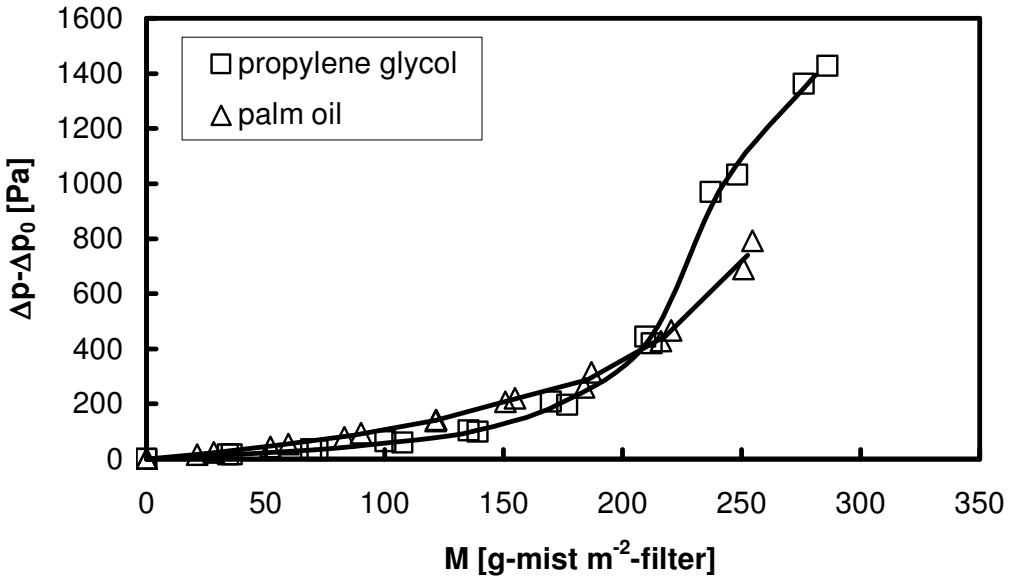

Figure 4.30 The change in pressure drop across a single filter as a function of collected mass at 14 cm s^{-1}.

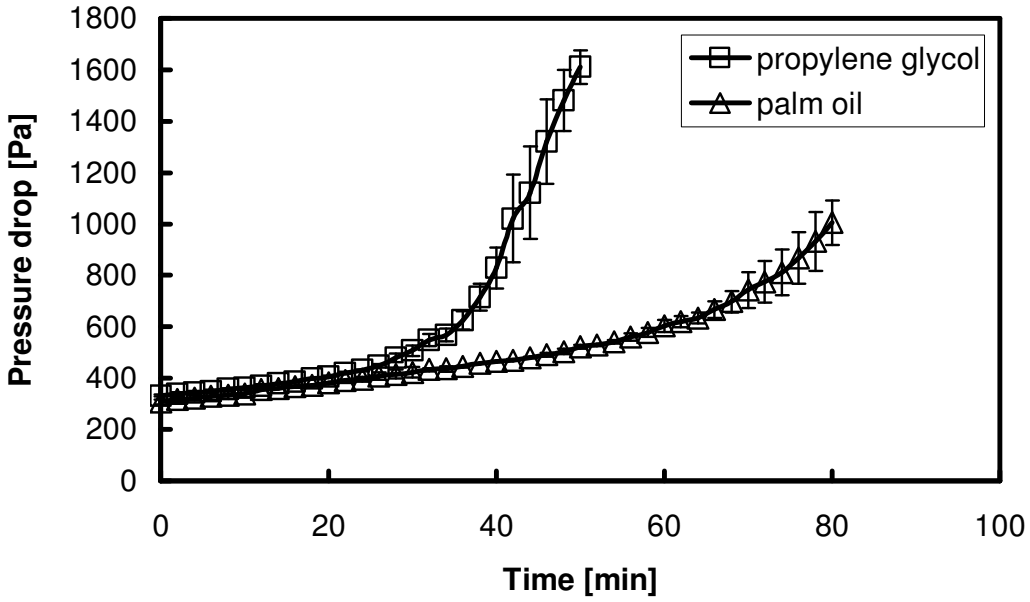

Figure 4.31 The change in pressure drop across five filters as a function of filtration time at 14 cm s^{-1}.

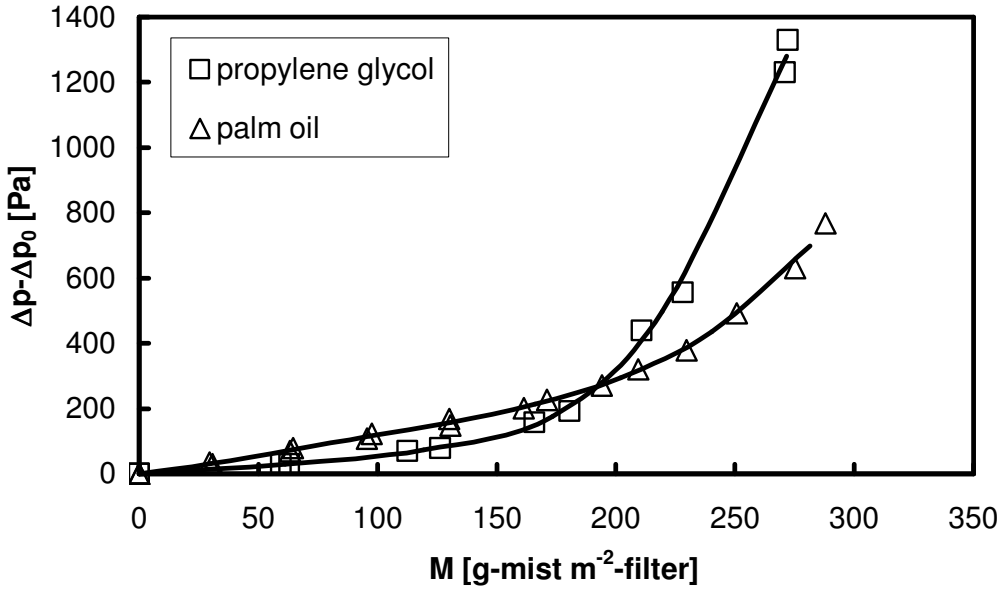

Figure 4.32 The change in pressure drop across five filters as a function of collected mass at 14 cm s^{-1}.

Figs. 4.33 and 4.34 show the optical microscope photographs of a single filter at different stages when the filter collected propylene glycol and palm oil, respectively. The photographs for propylene glycol (Fig. 4.33) suggest that at the beginning of filtration the deposit is made up of droplets deposited around the fibers [Fig. 4.33 (a)]; the beads then get bigger and join to form bridges at the intersection of fiber [Fig. 4.33 (b) and (c)]. Subsequently all interstices are bridged and these bridges combine to form a liquid film on the surface of the filter medium [Fig. 4.33 (d)] and cause higher pressure drop after some period. However, from Fig. 4.34, the deposition of palm oil aerosol particles is only made up of droplets deposited around the fibers even after 80 min of filtration. This is because propylene glycol has a higher surface tension than palm oil so the fibrous filter that is exposed to propylene glycol aerosol has a higher pressure drop because propylene glycol droplets deposited on the fibrous filter join to form bridges and liquid film on the surface of the filter.

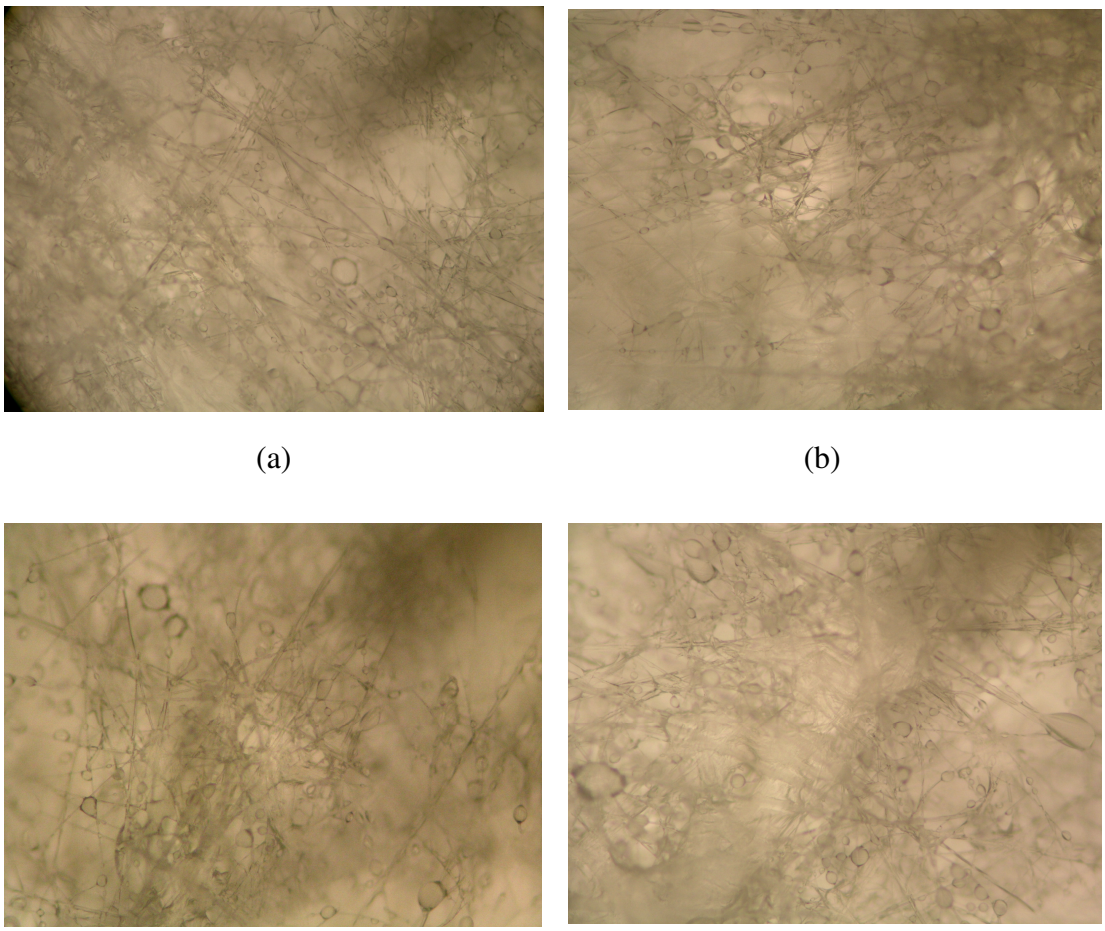

(a) (b)

(c) (d)

Figure 4.33 Optical microscope photographs of a single filter exposed to propylene glycol aerosol for (a) 20, (b) 40, (c) 60, and (d) 80 min (100×).

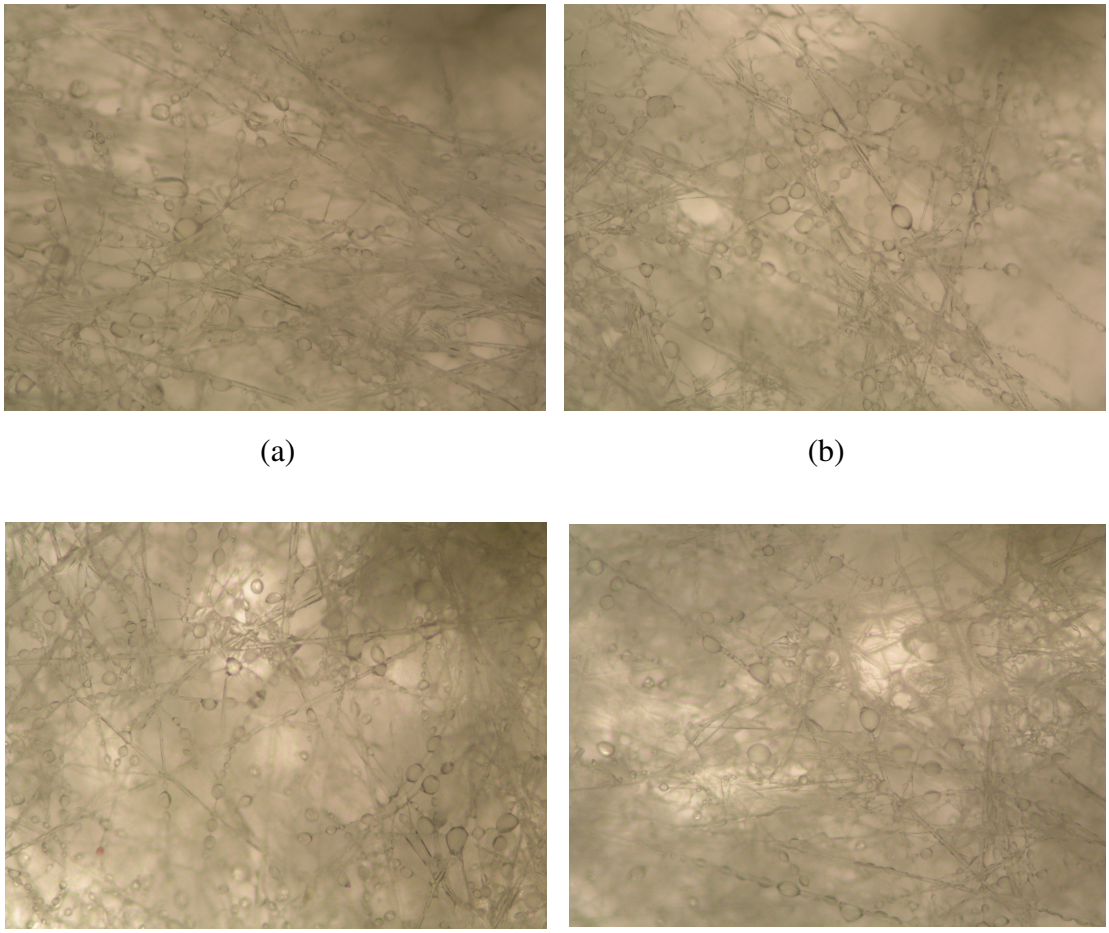

(a) (b)

(c) (d)

Figure 4.34 Optical microscope photographs of a single filter exposed to palm oil aerosol for (a) 20, (b) 40, (c) 60, and (d) 80 min (100×).

Fig. 4.35 shows the change in the collected mass as a function of filtration time of five filters using palm oil aerosol at filtration velocity of 14 cm s^{-1}. The results indicate that as filtration time increases, the collected mass of each filter increases as in the case of propylene glycol aerosol. The collected mass on the first filter sheet is about 26 and 232 g m^{-2} at 10 and 80 min, respectively. Moreover, at the same filtration time, the collected mass of the first filter sheet is lower when compared with the clogging of five filters by propylene glycol as shown in Fig. 4.36. This is because palm oil aerosol particles have lower concentration than propylene glycol aerosol particles. As filtration time elapses, palm oil aerosol particles can penetrate further to the subsequent filter sheets. This causes the increase of the collected mass on those filter sheets compared with propylene glycol aerosol particles, shown in Figs. 4.37 to Fig. 4.40. This is because palm oil aerosol particle has smaller particle size than propylene glycol aerosol particle and, hence, more palm oil aerosol particles can penetrate to the subsequent filter sheets. Mass of palm oil aerosol particles collected on the second filter sheet to the fifth filter sheet increases with filtration time.

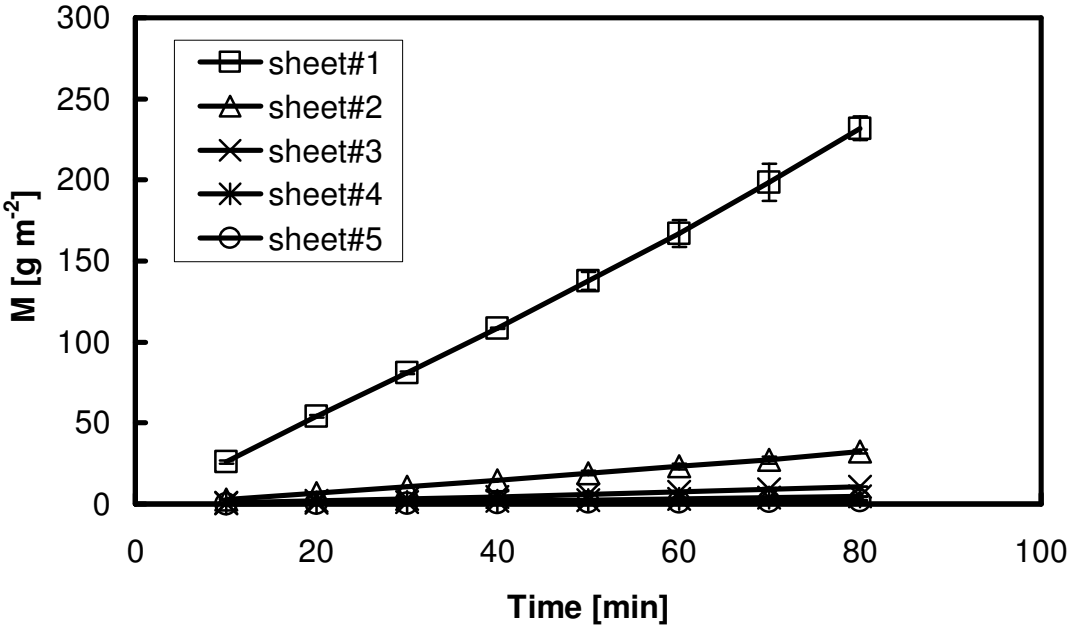

Figure 4.35 The change in the distribution profile during clogging of five filters for palm oil aerosol particles. (v = 14 cm s^{-1}; t = 10, 20, 30, 40, 50, 60, 70 and 80 min)

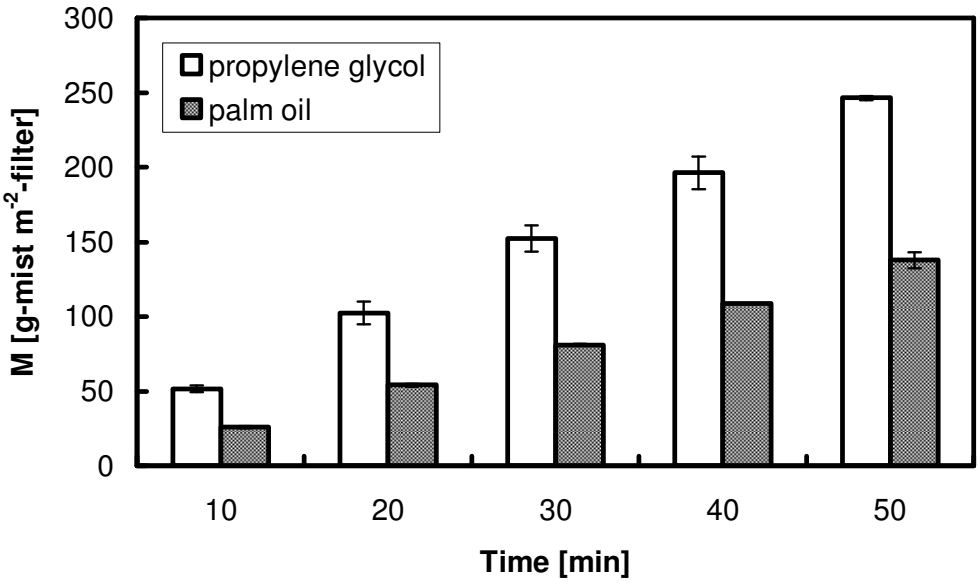

Figure 4.36 Effect of physical properties of the aerosol particles on the collected mass evolutions on the first filter sheet as a function of the filtration time at 14 cm s^{-1}.

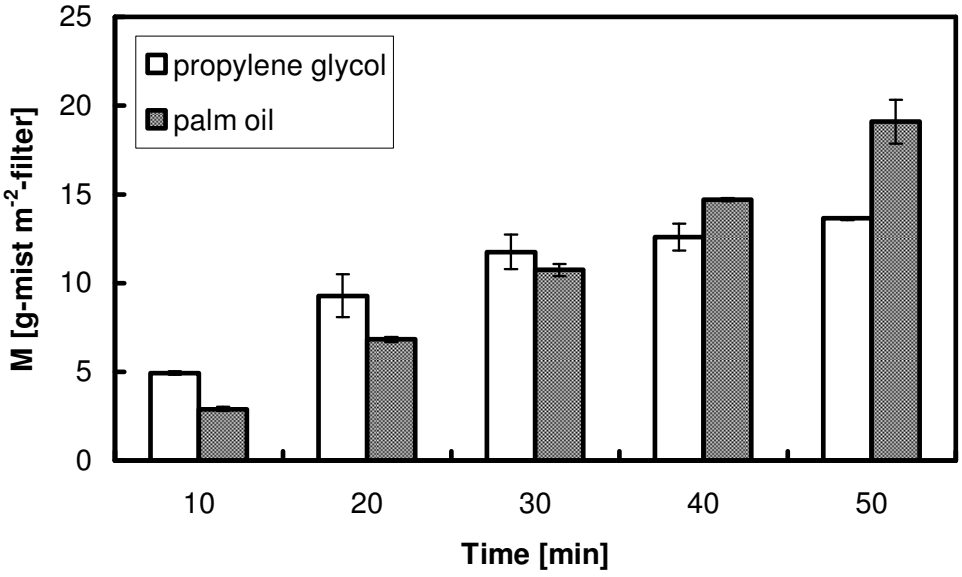

Figure 4.37 Effect of physical properties of the aerosol particles on the collected mass evolutions on the second filter sheet as a function of the filtration time at 14 cm s^{-1}.

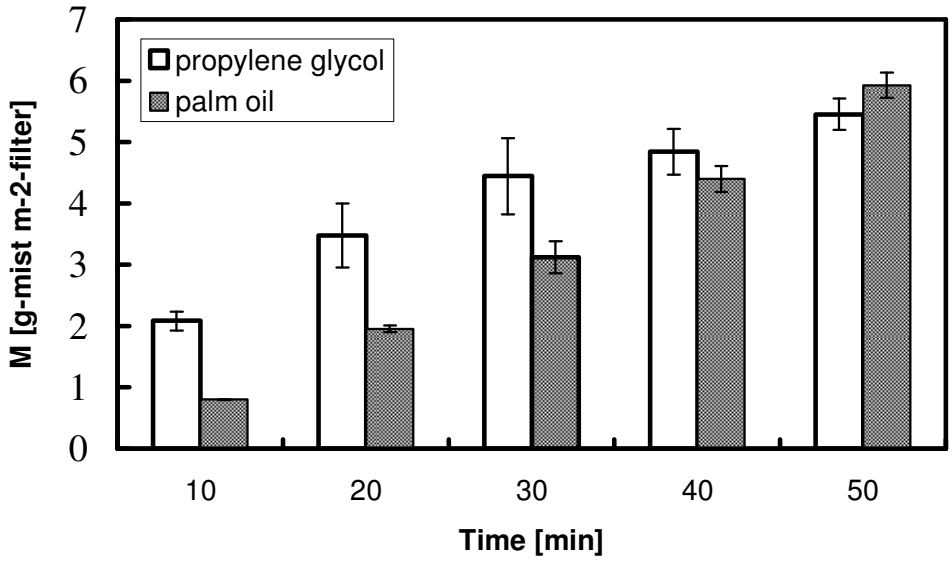

Figure 4.38 Effect of physical properties of the aerosol particles on the collected mass evolutions on the third filter sheet as a function of the filtration time at 14 cm s^{-1}.

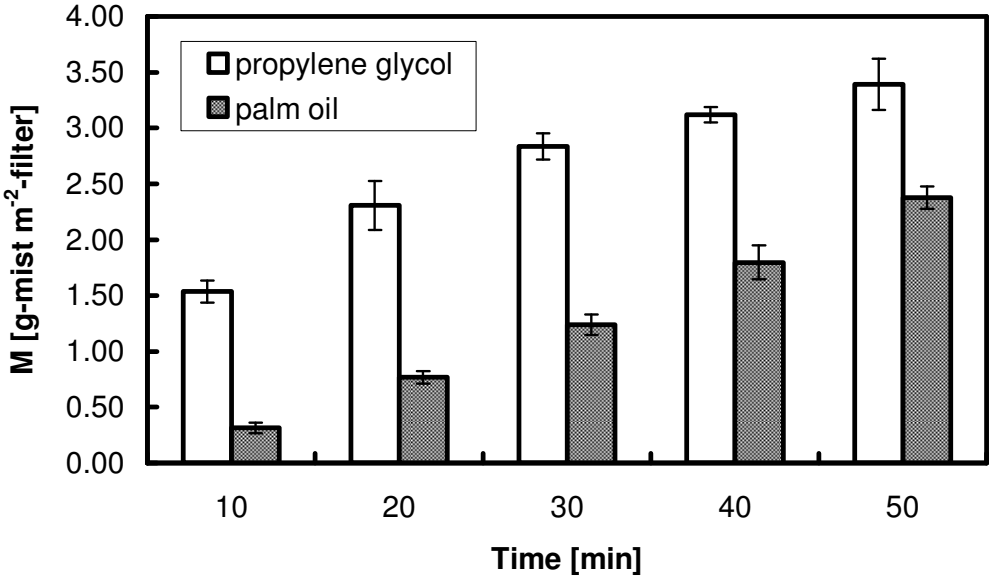

Figure 4.39 Effect of physical properties of the aerosol particles on the collected mass evolutions on the fourth filter sheet as a function of the filtration time at 14 cm s^{-1}.

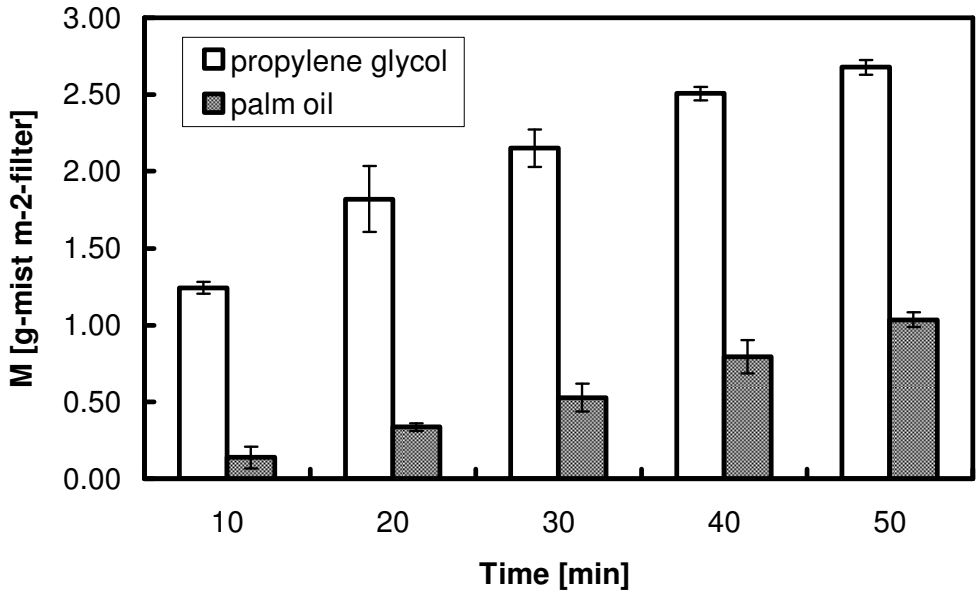

Figure 4.40 Effect of physical properties of the aerosol particles on the collected mass evolutions on the fifth filter sheet as a function of the filtration time at 14 cm s^{-1}.

4.3.4 Comparison between Experimental and Modelling Results

The pressure drop evolution was estimated by an adapted version of Davies' equation (1973). It was calculated by different equations because different layers exhibit different filtration stages. Frising et al. (2005) described the pressure drop evolution in four filtration stages. During the first filtration stage, the liquid is only deposited on the surface of the fiber. No drainage or liquid migration from one layer to the next layer is observed. In this work, the evolution of the pressure drop of a fibrous filter was investigated only in the first filtration stage because at the beginning of filtration the deposit is made up of droplets deposited around the fibers and no drainage is observed.

Frising et al. (2005) suggested the following expression to estimate the pressure drop for a fibrous filter during the first filtration stage:

$$\Delta P = 64\mu U_0 dZ \frac{(\alpha_f + \alpha_l)(\alpha_f + \alpha_l)^{0.5}}{d_{f\ Davies\ wet}^2} \times \left[1 + 16(\alpha_f + \alpha_l)^{2.5}\right] \qquad (4.3)$$

where μ is liquid viscosity, U_0 is filtration velocity, $d_{f\,Davies\,wet}$ is mean wet fiber Davies diameter which can be calculated from Eq. (2.18), α_f is clean filter packing density, α_l is liquid packing density and dZ is filter layer thickness which can be written as

$$dZ = \frac{Z}{np} \tag{4.4}$$

where Z is filter thickness, np is number of layers. This model was chosen because it gave the best results for initial pressure drop evolution.

Fig. 4.41 represents the comparison between experimental values and those calculated from Eq. (4.3) for the pressure drop evolutions of a single filter as function of collected mass during clogging by propylene glycol aerosol with different filtration velocities: 7, 14, 21 and 28 cm s^{-1} during the first filtration stage.

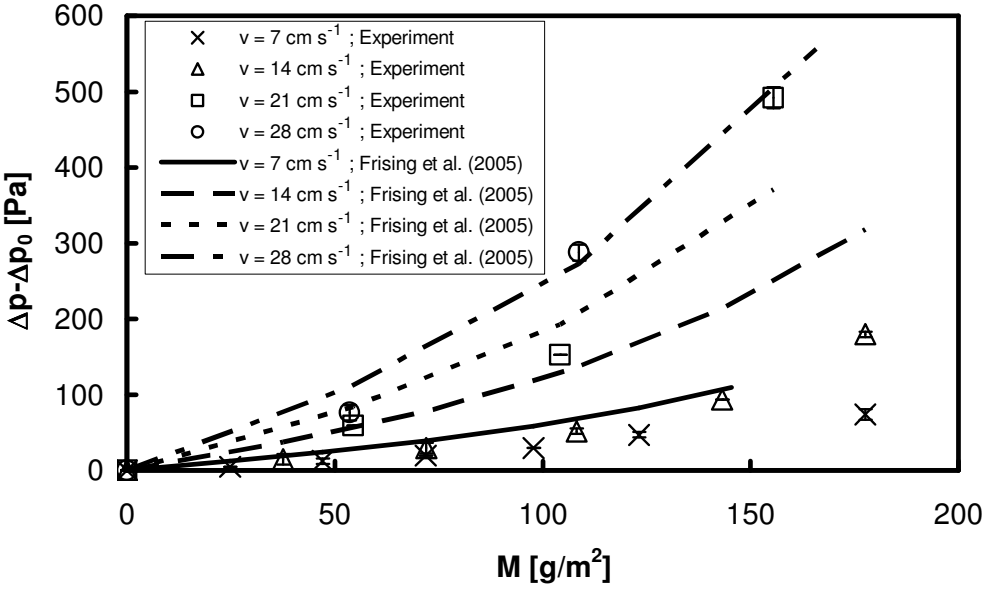

Figure 4.41 Comparison between experimental and modelling values of the pressure drop evolutions of a single filter as function of collected mass during clogging by propylene glycol aerosol with different filtration velocities during the first filtration stage.

From the result, it was found that the modeled pressure drop evolutions overestimated the experimental results for all filtration velocities. The discretization is low, however, at high velocity. This may be because of two reasons: First, at the beginning of filtration the deposition of propylene glycol aerosol particles is made up of droplets deposited around the fibers. The beads then get bigger and join to form bridges at the intersection of fiber. Subsequently all interstices are bridged and these bridges combine to form liquid films on the surface of the filter medium but the fibers was not perfectly wetted with liquid. Second, an adapted version of Davies' (1973) pressure drop model needs the liquid to wet the fibers perfectly and to be uniformly distributed throughout the fibrous filter. It gives, however, quite satisfactory results for the first filtration stage (Frising et al., 2005).

4.4 Saturation Characteristics of a Medium Performance Fibrous Filter

The saturation characteristics of the medium performance fibrous filter saturated with water, propylene glycol and palm oil were studied.

Initially, the test filter was immersed in the test liquid (water or propylene glycol or palm oil) until it was saturated. It was then exposed to an air stream at four different initial velocities: 7, 14, 21 and 28 cm s^{-1}. The velocity was then reduced to a minimum value of 1 cm s^{-1} for each case.

4.4.1 The Filter Sheet Saturated with Water

The change in the pressure drop across a single filter as a function of time and velocity when the liquid is water are shown in Figs. 4.42 and 4.43, respectively. It was found that the change in the saturation pressure drop at different initial velocities take nearly the same time. The saturation pressure drop from the initial velocity of 7 cm s^{-1} is greater than that from initial velocities of 14, 21 and 28 cm s^{-1}, respectively. The remained mass on the filter sheet saturated with water after the pressure drop is constant is decreased when the velocity is increased as shown in Fig. 4.44. This is because at the higher initial velocity, re-entrainment of liquid hold-up is greater.

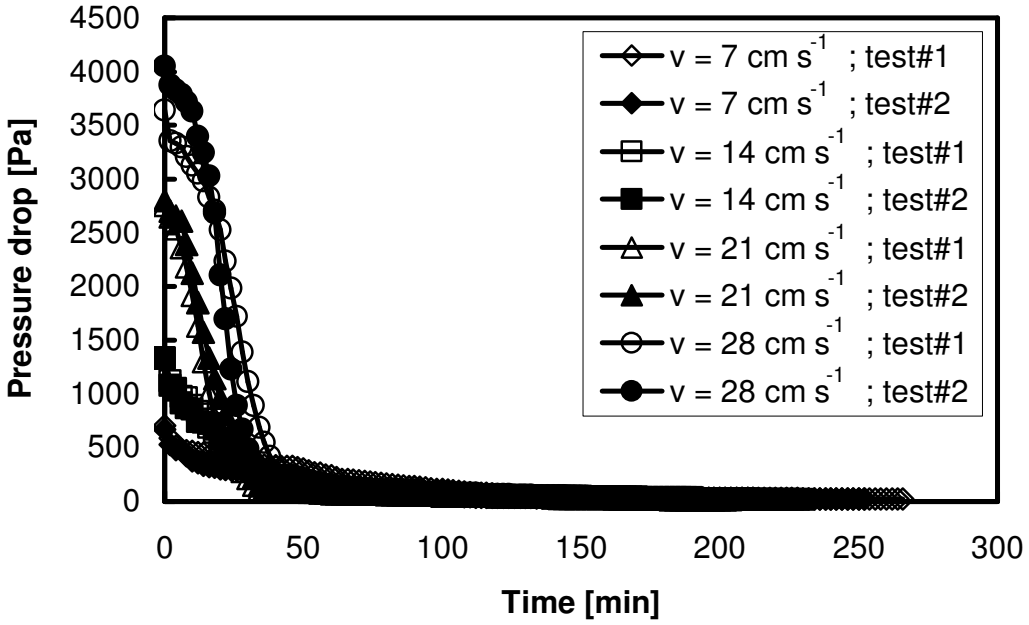

Figure 4.42 Change in pressure drop across the filter sheet saturated with water as a function of time at different velocities.

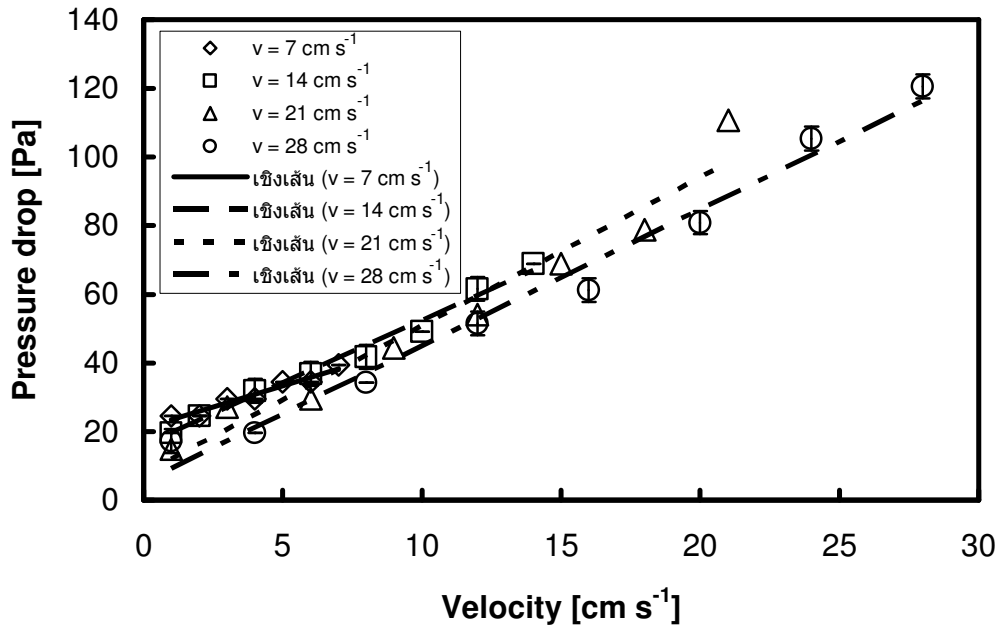

Figure 4.43 Saturation pressure drop across the filter sheet saturated with water as a function of velocity.

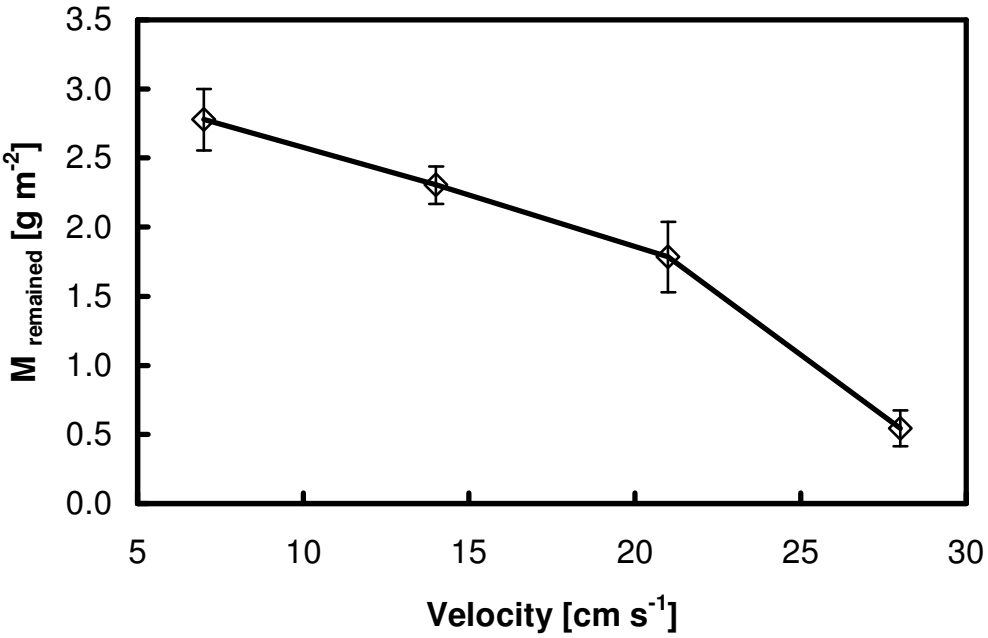

Figure 4.44 Remained mass on the filter sheet saturated with water after the pressure drop is constant as a function of velocity.

4.4.2 The Filter Sheet Saturated with Propylene Glycol

The change in the pressure drop across a single filter as a function of time and velocity when the liquid is propylene glycol are shown in Figs. 4.45 and 4.46, respectively. It was found that the change in the saturation pressure drop from the initial velocity of 7 cm s^{-1} takes longer than that from initial velocities of 14, 21 and 28 cm s^{-1}, respectively. The saturation pressure drop from the initial velocity of 7 cm sec^{-1} is greater than that from initial velocities of 14, 21 and 28 cm s^{-1}, respectively as in the previous case. The remained mass on the filter sheet saturated with propylene glycol after the pressure drop is constant is decreased when the velocity is increased as shown in Fig. 4.47 as in the previous case. This is because at the higher initial velocity, re-entrainment of liquid hold-up is greater.

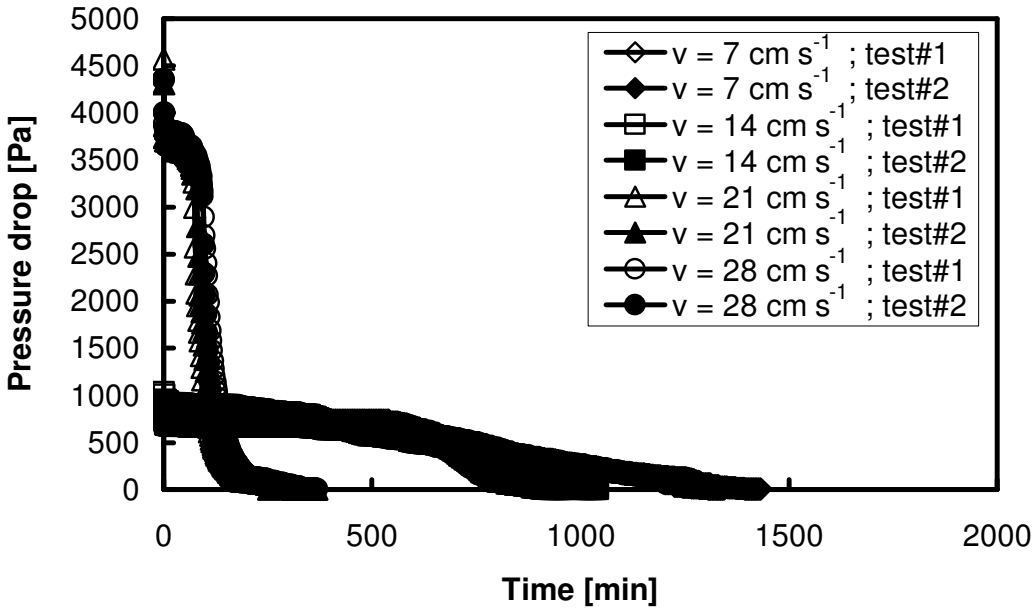

Figure 4.45 Change in pressure drop across the filter sheet saturated with propylene glycol as a function of time at different velocities.

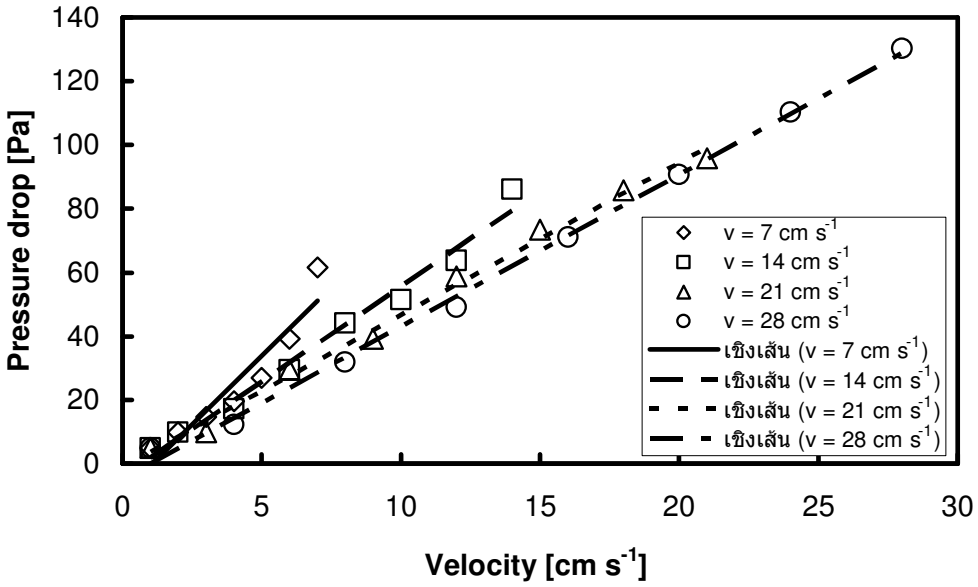

Figure 4.46 Saturation pressure drop across the filter sheet saturated with propylene glycol as a function of velocity.

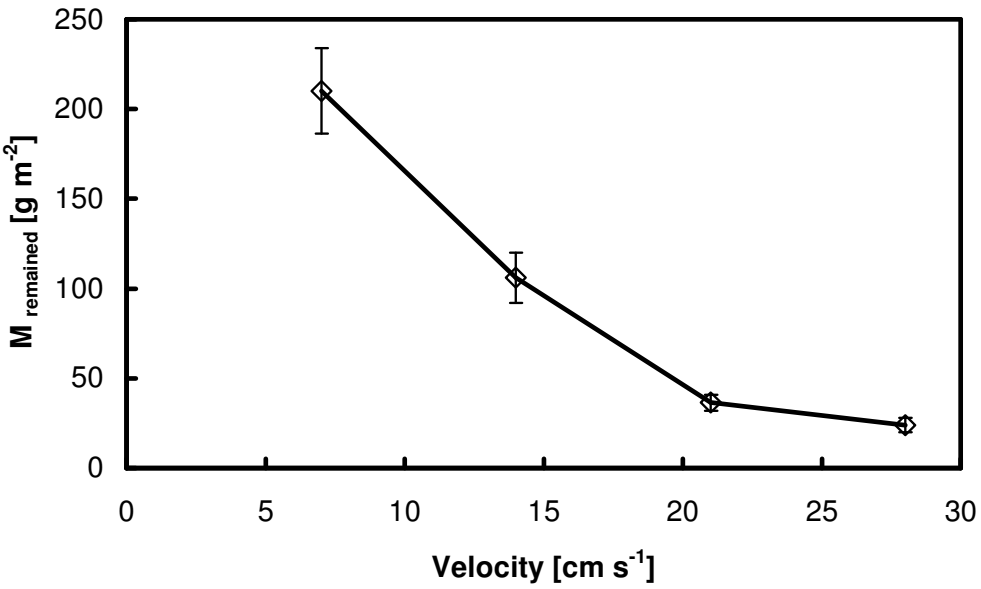

Figure 4.47 Remained mass on the filter sheet saturated with propylene glycol after the pressure drop is constant as a function of velocity.

4.4.3 The Filter Sheet Saturated with Palm oil

The change in the pressure drop across a single filter as a function of time and velocity when the liquid is palm oil are shown in Figs. 4.48 and 4.49, respectively. It was found that the change in the saturation pressure drop from the initial velocity of 28 cm s^{-1} take longer than that from initial velocities of 21, 14 and 7 cm s^{-1}, respectively. When the period is long, the weight of filter sheet saturated with palm oil decreases. From Fig. 4.48, it was found that the saturation characteristics of the medium performance fibrous filter saturated with palm oil is different from the case of water and propylene glycol. This result possibly occurs out of the viscosity effect. Palm oil is more viscous than propylene glycol so that palm oil can not re-entrain easily. The remained mass on the filter sheet saturated with palm oil after the pressure drop is constant is decreased when the velocity is increased as shown in Fig. 4.50 as in the previous case. This is because at the higher initial velocity, re-entrainment of liquid hold-up is greater. The constant pressure drop characteristics behave in the same manner as in the case of water and propylene glycol.

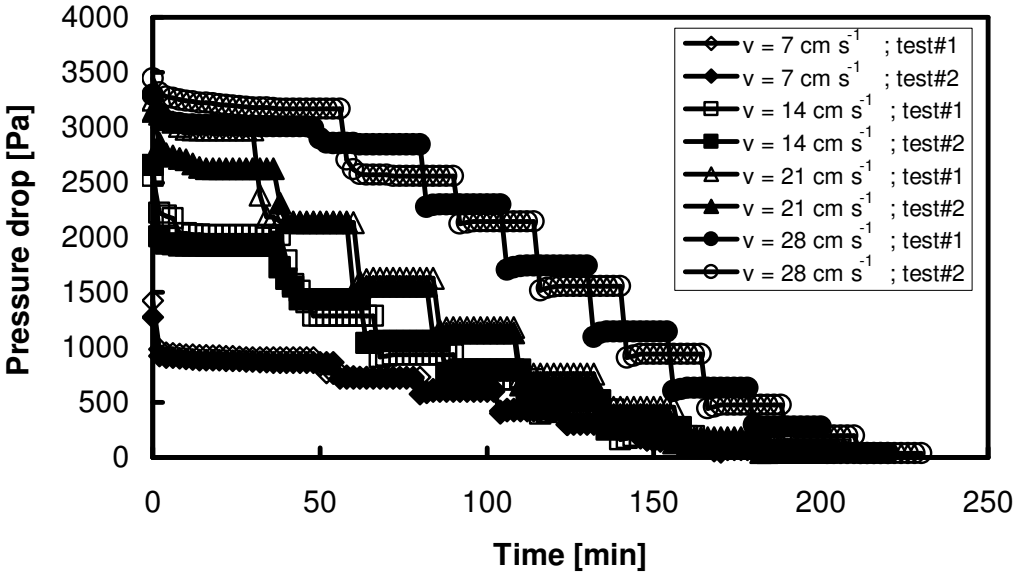

Figure 4.48 Change in pressure drop across the filter sheet saturated with palm oil as a function of time at different velocities.

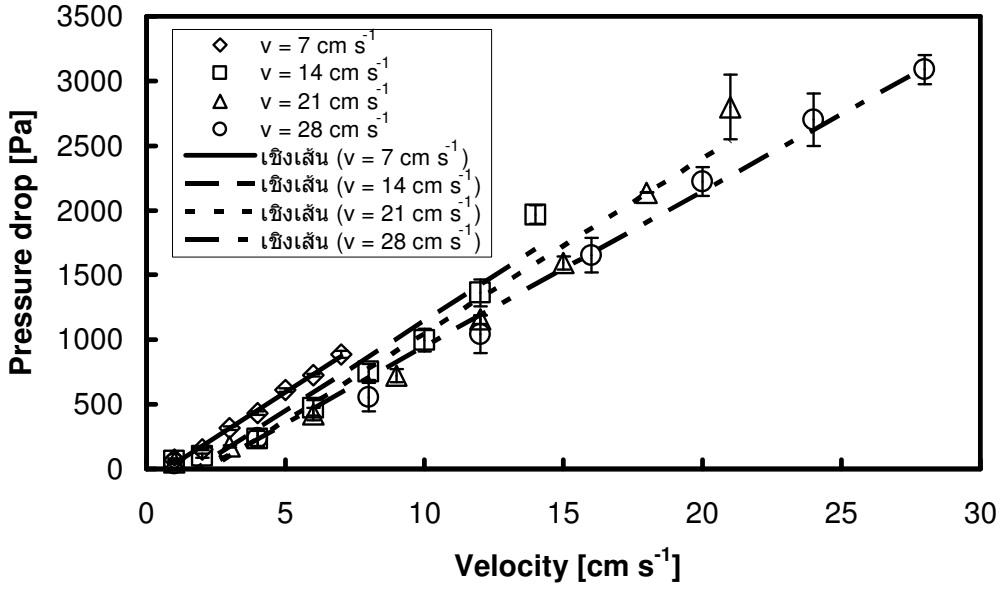

Figure 4.49 Saturation pressure drop across the filter sheet saturated with palm oil as a function of velocity.

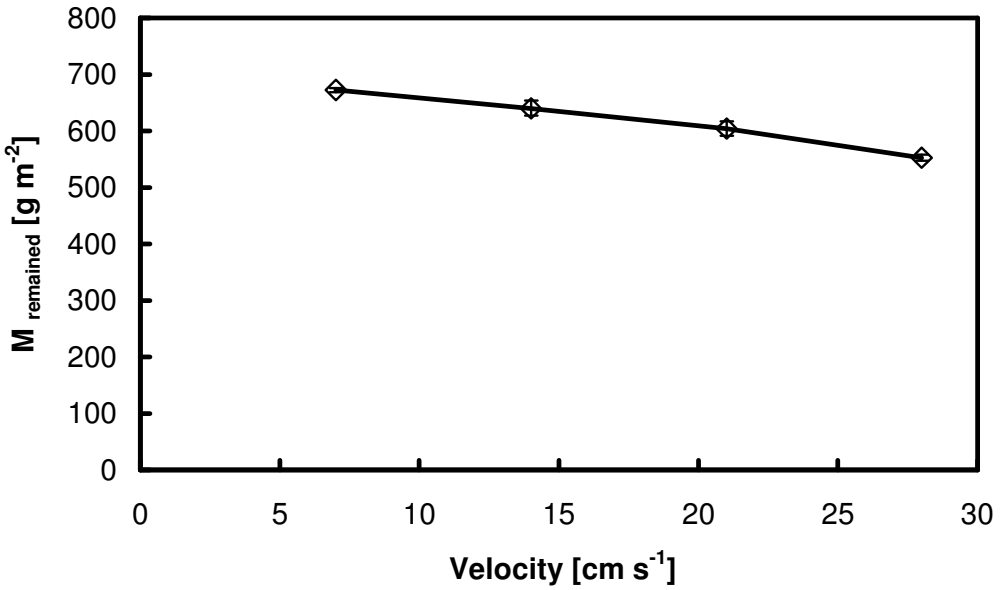

Figure 4.50 Remained mass on the filter sheet saturated with palm oil after the pressure drop is constant as a function of velocity.

Figs 4.51 to 4.53 show the optical microscope photographs of a single filter after the pressure drop is constant at each initial velocity when the filter was saturated with water, propylene glycol and palm oil, respectively. The photographs in Fig. 4.51 suggest that when the pressure drop of the initial velocity is constant, the fibrous filter saturated with water is made up of droplets partially deposited around the fibers. However, from Fig. 4.52 and 4.53, the fibrous filter saturated with propylene glycol and palm oil formed liquid films on the surface of the filter. This is due to the difference in the surface tension of liquids. Water and propylene glycol have higher surface tension than palm oil. Then the periods that the filter sheet saturated with water and propylene glycol formed liquid films on the surface of the filter is longer than that with palm oil.

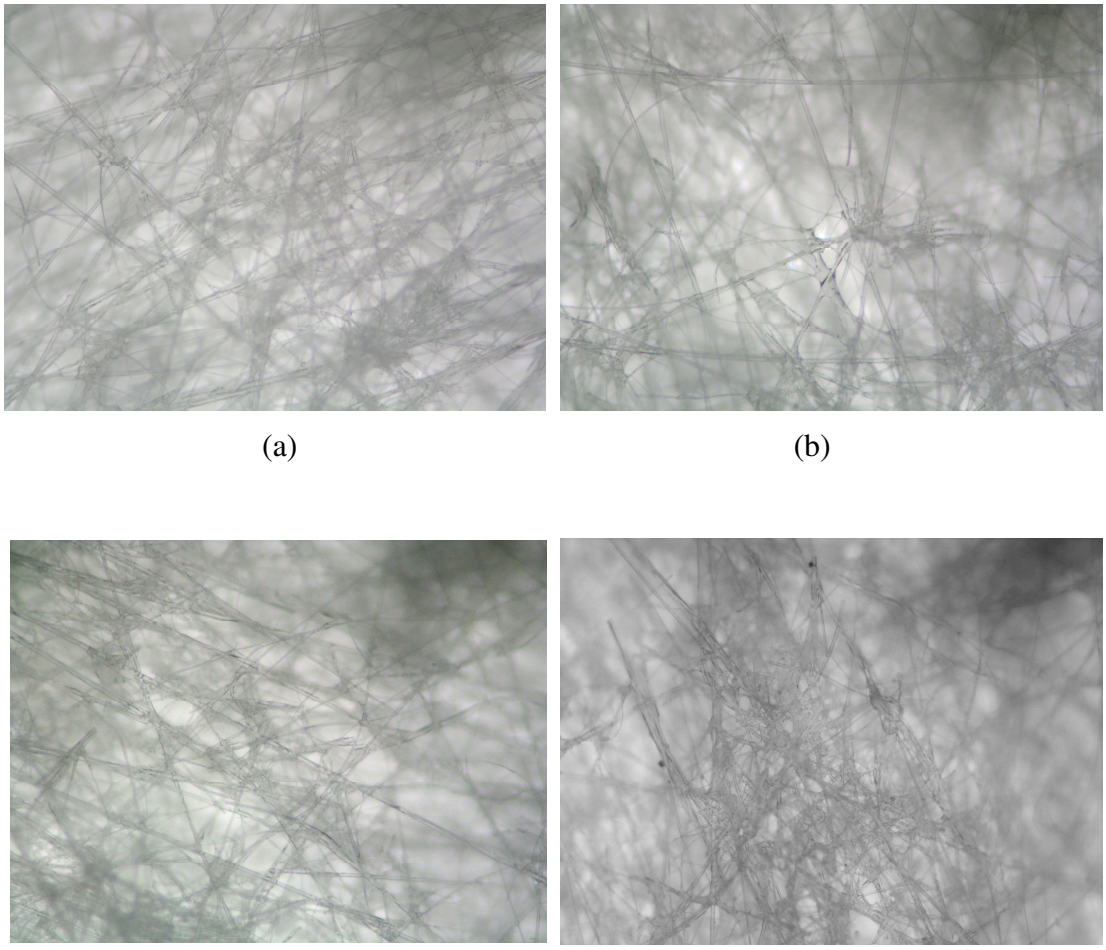

(a) (b)

(c) (d)

Figure 4.51 Optical microscope photograph of a single filter saturated with water at different initial velocity (×100). (a) initial velocity of 28 cm s^{-1}. (b) initial velocity of 21 cm s^{-1}. (c) initial velocity of 14 cm s^{-1}. (d) initial velocity of 7 cm s^{-1}.

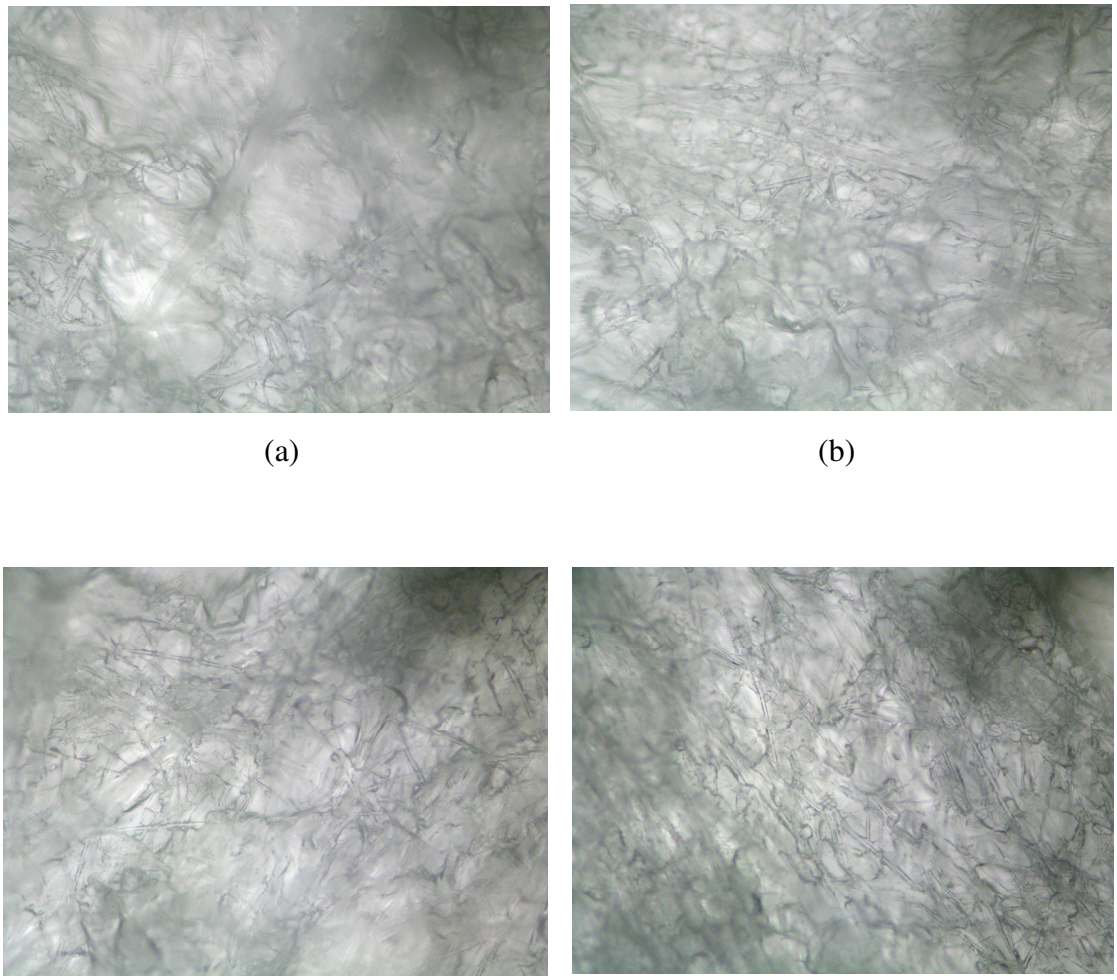

(a) (b)

(c) (d)

Figure 4.52 Optical microscope photograph of a single filter saturated with propylene glycol at different initial velocity (×100). (a) initial velocity of 28 cm s^{-1}. (b) initial velocity of 21 cm s^{-1}. (c) initial velocity of 14 cm s^{-1}. (d) initial velocity of 7 cm s^{-1}.

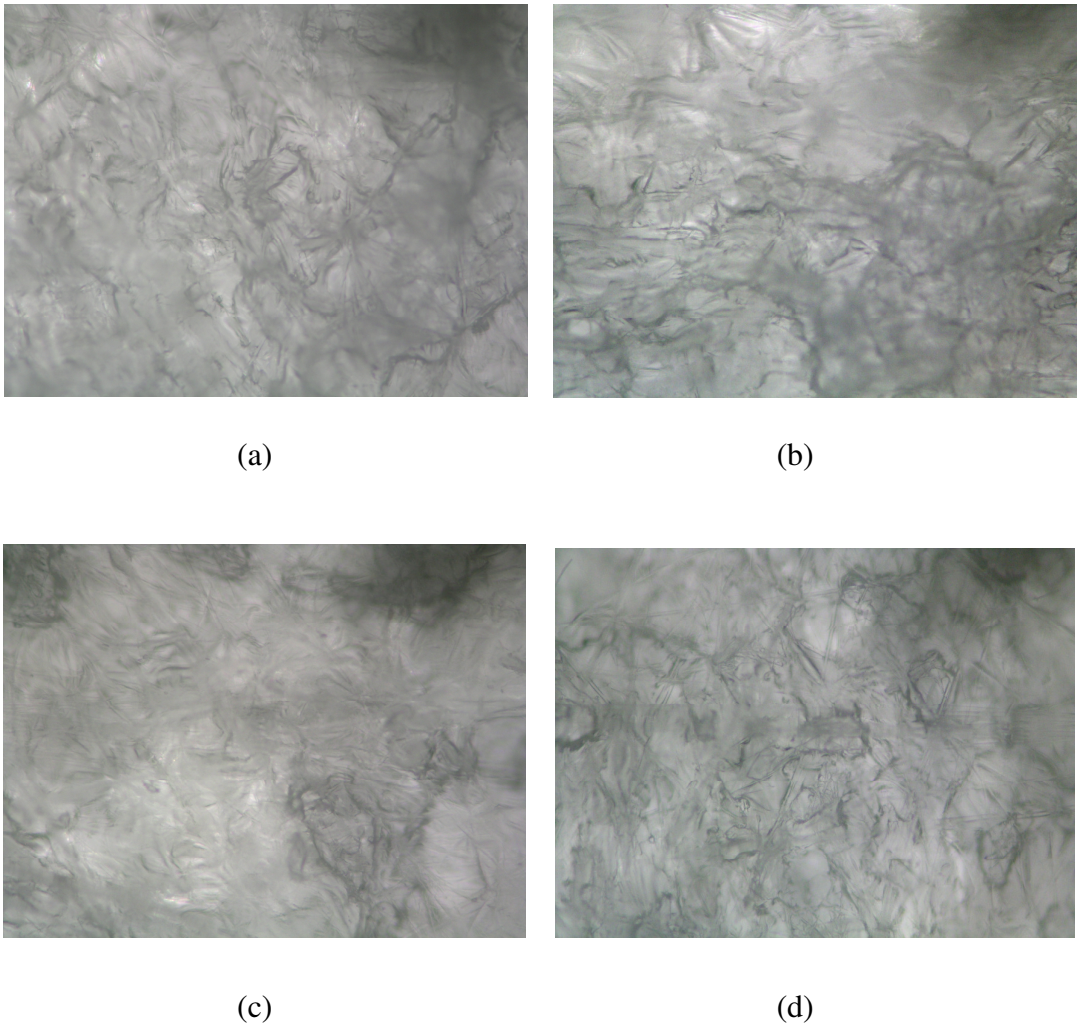

(a) (b)

(c) (d)

Figure 4.53 Optical microscope photograph of a single filter saturated with palm oil at different initial velocity (×100). (a) initial velocity of 28 cm s^{-1}. (b) initial velocity of 21 cm s^{-1}. (c) initial velocity of 14 cm s^{-1}. (d) initial velocity of 7 cm s^{-1}.

CHAPTER 5
CONCLUSIONS

In this work, an experimental set-up was designed and built for investigation of the collection characteristics of mist aerosol particles by a medium-performance fibrous filter. Initially, its collection performance was studied by varying various parameters. As a result of the present experimental study, the following conclusions can be reached:

(1) The average concentration of propylene glycol is higher than that of palm oil for identical operating condition because propylene glycol is less viscous than palm oil and, hence, easier to be atomized by the Laskin nozzle.

(2) The efficiency of a virgin filter slightly decreases when the filtration velocity increases for all particle sizes.

(3) At low velocity, the efficiency of a virgin filter is very high for all particle sizes due to the influence of the Brownian motion of small particles.

(4) At the highest velocity, collection efficiency of large particles is higher for virgin filter than that of small particles due to the influence of the impaction mechanism.

(5) The change in pressure drop during clogging increases when the filtration velocity increases. At high filtration velocity, the mist aerosol particles deposit on the collecting surface rapidly. This result causes the pressure drop of a single filter to increase.

(6) The change in pressure drop increases linearly with increasing the number of filter sheets for all velocities since the pressure drop is directly proportional to the thickness of the filter.

(7) The changes in pressure drop during clogging of a single filter and five identical filters are in the same direction. For five filters, while liquid

aerosol particles were collected on the surface of the filter, these particles can partially penetrate to the thickness of the medium.

(8) At the first stage of clogging, the collected mass of the filters is dependent on filtration velocity. At the same filtration time, the collected mass on the first filter sheet at higher filtration velocity is higher than that at lower filtration velocity.

(9) In an initial period, the clogging of the filter by palm oil aerosol is higher than that by propylene glycol aerosol due to the particle size effect. Palm oil has smaller particle size and larger surface area than propylene glycol then the amount of collected palm oil aerosol on the surface of the filter medium is greater than propylene glycol aerosol. After some period the fibrous filter that is exposed to propylene glycol aerosol has a higher pressure drop because the large propylene glycol droplets deposited on the fibrous filter join to form bridges and liquid films on the surface of the filter as shown in the optical microscope photographs.

(10) For five identical filters, while filtration time increases, the collected mass of each filter increases as in the case of propylene glycol aerosol. At the same filtration time, the collected mass of the first filter sheet when clogged by palm oil aerosol is lower when compared with the clogging of five filters by propylene glycol. This is because palm oil aerosol particles have lower concentration than propylene glycol aerosol particles.

(11) More palm oil aerosol particles can penetrate to the subsequent filter sheets because they have smaller particle size than propylene glycol aerosol particles.

(12) From the optical microscope photographs of five filters after filtration for 50 min, liquid aerosol particles can penetrate to the second, the third, the fourth and the fifth filter sheets. The quantity of palm oil droplets on the surface of the second and the third filter sheets is greater when compared with propylene glycol aerosol particles due to particle size and surface area effects.

(13) The period that the saturation pressure drop from all the initial velocity for propylene glycol is longer than that for water and palm oil. This is because propylene glycol has lower vapor pressure and higher boiling point than water so that propylene glycol can not evaporate easily. This causes the remained mass on the filter sheet saturated with water after the pressure drop is constant at all the initial velocity is lower than when filter sheet saturated with propylene glycol.

(14) The remained mass on the filter sheet saturated with propylene glycol after the pressure drop is constant at all the initial velocity is lower than when filter sheet saturated with palm oil. This is because propylene glycol is less viscous than palm oil so that propylene glycol can re-entrain easily.

REFERENCES

Agranovski, I.E., Shapiro, M. 2001. "Clogging of wet filters by dust particles", *Aerosol Scienc.* 32, 1009-1020.

Agranovski, I.E., Myojo, T., Braddock, R.D. and Jarvis, D. 2002. "Inclined wettable filter for mist purification", *Chemical Engineering Journal.* 89, 229-238.

Baron, P.A., Willeke, K. 2005. "Aerosol Measurement", 2nd ed. John Wiley & Sons, Inc., New York.

Briscoe, B.J., Galvin, K. P., Luckham, P.F. and Saeid, A.M. 1991. "Droplet coalescence on fibres", *Colloida and Surfaces*. 56, 301-312.

Brown, R.C. 1993. "Air Filtration", Health and Safety Executive Research and Laboratory Services Division, Sheffield, UK.

Contal, P., Simao, J., Thomas, D., Frising, T. and Calle, S. 2004. "Clogging of fibre filters by submicron droplets. Phenomena and influence of operating conditions", *Aerosol Science*. 35, 263-278.

Destephen, J.A., Kyung-Ju Choi. 1996. "Modelling of filtration processes of fibrous filter media", *Separations Technology.* 6, 55-67.

Frising, T., Thomas, D., Contal, P., Bemer, D. and Leclerc, D. 2003. "Influence of filter fibre size distribution on filter efficiency calculations", *Trans IChemE.* 81, 1179-1184.

Frising, T., Thomas, D., Bemer, D. and Contal, P. 2005. "Clogging of fibrous filters by liquid aerosol particles: Experimental and phenomenological modeling study", *Chemical Engineering Science.* 60, 2751-2762.

Gougeon, R., Boulaud, D. and Renoux, A. 1994. "Theoretical and experimental study of fibrous filters loading with liquid aerosols in the inertial regime", *J. Aerosol Sci*. 25, Suppl I, s189-s190.

Gougeon, R., Boulaud, D. and Renoux, A. 1996. "Comparison of data from model fiber filters with diffusion, interception and inertial deposition models" *Chem. Eng. Comm*. 151, 19-39.

Hajra, M. G., Mehta, K. and Chase, G.G. 2003. "Effects of humidity, temperature, and nanofibers on drop coalescence in glass fiber media", Separation and Purification Technology. 30, 79-88.

Hinds, W.C. 1999. "Aerosol Technology", 2nd ed. John Wiley & Sons, Inc., New York.

Ito, T., Otani, Y. and Inomata, H. 2004. "Performance of air filters cleaned by supercritical carbon dioxide", Separation and Purification Technology. 40, 41-46.

Letts, G.M., Raynor, P.C. and Schumann. 2003. "Selecting fiber materials to improve mist filters", *Aerosol Science.* 34, 1481-1492.

Liew, T. P., Conder, J.R. 1985. "Fine mist filtration by wet filters-I. liquid saturation and flow resistance of fibrous filters", *J. Aerosol Sci.* 16, 497-509.

Mullins, B.J., Braddock, R.D., Agranovski, I.E. and Cropp, R.A. 2006. "Observation and modeling of barrel droplets on vertical fibres subjected to gravitational and drag forces", *Journal of Colloid and Interface Science.* 300, 704-712.

Mullins, B.J., Kasper, G. 2006. "Comment on: "Clogging of fibrous filters by liquid aerosol particles: Experimental and phenomenological modeling study" by Frising et al.", *Chemical Engineering Science.* 61, 6223-6227.

Payet, S., Boulaud, D., Madelaine, G. and Renoux, A. 1992. "Penetration and pressure drop of a HEPA filter during loading with submicron liquid particles", *J. Aerosol Scit.* 23, 723-735.

Penicot, P., Thomas, D., Contal, P., Leclerc, D and Vendel, J. 1999. "Clogging of HEPA fibrous filters by solid and liquid aerosol particles: An experimental study", *Filtration & Separation.*, 59-64.

Raynor, P.C., Leith, D. 2000. "The influence of accumulated liquid on fibrous filter performance", *J. Aerosol Sci.* 31, 19-34.

Raynor, P.C., Volckens, J. and Leith, D. 2000. "Modeling evaporative loss of oil mist collected by sampling filters", *Applied Occupational and Environmental Hygiene.* 15, 90-96.

Reist, P.C. 1993. "Aerosol science and technology", New York: McGraw-Hill, 2nd ed.

Sakano, T., Otani, Y., Namiki, N. and Emi, H. 2000. "Particle collection of medium performance air filters consisting of binary fibers under dust loaded conditions", *Separation and Purification Technology.* 19, 145-152.

Thomas, D., Contal, P., Renaudin, V., Penicot, P., Leclerc, D. and Vendel, J. 1999. "Modelling pressure drop in HEPA filters during dynamic filtration", *J. Aerosol Sci.* 30, 235-246.

Vasudevan, G., Chase, G. G. 2004. "Performance of B-E-glass fiber media in coalescence filtration", *Aerosol Science*. 35, 83-91.

Walsh, D.C., Stenhouse, J.I.T., Scurrah, K.L. and Graef, A. 1996. "The effect of solid and liquid aerosol particle loading on fibrous filter material performance", *J. Aerosol Sci.* 27, Suppl. I, s617-s618.

Yeh, H.C., Liu, B.Y.H. 1974. “Aerosol filtration by fibrous filters –II. Experimental”, *J. Aerosol Science.* 5, 205-217.

Appendix A

Drawing of a Laskin nozzle

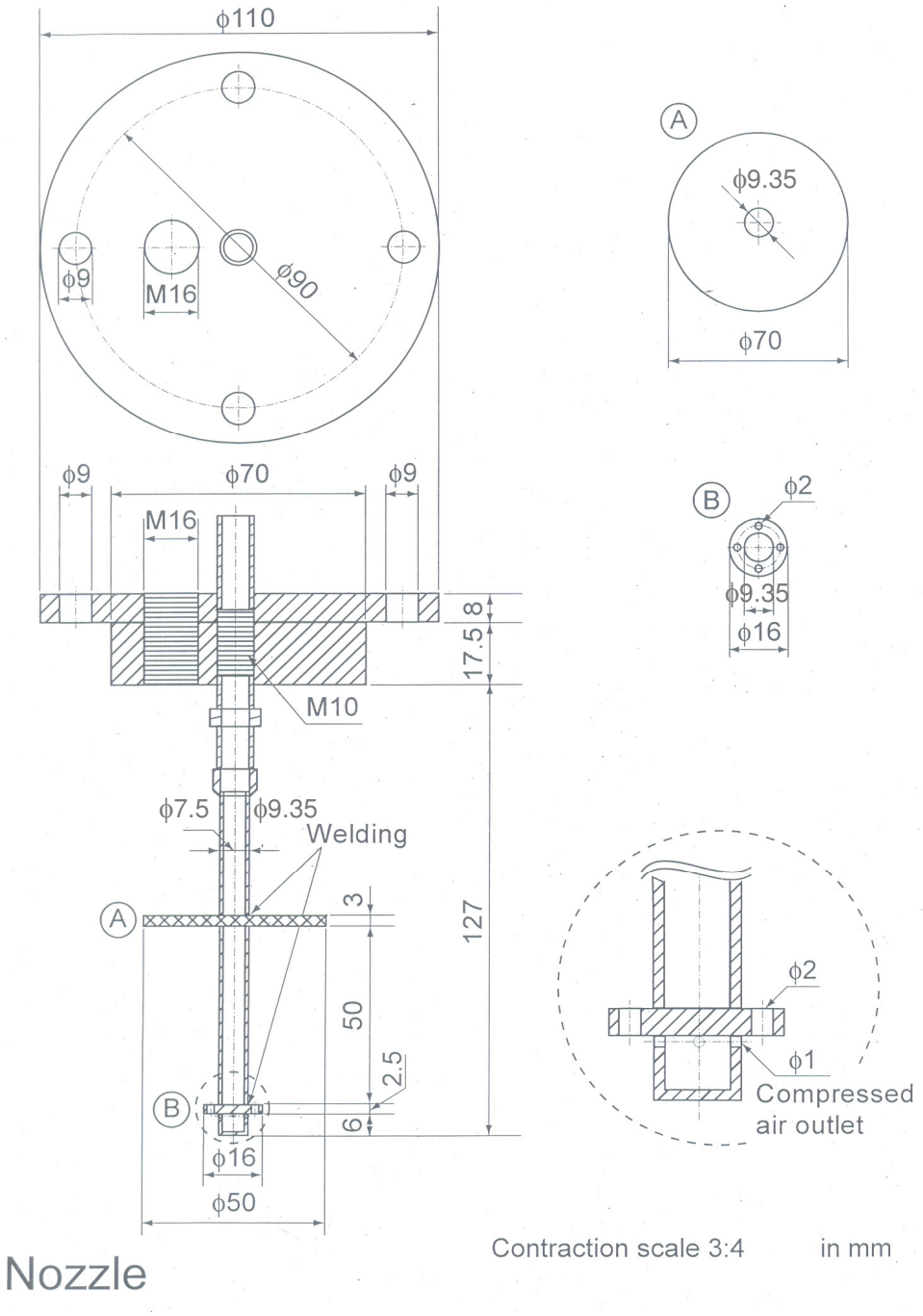

Figure 1. Model of nozzle.

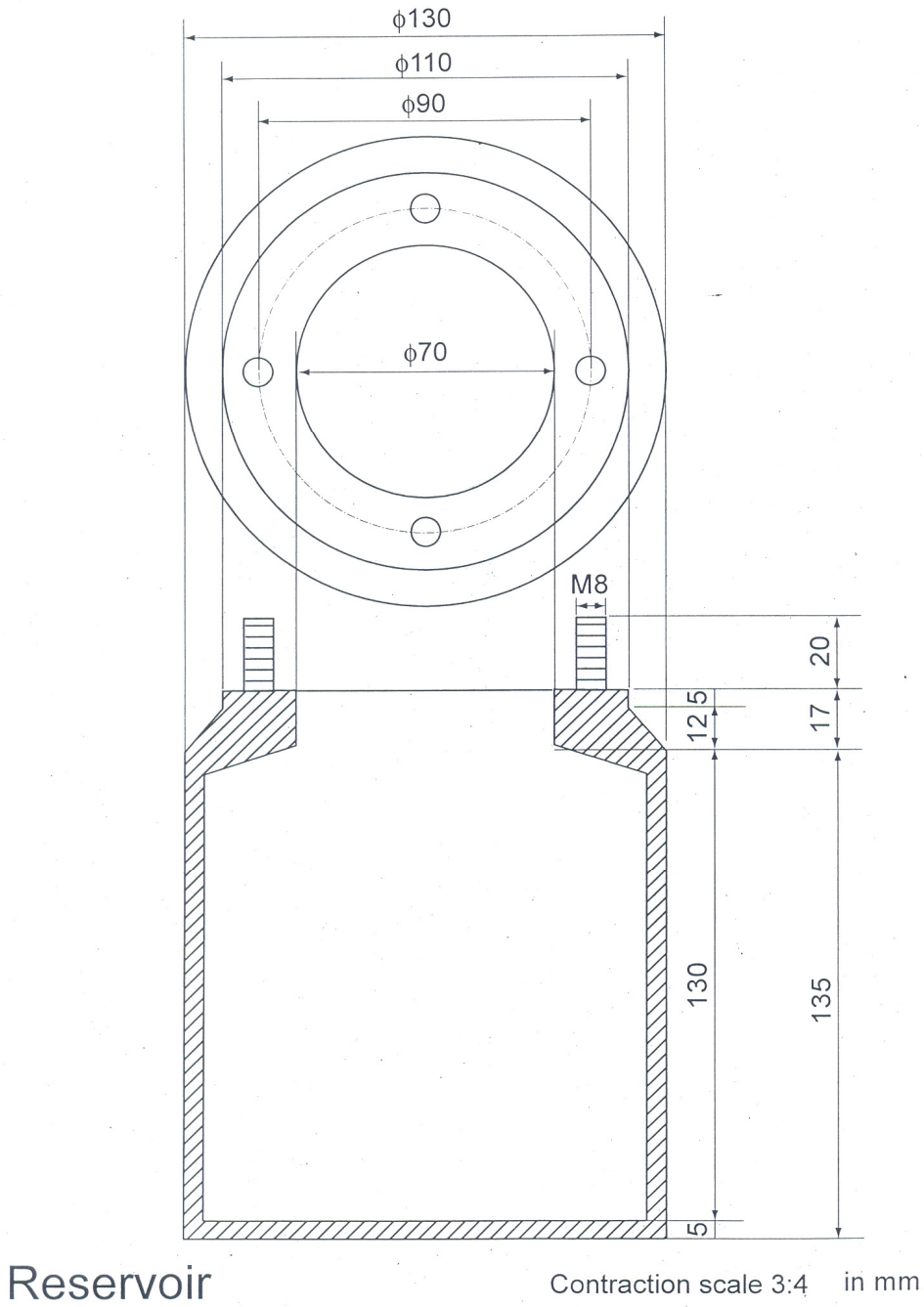

Figure 2. Model of reservoir.

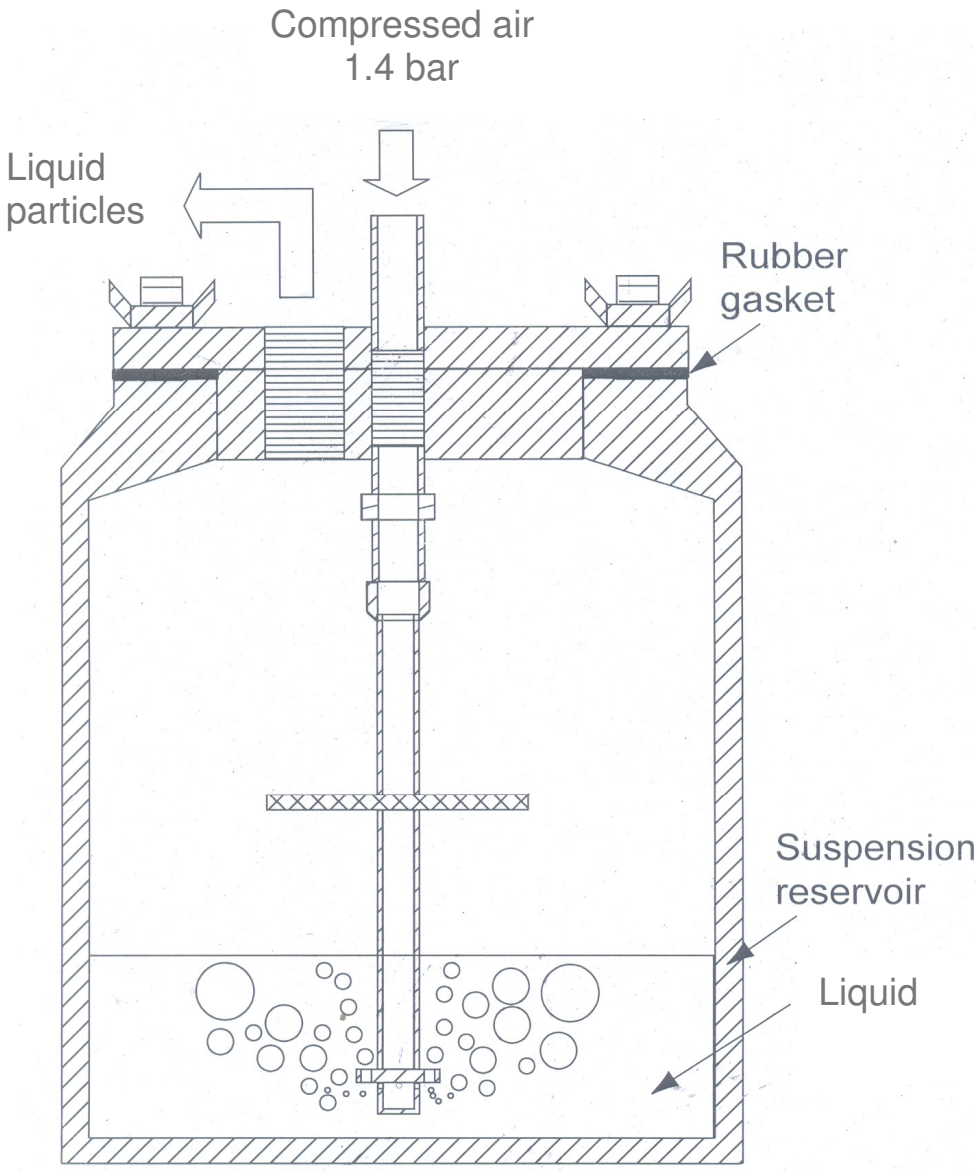

Figure 3. The Laskin nozzle.

Appendix B

Size distribution of aerosol particles from the Laskin nozzle

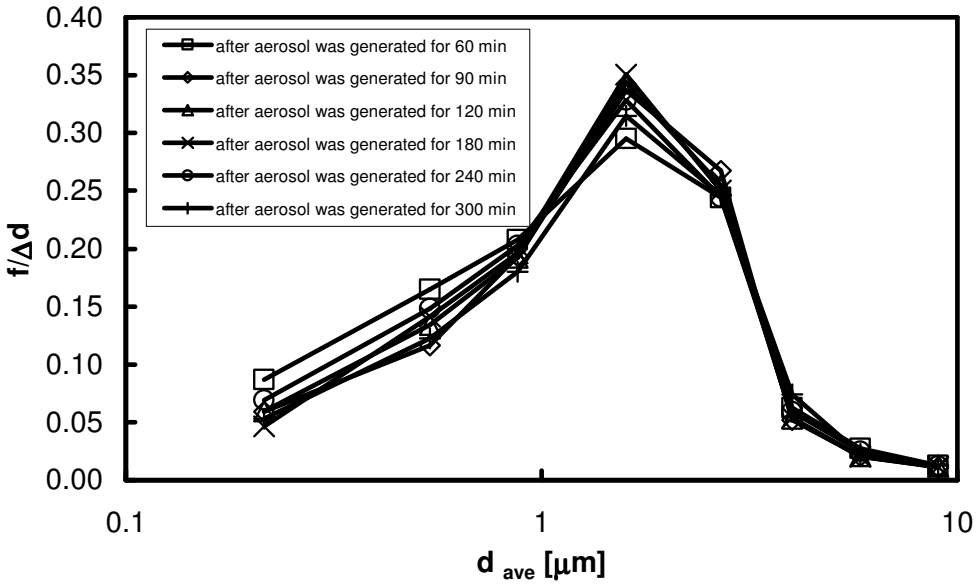

Figure 4. Size distribution of propylene glycol aerosol particles from the Laskin nozzle (Test#1).

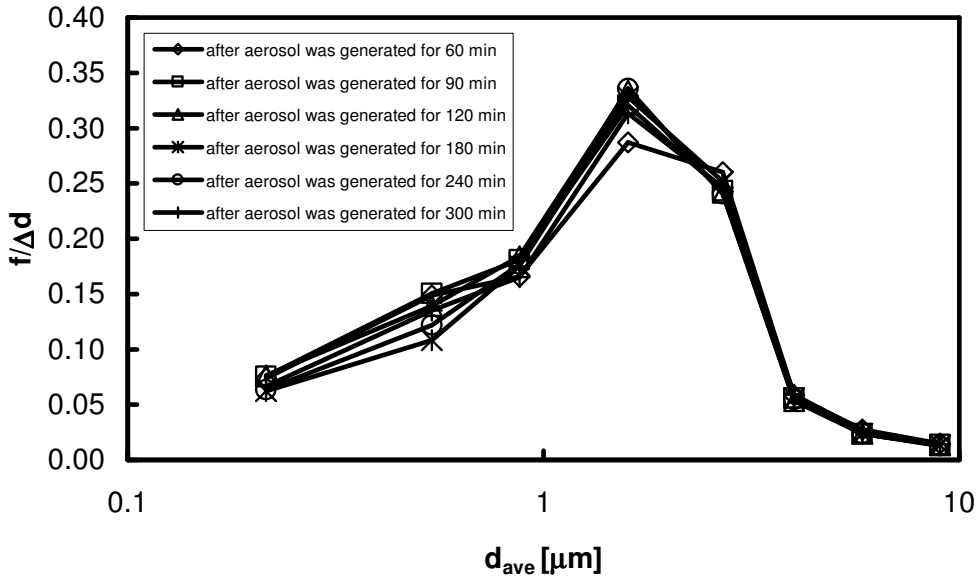

Figure 5. Size distribution of propylene glycol aerosol particles from the Laskin nozzle (Test#2).

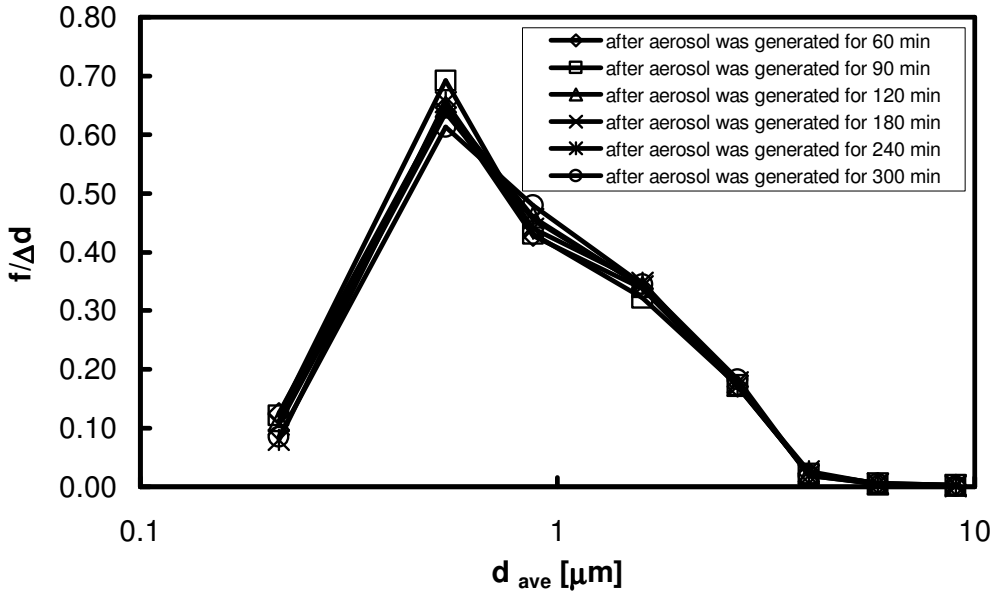

Figure 6. Size distribution of palm oil aerosol particles from the Laskin nozzle (Test#1).

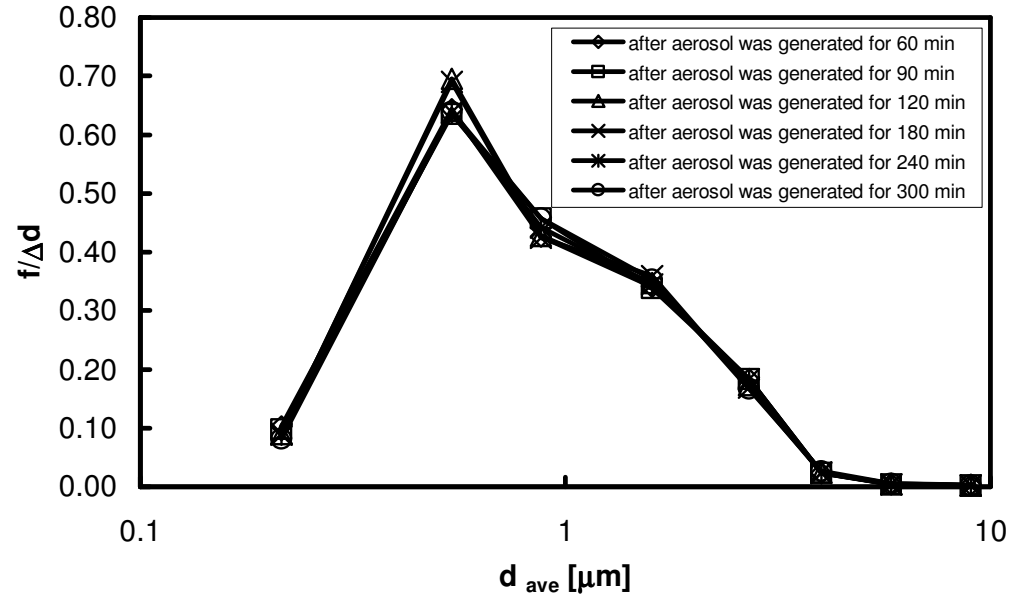

Figure 7. Size distribution of palm oil aerosol particles from the Laskin nozzle (Test#2).

VITAE

Name Miss Punnida Suwanwong

Student ID 4722041

Educational Attainment

Degree	Name of Institution	Year of Graduation
Bachelor of Science (Chemistry)	Prince of Songkla University	2003

Scholarship Awards during Enrollment

The scholarship from Higher Education Development Project: Center for Innovation in Chemistry: Postgraduate Education and Research Program in Chemistry, funded by The Royal Thai Government (PERCH-CIC).